UNIVERSITY OF CALIFORNIA, SAN DIEGO

Crosstalk Modeling, Analysis and Reduction in Stereoscopic Displays

A dissertation submitted in partial satisfaction of the
requirements for the degree
Doctor of Philosophy

in

Electrical Engineering (Signal and Image Processing)

by

Menglin Zeng

Committee in charge:

Professor Truong Nguyen, Chair
Professor Serge Belongie
Professor Pamela Cosman
Professor Yeshaiahu Fainman
Professor William Hodgkiss

2017

The dissertation of Menglin Zeng is approved, and it is acceptable in quality and form for publication on microfilm and electronically:

_____

_____

_____

_____

_____
Chair

University of California, San Diego

2017

DEDICATION

To my family and those who are interested in crosstalk.

EPIGRAPH

And God said, "Let there be light", and there was light.

—Genesis 1:3

In Him was life, and the life was the light of men.

—John 1:4

TABLE OF CONTENTS

LIST OF FIGURES

LIST OF TABLES

ACKNOWLEDGEMENTS

I would like to thank Prof. Nguyen for his extraordinary support and care. Without his patience in giving advice, encouragement with new ideas and continuous involvement this research could not start nor be completed. When this project encountered difficulties, his positive attitude encouraged me greatly, kept the project moving at a reasonable pace and pushed me onward to the finish line.

Thanks to Stanley who helped me with my first conference paper when I was a beginner in this topic. I also would like to thank Haleh who patiently helped me in revising a rejected conference paper until it eventually was accepted. Many thanks to my colleagues in the lab who participated in the subjective test and gave me precious advice in our group seminars.

I appreciate Alans help, who came to campus countless times with his baby girl to help revising my first journal paper and providing guidance for the subjective test. Furthermore, I thank Prof. Macleod who generously let us use his vision lab for the subjective test.

Also thanks to all the committee members for using your precious time to attend the preliminary, candidacy exams and this thesis defense with constructive advice.

Finally, I thank all the brothers and sisters in the Lord who shepherded me and prayed for me during this process. I surely could not make it without you. Most importantly, I thank You dear Lord Jesus, for leading me through this wonderful journey as my greatest companion and counselor.

Chapter 2, in full, is a reprint of the material as it appears in Numerical Grid Generational in Image Analysis and Interpretation (SSIAI). Menglin Zeng, Truong Nguyen, 2012. The dissertation author was the primary investigator and author of this paper.

Chapter 3, in full, is a reorganized composition of the materials as they appear

in International Conference on Acoustics, Speech and Signal Processing (ICASSP), IEEE, 2012, Menglin Zeng, Truong Nguyen, and, International Conference on Image Processing (ICIP), IEEE, 2014, Menglin Zeng, Haleh Azartash, and Truong Nguyen, and IEEE Transactions on Image Processing, Vol. 24, Number 12, 2015, Menglin Zeng, Alan Robinson, and Truong Nguyen. The dissertation author was the primary investigator and author of these papers.

Chapter 4, in full, is a reorganized composition of the materials as they appear in International Conference on Image Processing (ICIP), IEEE, 2014, Menglin Zeng, Haleh Azartash, and Truong Nguyen, and, IEEE Transactions on Image Processing, Vol. 25, Number 3, 2016, Menglin Zeng, Truong Nguyen. The dissertation author was the primary investigator and author of these papers.

Chapter 5, in part is currently being prepared for submission for publication of the material, Menglin Zeng, Alan Robinson, and Truong Nguyen. The dissertation author is the primary investigator and author of this material.

VITA

2006-2010	B. S. in Physics Science and Engineering (Optics and Photonics), Sun Yat-San University, Guangzhou, China
2010-2012	M. S, in Electrical Engineering (Signal and Image Processing), University of California, San Diego
2012-2017	Ph. D. in Electrical Engineering (Signal and Image Processing), University of California, San Diego

PUBLICATIONS

Menglin Zeng, Truong Nguyen "Crosstalk Analysis in LCD Stereoscopic Displays with Active Shutter Glasses", *Image Analysis and Interpretation (SSIAI), IEEE*, 165-168, 2012.

Menglin Zeng, Truong Nguyen "Crosstalk Modeling, Analysis, Simulation and Cancellation in passive-type stereoscopic LCD displays", *International Conference on Acoustics, Speech and Signal Processing (ICASSP), IEEE*, 1840-1844, 2012.

Menglin Zeng, Haleh Azartash, and Truong Nguyen "Crosstalk modeling in circularly polarized stereoscopic LCDs", *International Conference on Image Processing (ICIP), IEEE*, 3464-3468, 2014.

Menglin Zeng, Alan E. Robinson, and Truong Q. Nguyen, "Modeling, prediction, and reduction of 3D crosstalk in circular polarized stereoscopic LCDs", *IEEE Transactions on Image Processing*, Vol. 24, Number 12, pp 5516-5530, 2015.

Menglin Zeng, Truong Q. Nguyen, "Analysis of Crosstalk in 3D Circularly Polarized LCDs Depending on the Vertical Viewing Location", *IEEE Transactions on Image Processing*, Vol. 25, Number 3, pp 1070-1083, 2016.

ABSTRACT OF THE DISSERTATION

Crosstalk Modeling, Analysis and Reduction in Stereoscopic Displays

by

Menglin Zeng

Doctor of Philosophy in Electrical Engineering (Signal and Image Processing)

University of California San Diego, 2017

Professor Truong Nguyen, Chair

A Stereoscopic display enables viewers to see depth by showing horizontally shifted images to their left and right eye. This horizontal shift of the images with respect to one another is noted as disparity. When the brain fuses the left-eye and right-eye images into a single image, the amount of disparity creates different depth perception where the greater the disparity is the closer the object appears to be to the viewer. Since the left-eye and right-eye images are different, the complete separation of the left-eye and right-eye images in stereoscopic displays is the most critical condition for depth to be perceived properly. If the left eye sees the left-eye image as well as some portion of the right-eye image, and vice versa, then this result is crosstalk and produces undesirable 3D artifacts. With crosstalk, objects become blurry and double-edged which hinders the fusion of the left-eye and right-eye images and significantly degrades depth perception. In addition, watching stereoscopic displays with crosstalk for a long time causes increased eye pressure and even nausea in the viewer.

In this work, we focus on two types of stereoscopic displays: active 3D LCD

with shutter glasses and circularly-polarized 3D LCD with passive glasses which are the main-stream 3D displays in the consumers' market. Initially, we built the display model from the optical characteristics. For active 3D LCD, the model captures the temporal response of liquid crystal. For passive 3D LCD, the model is based on the polarization of light. Afterwards, we compare the simulation of the model with real displays to verify the accuracy of the modeling. Next, we analyze the temporal change of crosstalk in active 3D LCDs and the spatial change of crosstalk in passive 3D LCDs. Then, the proposed modeling includes the polarizing system and vertical misalignment in the LCD panel. In addition, we analyze how crosstalk changes with the image content including image contrast, texture, and at different viewing angles and head posts. Furthermore, we proposed effective crosstalk reduction methods that reduces crosstalk while preserving the image quality. Lastly, we conducted experimental study to find the relationship between motion and crosstalk visibility.

Chapter 1

Introduction

1.1 Introduction

Media with 3D content such as 3D movies and 3D gamings have found an increasing popularity in the market. Stereoscopic displays utilize the horizontal parallax between the left-eye (LE) and right-eye (RE) images, which is defined as disparity. As the object moves towards the viewer, disparity increases. Objects with different disparities in the stereo images create the sense of depth. The most critical factor in a 3D stereoscopic display is to separate the LE and RE view, such that the left eye only sees the LE view and vice versa.

The stereoscopic display technologies that can be found in the market include anaglyph, head-mounted display, active 3D LCD with shutter glasses, linearly-polarized passive 3D LCD with passive glasses, circularly-polarized LCD (CP LCD) with passive glasses, lenticular-lens autostereoscopic LCD and parallax-barrier LCD. Among these technologies, the most widely used are active 3D LCD with shutter glasses and circularly-polarized LCD with passive glasses.

1.2 Motivation

To observe depth, the left eye is supposed to be shown the left-eye (LE) images only, and the right eye should be shown right-eye (RE) images only. However, if the LE image contains some portion of the RE image and vice versa, crosstalk occurs. Crosstalk is one of the most disturbing factors in stereoscopic displays [Woo12].

Within a low level of crosstalk ($< 0.8\%$ in [LWH11]), the human visual system (HVS) is still able to fuse the LE and RE images to perceive depth. Thus, low level crosstalk is rather a type of "3D noise" [BPJ+11] appearing as faint shadows from the other view. An increasing level of crosstalk hinders the HVS's ability to search for the correct correspondences between the LE and RE images [Pat07]. In this case, stereo images are not fused by the HSV [YS90], and objects appear to be double-contoured. Fusing the stereo images into 3D is already a challenging task for HVS [HR12]: consider the conflict between the plane of focus and the plane of convergence of the eyes. Crosstalk makes fusing even harder, degrades depth resolution significantly [SMI05], [CCCH09], [TWA11], and increases eye strain and nausea [SMI05].

The source of crosstalk is mainly the display. Some of the commonly used stereoscopic display technologies include anaglyph displays, head-mounted displays, active-shutter displays, polarized displays and autosterescopic displays. Among these technologies, the currently most widely used are active 3D LCD with shutter glasses and CP LCDs with passive glasses. However significant crosstalk is observed in both types. Therefore, it is desirable to find out the reason why crosstalk exists in active and passive 3D LCDs and also to propose image-processing-based crosstalk reduction methods.

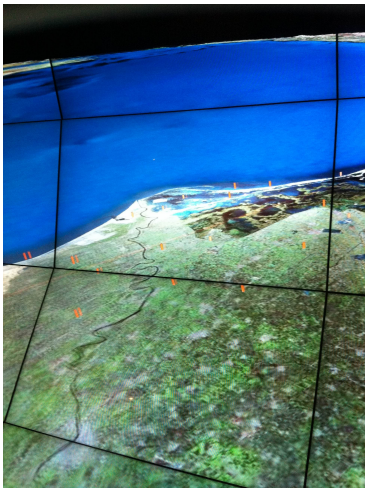

(a) Immersive 3D made of multiple CP LCDs.

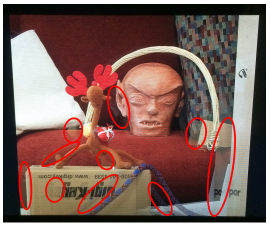

(b) Left-eye view.

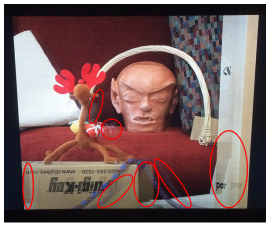

(c) Right-eye view.

Figure 1.1: Crosstalk in CP LCD dependent on the vertical viewing location. (a) Crosstalk in an immersive 3D display formed by the CP LCD grid. (b) and (c) Crosstalk in a single CP LCD.

1.3 3D crosstalk

If, in the display, the LE image contains some portion of the RE image and vice versa, crosstalk occurs. Crosstalk is the percentage of the RE images perceived by the left eye and the percentage of the LE images perceived by the right eye. The qualitative as well as mathematical definitions of crosstalk are summarized in [Woo12]. We adopt Eq. (1.1) [WH10] as the definition of crosstalk, where *leakage* is the intensity of the undesired image, and *signal* is the intensity of the desired image.

$$crosstalk(\%) = \frac{leakage}{signal} \times 100 \tag{1.1}$$

Crosstalk appearance includes ghosting or double-edged objects. Fig. 1.1 shows examples of crosstalk in CP LCD. In Fig. 1.1 (a), a 3D immersive display, which is formed by multiple CP LCDs, shows the doublings of the orange dots, and the black line especially at the bottom screens. In Fig. 1.1 (b) and (c), which are respectively the left-eye (LE) and right-eye (RE) views of a single CP LCD, we can observe severe crosstalk, which is highlighted by the red ellipses.

Crosstalk is the most detrimental factor in stereoscopic view [Woo12]. As stated previously, fusing the stereo images into 3D is already a challenging task for HVS [HR12] because of the conflict between the plane of focus and the plane of convergence of the eyes. Crosstalk makes fusing even harder, degrades depth resolution significantly [SMI05], [CCCH09], [TWA11], and increases eye strain and nausea [SMI05]. Crosstalk depends on both the stereoscopic displays and the human visual system (HSV). In this paper, we only consider crosstalk caused by the device.

The comparatively complete list of the causes of crosstalk in CP LCD is presented in [Woo12] and [YUT08]. These causes can be summarized as fabrication defects, including inaccuracy in PR alignment, limitations in the polarizing system, including angle dependency and wave-length dependency of PR and passive glasses [LL12], [HHS10], [HWZ+05], [LL10], [ZN14], and the vertical misalignment of light between liquid crystal and PR [ZN14], [ZN13], which takes place if the viewer deviates from the screen center.

1.4 Contribution

The contributions of this thesis are as follows:

1. We propose an accurate model of active 3D LCD that captures the temporal characteristics. The major cause of crosstalk in active 3D LCD is found by testing combinations of ideal/real LCD and ideal/real shutter glasses.

2. In the modeling of the polarizing system of CP LCD, the coordinate transformation from the LCD to the passive glasses is computed such that the resulted simulation no longer has erroneous color bleeding as in previous related works.

3. For the modeling of vertical misalignment in CP LCD, we propose a novel calibration method that only requires observation of the display at four viewing locations. Furthermore, we prove mathematically that VM-based crosstalk can not be efficiently reduced through the polarizing system. In addition, from the display calibration, we

present an analytic solution of the VM-free viewing zone of CP LCD and also a solution for maximizing the VM-free viewing zone in the case of multiple screens.

4. For crosstalk reduction, we propose a linear-programming problem that maximizes the dynamic range of the output image. We also show that areas in the image with high texture conceal the visibility of crosstalk. Thus, we propose neglecting the textured regions in the input images to further improve the image contrast of the output images.

5. We demonstrate through a rigorous subjective test that as the speed goes beyond certain threshold, motion blur becomes more dominant than crosstalk thus concealing the crosstalk visibility. Furthermore, we quantify the range of crosstalk and moving speed where crosstalk is visually distinguishable and indistinguishable.

1.5 Organization

The thesis is organized as follows:

Chapter 2 discusses the modeling of active 3D LCD with shutter glasses where the rising and falling responses of liquid crystal in both LCD and shutter glasses are considered. The model is verified by tested results. A crosstalk reduction method is proposed.

Chapter 3 focuses on the modeling of the polarizing system in CP LCD using Mueller calculus. The results of the modeling when the viewer is in an upright pose and in a head-tilted pose are shown. In addition, an efficient crosstalk reduction method is proposed.

Chapter 4 models crosstalk caused by vertical misalignment in CP LCD by a novel display calibration method. The VM-free viewing zone is analytically calculated.

Chapter 5 finds the relationship between crosstalk visibility and motion by subjective test.

Chapter 6 concludes this work and proposes future work.

Chapter 2

Crosstalk Modeling, Analysis and Simulation in stereoscopic LCDs using Active Shutter Glasses

Improvements in the quality of Liquid Crystal Displays (LCD) triggers a significant surge in the 3DTV market. A large segment of the 3DTV market has adopted active shutter glasses (active 3DTV). In this system, crosstalk is an important factor that affects the viewing quality of active 3DTV.

In active displays (or frame-sequential, time-sequential displays), only the left view or the right view is displayed by the monitor at a given instant time, and then switched to another view in the next time period. In combination with liquid crystal shutter glasses (LCS), an image is displayed to one eye only while the other eye is blocked. Thus the left eye sees the left view only and vice versa for the right eye. The system is called active because the glasses are actively controlling which view is displayed by turning on and off the liquid crystal.

Ideal isolation of the left and right views requires perfect temporal separation of the left and right channels of the monitor, perfect opening and closing of the glasses, as well as perfect synchronization between monitor and glasses. Liquid crystal (LC) is used in both LCD and LCS. Because of the hold type behavior in the LC, it takes

a finite amount of time for the LCD to change from one gray level to another, and for the LCS to go from transparent to fully opaque. Those transient states of LCDs and LCSs together contribute to crosstalk. In this work, we focus on the evaluation of crosstalk, simulating and analyzing how the LCD and the LCS contribute to crosstalk respectively, and we present the major components of crosstalk.

2.1 Mathematical Model of Crosstalk in Active 3D LCDs

$$C_L(x,y,t) = \frac{I(x,y,t) - I_L(x,y)}{I_R(x,y) - I_L(x,y)} \cdot g_L(t) \tag{2.1}$$

$$C_R(x,y,t) = \frac{I(x,y,t) - I_R(x,y)}{I_L(x,y) - I_R(x,y)} \cdot g_R(t) \tag{2.2}$$

The mathematical model of crosstalk is given by Eq. (2.1) and (2.2), where crosstalk is a function of space and time under the condition that $I_L(x,y) \neq I_R(x,y)$. $I(x,y,t)$ is LCD intensity at location (x,y), and it considers LC temporal features by being defined as a function of time t. and are the ideal intensities at the LCD for the left and right views at location (x,y) respectively. $g_L(t)$ and $g_L(t)$ are the time-dependent transmittances of the left and right glasses (LCS) respectively, and they change from 0 to 1. Eq. (2.1) and (2.2) model system crosstalk [LLT$^+$09] depending only on the display but not content (including contrast and HVS).

In Eq. (2.1) and (2.2), the first quantity in the fraction denotes crosstalk caused by LCD. Due to the response time of LC, the real intensity at the LCD should be between and (assuming no overdrive is used). Thus this leakage could be positive or negative. For example, if I_L is greater than I_R, I_L should also be greater than I, then the leakage $I(x,y,t) - I_L(x,y))$ in Eq. (2.1) for the left view is negative. Negative leakage results in a darkened image in the left view, and the darkened region in the left view brings about unwanted shadow from the right view. Similarly for the right

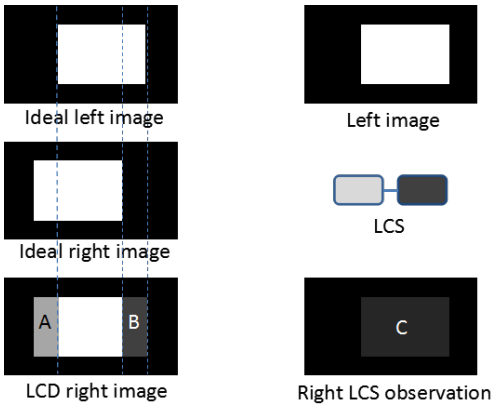

Figure 2.1: Crosstalk in active-glasses stereo display. Left column: LCD-based crosstalk; Right column : LCS-based crosstalk)

view, if the leakage $I(x, y, t) - I_R(x, y))$ in (2.2) is positive indicating a brightened glow from the left view. Thus the first quantities in Eq. (2.1) and (2.2) are LCD-based crosstalk and they could be either dark crosstalk or bright crosstalk.

The right quantity, or transmittance of LCS in Eq. (2.1) and (2.2) explain the fraction of crosstalk brought about by the LCS. Suppose that the LCD is displaying a left image, and I equals to I_L at time t at location (x, y), then the left crosstalk $C_L(x, y, t)$ is zero in Eq. (2.1). However, the left fraction is 1 in Eq. (2.2), and the larger g_R is the larger C_R will be. Only when g_R is 0, C_R becomes 0. This makes sense because in this example, when the LCD is showing a left image, the right LCS should be opaque. Thus the second quantity in Eq. (2.1) and (2.2) characterize LCS-based crosstalk.

In Fig. 2.1, the left column shows LCD-based crosstalk. The 3D content in Fig. 2.1 is a white box in black background. In the left column, the top frame is the left image and the middle frame is the right image, and the horizontal shift of the white box between the left and right image is due to disparity. The real display of the left image on the LCD is illustrated by the bottom left graph in Fig. 2.1, where region A is not completely white, and region B is not completely black due to the incorrect intensity in the LCD in A and B. A and B show contours in the right LCD view that belongs to the left image (top left in Fig. 2.1). Consequently, complete

isolation of the left and right channels on the LCD does not occur.

Region A is dark crosstalk that is caused by lower intensity at the same location in the previous frame (or the other view). Similarly, region B is the bright crosstalk caused by higher intensity.

In the right column in Fig. 2.1), the top image is the ideal left view and, the glasses in the middle are open on the left and closed on the right. Due to incomplete shuttering of the right lens, a darkened left image (region C) is observed in the right view. This type of crosstalk is LCS-based.

2.2 Crosstalk Analysis in Active 3D LCDs

2.2.1 Temporal Response of Liquid Crystal

Since liquid crystal (LC) response is one of the critical characteristics in LCD stereo displays, we need a mathematical model for LC. From [WWZW04], the intensity of rising edge and falling edge of LC are given by Eq. (2.3) and (2.4) respectively. Note the intensities in these equations are normalized intensities ranging from 0 to 1.

$$I_R(t) = \sin^2\left(\frac{1}{2}\cdot\frac{\delta_0}{1+(\frac{\phi_\infty^2}{\phi_0^2-1})\exp(-\frac{2t}{\tau_r})}\right) \tag{2.3}$$

$$I_F(t) = \sin^2\left(\frac{\delta_0}{2}\cdot\exp(-\frac{2t}{\tau_f})\right) \tag{2.4}$$

For the LCD, we set $\delta_0 = \pi$, $\phi_\infty = 80^{\text{deg}}$, $\phi_\infty = 10^{\text{deg}}$. In Eq. (2.3) and (2.4), as time goes to infinity, I_R becomes 1, and I_F becomes 0, so that I_R characterizes the black to white response, and I_F characterizes the white to black response. How fast the intensity can change is characterized by τ_r and τ_f. In order to determine the values of τ_r and τ_f, we need to refer to the response time provided in specification lists from LCD manufacturers. The LC response time is the time for the LC optical transmittance to change from 90% to 10%. For analysis, we set rise response time

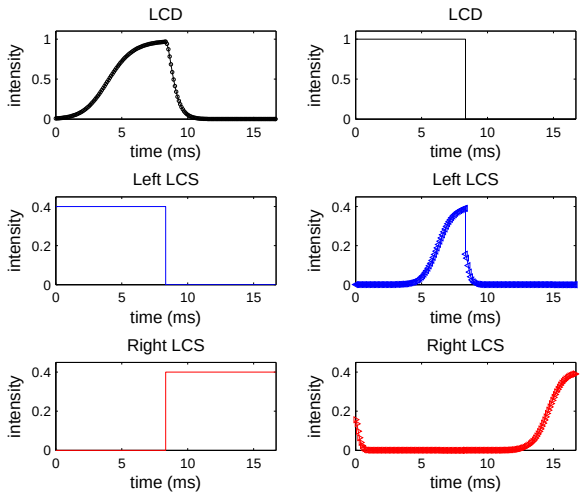

Figure 2.2: LCD response and LCS response. Left column: real LCD with ideal LCS; right column: ideal LCD with real LCS

$T_{rise} = 3.8ms$, fall response $T_{fall} = 1.2ms$. Eq. (2.3) and (2.4) yield $\tau_r = 2.8ms$, and $\tau_f = 1.8ms$.

For LCS, $g_L(t)$ has the same form as for LCD where $\delta_0 = \pi$, $\phi_\infty = 85^{\text{deg}}$ and $\phi_0 = 5^{\text{deg}}$, LC rise time $T_{rise} = 2.5ms$, fall response time $T_{fall} = 0.5ms$, and consequently $\tau_r = 3.4ms$, and $\tau_f = 0.34ms$. In addition, we need to multiply the transmittance constant $t_g = 40\%$ in the LC equation. The settings of these parameters for the LCD and LCS are for the purpose of simulating real LCD and LCS responses in 120Hz active 3DTVs. One example of this is given in [BTB+11], where measured 120Hz LCD and LCS responses are provided.

Simulation of Ideal LCD or Ideal LCS

In Fig. 2.2, when the LCD intensity is rising, the left LCS opens and the right LCS closes. Also, when the LCD intensity is falling, the left LCS closes and the right LCS opens. The right LCS has an $8.3ms$ shift compared with the left LCS. The left column of Fig. 2.3 shows the simulation results of the left and right observations and crosstalk when ideal LCS is assumed. In this column, zero crosstalk is observed during both $8.3ms - 16.6ms$ (closing of the left LCS) in the second plot and during

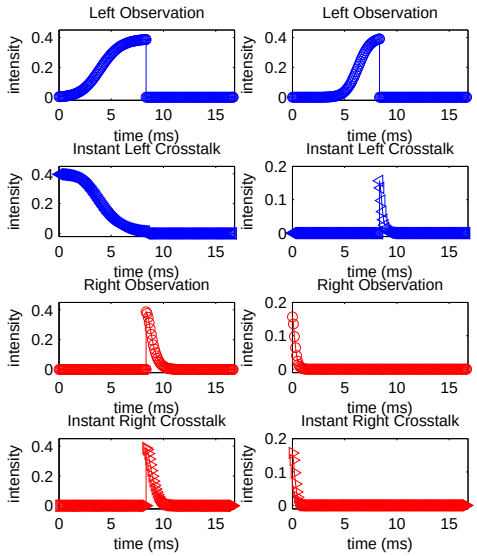

Figure 2.3: Simulation of observation and crosstalk. Left: real LCD with ideal LCS, right: ideal LCD with real LCS

$0ms - 8.3ms$ (closing of the right LCS) in the fourth plot. Because when the glass is fully closed, no residual in LCD from the previous frame (the other view) can be seen. In both $0ms - 8.3m$ duration in the second plot and $8.3ms - 16.6ms$ duration in the fourth plot crosstalk occurs due to the transient state of LCD. Here, because the LCS is ideal, this crosstalk is LCD-based, and its due to the transient state of LCD. In the second plot for the left view, the crosstalk is dark crosstalk, and in the fourth plot for the right view, the crosstalk is bright crosstalk.

In the right column of Fig. 2.3 where ideal LCD is assumed, no crosstalk is observed during $0ms - 8.3ms$ (opening of the left LCS) in the second plot and during $8.3 - 16.6ms$ (opening of the right LCS) in the fourth plot. Its due to the ideal LCD. Crosstalk happens during the closing of the LCS for both views and its because the LCS isnt fully opaque when the LCD hasnt evolved into the next view. Thus the crosstalk here is induced by LCS. Crosstalk in the second right plot (left view) is dark crosstalk, and is bright crosstalk in fourth right plot (the right view).

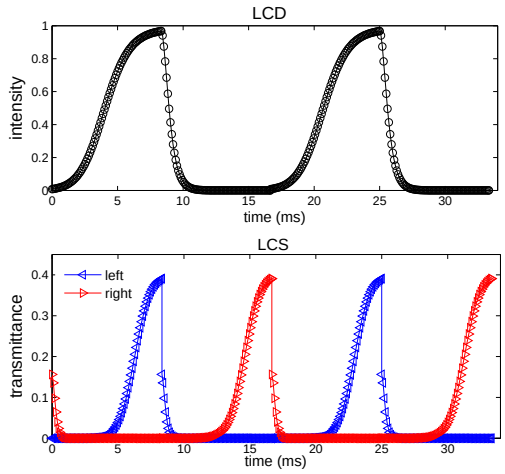

Figure 2.4: Simulation of LCD Response and LCS Response

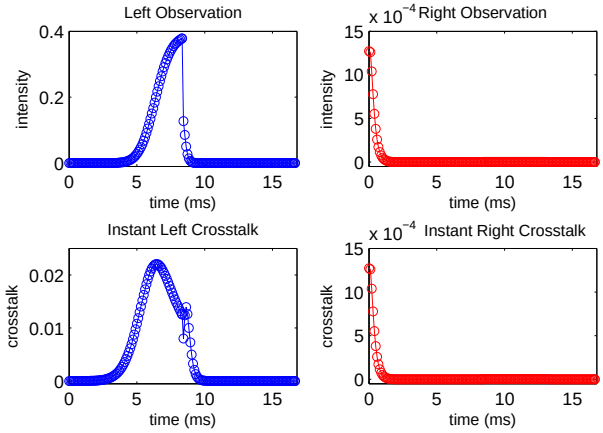

Figure 2.5: Simulation of observation after glasses and crosstalk.

2.2.2 Simulation of Real LCD with Real LCS

The simulation of real 120Hz LCD and real LCS responses are shown in Fig. 2.4, which is quite similar to the measured results given in [BTB+11]. As shown by Fig. 2.4, both the LCD and the LCS have faster fall response than rise response; the LCD has slower response than the LCS; The LCS does not start to open until the LCD has already changed its intensity quite close to the ideal.

$$\bar{C}_{time}(x,y) = \frac{1}{2/f}\int_0^{2/f} C_L(x,y,t) + C_R(x,y,t)dt \tag{2.5}$$

In the second row in Fig. 2.5, how crosstalk of the left and right view changes with time is shown. Averaging the simulated crosstalk in time domain Eq. (2.5), the

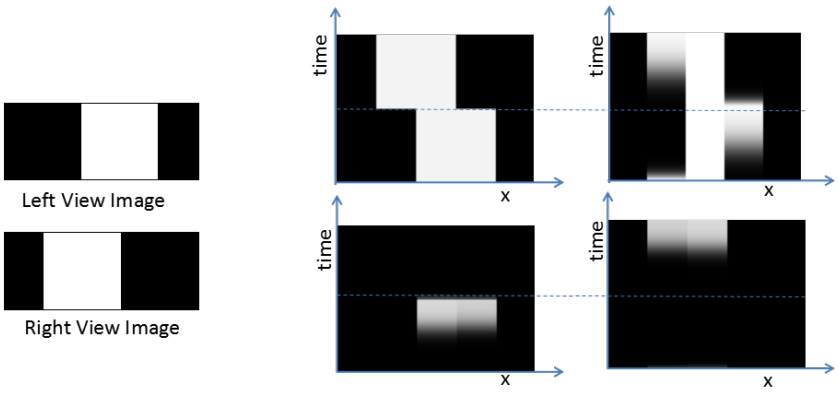

Figure 2.6: Ideal stereo images and space-time plots of simulation results. Left column: top graph is left view input image; bottom graph is right view image. Right 4 plots: top left:ideal LCD, top right: real LCD, bottom left: left Observation, bottom right: right observation.

sum of crosstalk for the left and the right views is 0.4% which is close to the results of 120Hz Samsung-3DTV in [BTB+11] when the tested gray level changes between 0 and 255 (black and white). Thus using our method of crosstalk analysis, the temporal characteristics of 3D crosstalk in active 3DTV can be simulated, and the level of temporally averaged crosstalk can be estimated given specifications including LCD refresh rate, LCD response time and LCS response time. Fig. 2.6 presents space-time plots describing our analysis, for the 3D content shown on the left of Fig. 2.6, here at a given point in time, every horizontal line on the screen is identical (top-to-bottom frame update is ignored). In the left 4 plots in Fig. 2.6, the top right plot shows simulated LCD. We can observe transient states from black to white and from white-to-black in the LCD instead of instant change between black and white shown in ideal LCD (top left) as time evolves. The black to white transition produces dark crosstalk, and the white-to-black transient state produces bright crosstalk. Also, we can see that the black to white response is slower than the white-to-black transition.

In the left 4 plots in Fig. 2.6, the bottom two plots show the observed left view and right view after light passes through the glasses. These two plots indicate two usages of the glasses. First, the glasses achieve temporal separation of the left and

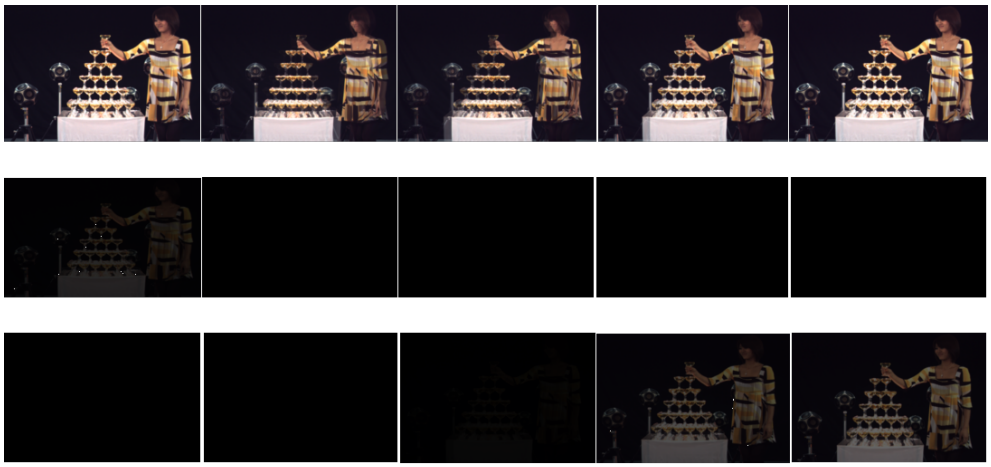

Figure 2.7: Simulation of 120Hz LCD and the LCS. First row: LCD, second row: left LCS, third row: right LCS.

right views, as we can see the bright bar appearing and vanishing in synchronization with the LCD. Second, the timing of LCSs opening with regard to the LCD reduces LCD-based dark crosstalk: the LCS doesnt open until the LCD has changed its intensity quite close to the ideal. However, we can also see that they come at the price of flickering (for view separation) and lowered brightness. Fig. 2.7 presents simulation of 3D video display on LCD and through LCS. From the left to the right, the LCD starts from the left image and is displaying the right image; the left LCS closes and the right LCS opens. We can easily observe bright and dark crosstalk in LCD, and opening and closing of LCS.

To briefly sum up here: when LCS opens, crosstalk is LCD-based and it is induced by the residual of previous frame in LCD; when LCS closes, crosstalk is LCS-based and it is caused by incomplete light blocking of LCS.

2.2.3 Crosstalk Reduction in Active Shutter 3D LCDs

In this section, how crosstalk changes with the parameters of both the LCD and LCS is analyzed first, and an efficient method for crosstalk reduction is discussed accordingly. We measure the change in crosstalk by comparing temporally averaged crosstalk instead of instant crosstalk. Temporally averaged crosstalk is defined by

Figure 2.8: Space-time plots when better LCD rise response is assumed. Left: LCD display, middle: left LCS display, right: right LCS display.

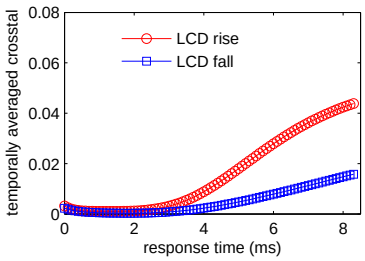

(a) Temporal change of crosstalk with LCD.

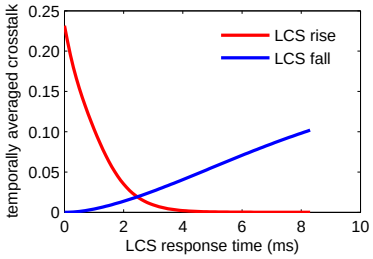

(b) Temporal change of crosstalk with LCS.

Figure 2.9: Temporally averaged crosstalk when rise response and fall response are changed.

Eq. (2.5), where is the LCD refresh frequency and, is a complete LCS period of opening and closing.

Shown in the left plot in Fig. 2.8, shortened LCD responses (fall and rise) alleviate crosstalk. However, further reducing LCD response (less than around $1ms$) would slightly increase crosstalk due to imperfect LCS. In the right plot of Fig. 2.9, a faster LCS fall response always reduces the magnitude of crosstalk, while a faster LCS rise response aggravates crosstalk due to slow LCD rise response. Fig. 2.9 shows that changing the rise response time of the LCD to around $1ms$ will reduce the amount of average crosstalk the most. Fig. 2.8 gives space-time plots illustrating the effect of crosstalk reduction after setting the rise response time of the LCS to 1ms. The left plot of Fig. 2.8 shows that the black-to-white transit is faster in comparison to the top left plot in Fig. 2.7, the white bars in the middle and right plots in Fig. 2.8 show hardly visible wrong edges compared with the bottom left and right plots in Fig. 2.7.

2.3 Conclusion

In this chapter, a mathematical model to characterize crosstalk in active stereoscopic displays is proposed. The model demonstrates the ability to simulate and evaluate crosstalk in both temporal and spatial domain. Simulations of ideal LCD with real LCS, ideal LCS with real LCD and real 120Hz LCD and LCS are presented with the correspondent crosstalk analysis. The simulated results of crosstalk match the measured crosstalk. Consequently, our method can be used to estimate crosstalk given the specifications of active 3DTV. By changing parameters in active 3DTV, the results show the efficient way to reduce crosstalk in active displays is to improve the LCD rising response.

2.4 Acknowledgment

Chapter 2, in full, is a reprint of the material as it appears in Numerical Grid Generational in Image Analysis and Interpretation (SSIAI). Menglin Zeng, Truong Nguyen, 2012. The dissertation author was the primary investigator and author of this paper.

Chapter 3

Modeling, Prediction and Reduction of 3D crosstalk in Circular Polarized Stereoscopic LCDs

Crosstalk, which is the incomplete separation between the left and right views in 3D displays, induces ghosting and causes difficulty of the eyes to fuse the stereo image for depth perception. Circularly polarized (CP) liquid crystal display (LCD) is one of the main-stream consumer 3D displays with the prospering of 3D movies and gamings. The polarizing system including the patterned retarder (PR) is one of the major causes of crosstalk in CP LCD. The contributions of this paper are the modeling of the polarizing system of CP LCD and a crosstalk reduction method that efficiently cancels crosstalk and preserves image contrast. For the modeling, practical orientation of the polarized glasses (PG) is considered. In addition, this paper calculates the rotation of the light-propagation coordinate for the Stokes vector as light propagates from LCD to PG, and this calculation is missing in previous works when applying Mueller calculus. The proposed crosstalk reduction method is formulated as a linear programming problem which can be easily solved. In addition, we propose excluding

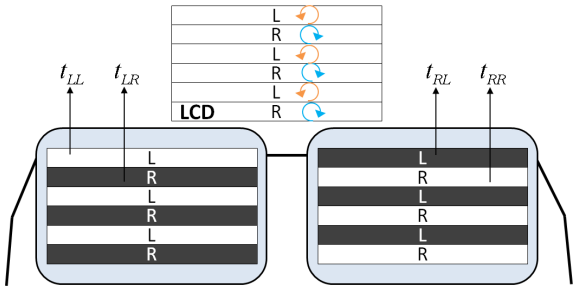

Figure 3.1: Circularly polarized LCD with passive glasses [ZN14]

the highly textured areas in the input images to further preserve image contrast in crosstalk reduction.

3.1 Introduction

3.1.1 How does CP LCD work?

Circularly polarized (CP) LCD CP, as one of the most popular type of stereoscopic displays in the consumer market, is the focus of this work. Stereoscopic displays create the sense of depth by showing the left eye and right eye with different images.

Fig. 4.1 illustrates how CP LCD separates the LE and RE views, that is, the screen allocates the odd-row pixels (LE field) display images for the left eye, and the even-row pixels (RE field) to display images for the right eye. Lights emitted from the LE field are in left-hand (LH) circular polarization, whereas the lights emitted from the RE field are in right-hand (RH) circular polarization. The LE lens of the polarized glasses transmits only LH-circularly polarized light, and the RE lens only transmits RH-circularly polarized light. Therefore, the left eye only sees the LE field of the screen, and the right eye only sees the RE field of the screen.

3.1.2 Definition of crosstalk

If the separation of the LE and the RE views is incomplete: the undesired images "blend" into the desired images, then ghosting appears as double-contoured objects known as crosstalk. Crosstalk causes difficulty for the human visual system

Figure 3.2: Crosstalk in passive-type circularly polarized LCD. Left: Immersive 3D formed by the CPLCD grid. Right: Crosstalk in the CPLCD grid.

(HVS) to find the corresponding features between the left and right images and thus hinders the fusing of the stereo images into 3D. An immersive 3D display formed by the CP LCD grid is shown in the left image of Fig. 3.2 with its crosstalk shown in the right image of Fig. 3.2. There is no standard terminology for crosstalk in stereoscopic vision. Lipton [Lip87] clarifies the difference between the "incomplete left and right channel isolation" and the "perceived doubling of the image or ghosting" because the former only depends on the display while the latter is also influenced by human vision. Huang et al. [HTLH00] use "system crosstalk" and "viewer crosstalk" to differentiate between these two concepts. In [Lip87], the perception of crosstalk is described as "ghosting". Crosstalk visibility depends on the amount of crosstalk (display-dependent) presented [PSI05], as well as image contrast and disparity [LWH11] and [LXP12], color [DKS12], and motion [SJMR14].

3.1.3 Causes of crosstalk in CP LCD

Mechanisms of crosstalk in various types of stereoscopic displays are studied by Woods [Woo12]. Yoshihara et al. [YUT08] and Boher et al. [BL11] measure and characterize crosstalk in CP LCD. In addition, optical designs of the wave retarders in CP LCD are proposed in [HW05] and [WKL12] to resolve polarization deviation and light dispersion at oblique incidence. These works address various factors causing crosstalk in CP LCD which can be categorized as:

- Manufacturing defects including the optical quality of the patterned retarder and the polarized glasses, and the mismatch between the patterned retarder

(PR) and the liquid crystal (LC) cells.

- Limitation in the polarizing system of CP LCD that induces crosstalk at oblique viewing angle. CP LCD's polarizing system includes the linear polarizer (LP), liquid crystal (LC), patterned retarder (PR) in the LCD and quarter-wave retarder (QWR) in glasses.

- The vertical misalignment (VM) of the incident light between the LC cells and the PR when the viewing location shifts vertically away from the screen center.

In this paper, the manufacturing defect is not considered. In addition, we assume that in the vertical direction, the viewing location is aligned in the vicinity of the screen center so that crosstalk induced by VM does not exist. Consequently, we investigate the impact of the polarizing system of CP LCD on crosstalk varying the horizontal viewing angle and propose the corresponding crosstalk cancellation method.

3.1.4 Related works

The modeling of the polarizing system of CP LCD can be found in [HW05] and [WKL12] where phase compensation schemes in the PR to reduce crosstalk are proposed. In [WKL12] and [LL10], the polarization of light on a single point in the LCD is analyzed at two scenarios. The first scenario is that light incidents obliquely at the LCD but normally at the glasses. The second scenario is that the LCD and the glasses are parallel so that the incident angles are the same in the LCD and glasses. However, because polarization is sensitive to the incident angle, these incidence scenarios lack accuracy considering the entire CP LCD screen (especially for big-screen displays) as well as arbitrary viewing locations. For the first scenario, the lights from the entire screen can not all be at normal incidence in the glasses. For the second scenario, when the viewer moves away from the screen center and adjusts the glasses towards the screen, the LCD and the glasses are not parallel. Therefore, it's unclear how much the polarizing system of CP LCD contributes to crosstalk in the

realistic viewing scenario. Similar issue exists in [HHS10]. In addition, the rotation of the light-propagation coordinate (LPC) when light propagates from the LCD to the glasses is neglected in previous works. We show that without this rotation, the result of modeling shows erroneous pattern of display luminance and color bleeding. In this paper, we carefully estimate the orientation of the polarized glasses relative to the LCD, derive the analytic solution of the rotation of LPC, and validate the simulation result by human observations.

Regarding crosstalk reduction, most existing works are adapted from Lipscom et al. [LW94]. The idea in [LW94] is based on luminance compensation where the amount of crosstalk luminance is subtracted in the input image. If the luminance to be subtracted is greater than the original luminance, then the black level of the image has to be increased. However, increasing the black level degrades the contrast of the image. [JKD00] and [KRL$^+$11] follow the compensation scheme in [LW94] and have the same problem of losing image contrast. Instead of compensating luminance in the target image, Smit et. al [SLF07] propose adjusting the luminance in the image for the other eye at the 3D fused point according to disparity mapping. However, the difference between the LE and RE images induced by this method causes 3D luster which even "highlights" crosstalk. Extensions of the compensation scheme in [LW94] in color images can be found in [SLF07] and [DN11] where CIE Lab and YCbCr color spaces are used respectively. They proposed to modify the luminance channel and leave chrominance unchanged to avoid color shifting. However, we demonstrate that there is residual crosstalk in the chrominance channel which leads to considerable increasing of crosstalk visibility. Sohn et al. [Hon12] propose minimizing the contrast loss induced by crosstalk reduction by changing the disparity globally by a constant (equivalent to shifting the image for one eye horizontally) so that the area where the black-level luminance needs to be increased becomes smaller. However, since the relationship between disparity and depth is nonlinear, globally shifting the disparity will distort the depth view after fusing the stereo images. In this paper, we formulate

a linear programming problem which minimizes the background increment value for crosstalk reduction. In addition, we propose excluding the highly-textured areas in crosstalk reduction which further improves image contrast without increasing the visibility of crosstalk.

3.2 Display model

In this section, CP LCD with passive glasses is modeled in 4 steps: in Section 3.2.1, the eye response to the display luminance is derived using the line spread function [LHW58]; in Section 3.2.2, the display model as the relationship between the input and the output images is proposed; in Section 3.2.3, the optical system of CP LCD is solved by Mueller Calculus [YW06] together with the proposed head posture estimation. Furthermore, in Section 3.2.4, the result of the display modeling is compared with real display. Subjective test result also verifies the accuracy of the proposed model. In addition, the case with viewer's head tilt is discussed in Section. 3.2.5.

3.2.1 Eye response to the display

As illustrated in Fig. 4.1, in CP LCD, the image for one eye is shown in every other pixel row on the screen. However, when observing at a distance, the human eyes couldn't discern the vertical discontinuity but rather perceive the "smooth" images. Therefore in the display modeling, how the human eyes "blend" the odd and the even fields together needs to be considered. This problem can be formulated as: what is the perceived luminance when the luminance in odd field is I_1 and that in the even field is I_2?

Since each row on the screen forms a self-illuminating "line", we use Line Spread Function (LSF) defined by Lamberts et al. [LHW58] which is the light distribution of "the infinitely narrow line as measured along the direction perpendicular

to the line" on the retina as the impulse response of eye. Yang et al [YWS08] prove that LSF can be well characterized by Eq. (3.1):

$$L(\theta) = \frac{1}{\pi}\frac{\Gamma}{\theta^2 + \Gamma^2} \tag{3.1}$$

which is a Lorentzian function of visual angle θ (in $arcmin$), characterized by half width at half maximum (HWHM) Γ, and is integrated to 1. Setting $3.86mm$ [RMDM04] as the mean size of human pupil under room light, and according to the measured LSFs in [CG66] for different pupil sizes, $\Gamma = 3.4arcmin$ in Eq. (3.1). The luminace of a pixel row measured vertically on the screen is:

$$r_0(\theta; I) = \begin{cases} I, & \text{if } 0 \leq \theta \leq \theta_p, \\ 0, & \text{otherwise.} \end{cases} \tag{3.2}$$

where I is the luminance input, θ_p is the vertical span of a pixel row in terms of visual angle. θ_p can be calculated from:

$$\theta_p = \arctan\left(h_p/D_v\right)/\pi \cdot 60(arcmin) \tag{3.3}$$

where h_p is the pixel height, and D_v is the viewing distance. In this paper, we refer to LG 47LH55 ($1080p$) [Cor09] for our calculation, with the displaying area $58.5cm \times 104.0cm$ (h×w) in dimension. With $h_p = 58.5cm/1080 \approx 542\mu m$, the response of the human eye to a pixel row can be calculated by convolution of Eq. (3.1) and (3.2):

$$r_{eye}(\theta; I) = r_0(\theta; I) \otimes L(\theta) \tag{3.4}$$

To validate Eq. (3.4), we integrate it over θ as

$$\begin{aligned} \int_{-\infty}^{+\infty} r_{eye}(\theta; I)\mathrm{d}\theta &= \int_{-\infty}^{+\infty} r_0(\theta; I) \otimes L(\theta)\mathrm{d}\theta \\ &= \int_{-\infty}^{+\infty} r_0(\theta; I)\mathrm{d}\theta \cdot \int_{-\infty}^{+\infty} L(\theta)\mathrm{d}\theta \\ &= \theta_p \cdot I \end{aligned} \tag{3.5}$$

where the result $\theta_p \cdot I$ is the total energy of a pixel row on the retina measured vertically. Assume that the luminance input in the left-eye field is I_L, then the response to the left-eye-field (in the vertical direction) can be written as:

$$f_{\mathrm{L}}(\theta; I_L) = r(\theta; I_L) \otimes \sum_{k=-N}^{k=N} \delta(\theta - 2k\theta_p) \tag{3.6}$$

The period of the sampling function in Eq. (3.6) is $2\theta_p$, which is the vertical span of two pixel rows. N in Eq. (3.6) determines the number of rows, and we assume $N \to \infty$ within the smooth image region. Assuming the luminance input for the right-eye field is I_R, then the response to the screen becomes:

$$f(\theta; I_L, I_R) = f_{\mathrm{L}}(\theta; I_L) + f_{\mathrm{L}}(\theta - \theta_p; I_R) \tag{3.7}$$

where the second term is the right-eye-field response obtained by shifting the left-eye-field response by θ_p. Taking the magnitude response of Eq. (3.7) yields:

$$\begin{aligned} |\mathscr{F}(\omega; I_L, I_R)| = \frac{1}{2}\sqrt{I_L^2 + I_R^2 + 2I_L I_R \cos(2\pi\theta_p \cdot \omega)} \\ \cdot |\mathrm{sinc}(\theta_p \cdot \omega)| \cdot e^{-2\pi\Gamma|\omega|} \cdot \sum_{k=-N}^{k=N} \delta\left(\omega - \frac{k}{2\theta_p}\right) \end{aligned} \tag{3.8}$$

where ω is the visual-angle frequency in *cycles/arcmin*. Notice that Eq. (3.8) is discrete: the sampling term in Eq. (3.8) with the interval of $\frac{1}{2\theta_p}$, due to the periodic luminance as shown in Eq. (3.7). The maximum value of Eq. (3.8) is at $\omega = 0$ where the corresponding luminance (or the inverse Fourier transform) is $\frac{1}{2}(I_L + I_R)$, which indicates the visual averaging between the left-eye and the right-eye fields. In fact, the convolution with LSF in Eq. (3.4), which is low-pass, causes Eq. (3.8) to be low-frequency concentrated as expressed by the term $e^{-2\pi\Gamma|\omega|}$ in Eq. (3.8). By setting $I_L = 1$ and $I_R = 0$, Fig. 3.3 shows the magnitude response of the screen as the blue curve (Eq. (3.8) without the sampling term) multiplied with the red impulses (sampling term in Eq. (3.8)). When the viewing distance shown in Fig. 3.3 changes from $0.1m$ to $1.5m$, even though the blue curve becomes smoother and decays slower (because θ_p decreases, as implied in Eq. (3.3)), the interval of the red sampling increases

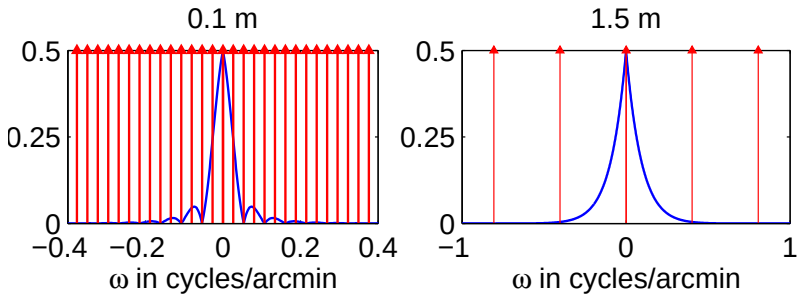

Figure 3.3: Magnitude response of the screen on retina when the luminance for the left-eye and the right-eye fields are 1 and 0 respectively. Left: viewing distance is $0.1m$. Right: viewing distance is $1.5m$.

which yields much less energy in the non-DC components for viewing distance $1.5m$. Henceforth, the DC luminance becomes more dominant when the viewing distance increases. Nevertheless, it's desirable to quantify the viewing distance beyond which the vertical discontinuity of the screen is negligible. From Eq. (3.8) and Fig. 3.3, we know the first non-DC component of the screen magnitude response is at $\omega = \frac{1}{2\theta_p}$ which corresponds to the luminance component that changes from row to row. After plugging $\omega = \frac{1}{2\theta_p}$ into Eq. (3.8) and taking the inverse Fourier transform, we derive the luminance amplitude of the first non-DC component as:

$$\frac{1}{2}|I_L - I_R| \cdot \mathrm{sinc}(0.5) \cdot e^{-\frac{\pi\Gamma}{\theta_p}} . \tag{3.9}$$

By forcing Eq. (3.9)≤ 0.01 (still assuming $I_L = 1$, $I_R = 0$), we arrive at $\theta_p \leq 1.5434$ $arcmin$. From Eq. (3.3), we conclude that $D_v \geq 0.60m$. Hence for model LG 47LH55, when the viewer stands farther than $0.60m$ away from the screen, the row pattern of the screen is invisible, and the perceived luminance is simply the average between the left-eye and the right-eye fields. Fig. 3.4 shows a CP LCD [Cor09] observed at the distance of $1.0m$ (without passive glasses), where the top-row squares are lit up in the left-eye field only while the bottom-row squares are evenly lit up in the two eye fields. The input grayscale level is 255 (luminance 1) for the top-row squares in the R, G, B and gray from left to right respectively whereas the input grayscale level is 186 (luminance 0.5 assuming the display gamma is 2.2) for the corresponding bottom-row

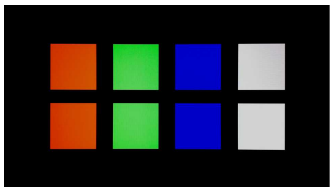

Figure 3.4: Demonstration of the luminance averaging between the left-eye and the right-eye fields of the screen. See text for the details.

squares. Fig. 3.4 suggests that the colors in the top-row squares match those in the bottom-row squares which verifies our conclusion that the perceived luminance when the viewing distance is greater than $0.60m$ is the luminance averaged between the two eye fields.

3.2.2 Relationship of the input and output of the display

We improve the display model proposed in [ZN13] in two aspects. Firstly, we change the optical modeling method in [ZN13] from Jones matrix into Mueller calculus. Compared to Jones matrix which characterizes coherent light, Mueller Calculus is able to characterized incoherent light which is the case for CP LCD. In addition, [ZN13] does not consider the realistic viewing condition. We model the relationship of the input and output of CP LCD in terms of luminance as [ZN13]:

$$\begin{bmatrix} L_o(i,j) \\ R_o(i,j) \end{bmatrix} = \begin{bmatrix} t_{LL} & t_{LR} \\ t_{RL} & t_{RR} \end{bmatrix} \begin{bmatrix} L_{in}(i) \\ R_{in}(j) \end{bmatrix} \tag{3.10}$$

where $L_{in}(i)$ and $R_{in}(j)$ are the luminance input in the LE and RE images respectively, $L_o(i,j)$ and $R_o(i,j)$ are the luminance output in the LE and RE views respectively, i and j denote the grayscale levels input in the LE and RE input images respectively. The 2x2 matrix in Eq. (4.2) is defined as the display transmission matrix (TM) whose entries (shown in Fig. 4.1) are t_{LL}, transmittance of the LE pixel after LE lens, t_{LR}, transmittance of the RE pixel after LE lens (t_{RL} and t_{RR} are similarly defined). Transmittance is the percentage of pixel luminance transmitted after the glasses which ranges from 0 to 1. Eq. (4.2) implies that crosstalk occurs if TM has

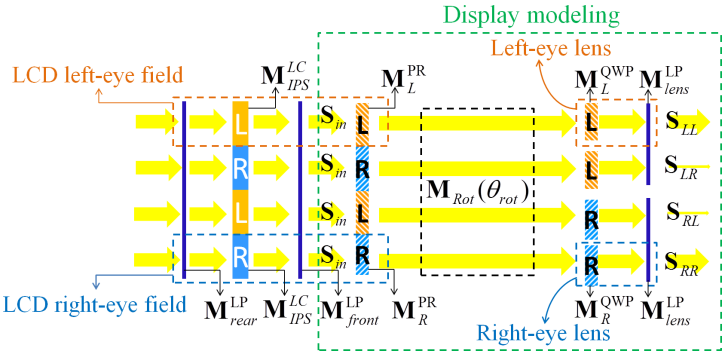

(a) Mueller calculus representation of the polarizing system.

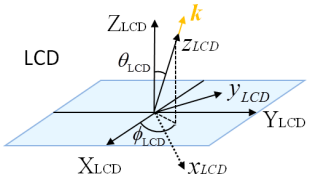

(b) Light coordinate in the LCD.

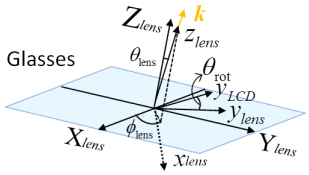

(c) Light coordinate in the glasses.

Figure 3.5: The polarizing system of circularly polarized LCD with polarized glasses.

non-zero off-diagonal entries. Then we define crosstalk in the left and right views as:

$$crosstalk_L(\%) = \frac{t_{LR}}{t_{LL}} \times 100 \tag{3.11}$$

$$crosstalk_R(\%) = \frac{t_{RL}}{t_{RR}} \times 100 \tag{3.12}$$

3.2.3 Modeling the polarizing system by Mueller calculus

There are many optical modeling methods for polarization, including Extended Jones matrix [Lie97], Barreman 4x4 method [Ber72], and Mueller Calculus (MC) [YW06]. We use Mueller calculus because it models incoherent light (true to CP LCD) and the calculation is intuitive. In Mueller calculus (MC), the polarizing state of the light is characterized by the 4x1 Stokes vector (SV) denoted as $\mathbf{S} = [S_0, S_1, S_2, S_3]^T$ [YW06], where S_0 is the intensity of light (normalized luminance in our case). The polarizing modules such as LP and WR are represented by the 4x4 Mueller matrix denoted as $\mathbf{M}$. As light propagates in CP LCD, the SV is left multiplied by the $\mathbf{M}$s of the polarizing modules along the light path.

Fig. 3.5(a) shows the 4 possible light paths in CP LCD's polarizing system where the polarizing modules are labeled with the corresponding MC notations. The orange and blue dashed boxes on the left-hand side of Fig. 3.5(a) show the left-eye-field

and the right-eye-field LCD respectively. The LCD panel comprises rear LP denoted as $\mathbf{M}_{rear}^{LP}$, LC of In-Plane-Switching (IPS) configuration [YW06] $\mathbf{M}_{IPS}^{LC}$, front LP $\mathbf{M}_{front}^{LP}$ and patterned retarder (PR) of LE field $\mathbf{M}_{L}^{PR}$ and PR of RE field $\mathbf{M}_{R}^{PR}$. The slow axis [YW06] of the left-eye-field PR and that of the right-eye-field PR are orthogonal. The orange and blue dashed boxes on the right-hand side of Fig. 3.5(a) highlight the LE and RE lenses of the polarized glasses respectively. The LE lens includes the LE quarter-wave plate (QWP) denoted as $\mathbf{M}_{L}^{QWP}$, and lens LP $\mathbf{M}_{lens}^{LP}$. Similarly, the QWP in the RE lens has the MC notation $\mathbf{M}_{R}^{QWP}$, and the MC notation of the LP in the lens is $\mathbf{M}_{lens}^{LP}$. The slow axes of the LE and RE QWPs are also orthogonal. $\mathbf{M}_{Rot}(\theta_{rot})$ is the MC notation of the LPC rotation from the LCD to the glasses. On the right-hand side of Fig. 3.5(a), $\mathbf{S}_{LL}$ denotes the output SV from the LE LCD field after the LE lens, $\mathbf{S}_{LR}$ denotes the output SV from the RE LCD field after the LE lens (and similarly are $\mathbf{S}_{RL}$ and $\mathbf{S}_{RR}$ defined). The rear LP, LC and the front LP form the conventional LCD without 3D function. In the following model, we assume the light emitted from the front LP is perfectly linear (the same as assuming the part of CP LCD that is equivalent to conventional LCD is ideal), which is $\mathbf{S}_{in} = [1, 1, 0, 0]$.

Fig. 3.5(b) shows axes of LCD coordinate where Z_{LCD} is the LCD normal, X_{LCD} and Y_{LCD} are the horizontal and vertical axes of LCD respectively. Fig. 3.5(c) shows axes of glasses coordinate where Z_{lens} is the surface normal of the lens, X_{lens} and Y_{lens} are the horizontal and vertical axes of the glasses respectively. The axes of light-propagation cooridnate are formed as follows: z axis is the same as the light propagation direction denoted by $\mathbf{k}$, x axis is on the incident plane, and y axis lies on the surface. Axes of the light-propagation coordinate (LPC) in the LCD frame are denoted by x_{LCD}, y_{LCD} and z_{LCD}, and those in the glasses frame are denoted by x_{lens}, y_{lens} and z_{lens}. z_{LCD} and z_{lens} are in the same direction.

Consequently, the Mueller calculus formula of the 4 light paths in Fig. 3.5 is:

$$\begin{pmatrix} \mathbf{S}_{LL} \\ \mathbf{S}_{LR} \\ \mathbf{S}_{RL} \\ \mathbf{S}_{RR} \end{pmatrix} = \mathbf{M}_{lens}^{LP} \cdot \begin{pmatrix} \mathbf{M}_{L}^{QWR} \\ \mathbf{M}_{L}^{QWR} \\ \mathbf{M}_{R}^{QWR} \\ \mathbf{M}_{R}^{QWR} \end{pmatrix} \cdot \mathbf{M}_{Rot}(\theta_{rot}) \begin{pmatrix} \mathbf{M}_{L}^{PR} \\ \mathbf{M}_{R}^{PR} \\ \mathbf{M}_{L}^{PR} \\ \mathbf{M}_{R}^{PR} \end{pmatrix} \mathbf{S}_{in} \tag{3.13}$$

where S_{LL} is resulted from matrix-vector multiplication when $\mathbf{M}_{L}^{QWP}$ and $\mathbf{M}_{L}^{PR}$ are selected on the right-hand side of Eq. (4.5), and so forth for the other output SVs. Note that on the right-hand side of Eq. (4.5), before multiplying with $\mathbf{M}_{Rot}(\theta_{rot})$, the first entries, which are luminance, of the SVs are changed into 1, and the other 3 entries (polarization status) are unchanged. This is for the purpose of excluding the effect of the LC and the crossed LPs have on display transmittance. The assembly of the 1^{st} entries of the output SVs in Eq. (4.5) becomes the transmittance matrix of CP LCD's polarizing system:

$$\begin{bmatrix} t_{LL} & t_{LR} \\ t_{RL} & t_{RR} \end{bmatrix} = \begin{bmatrix} S_{LL0} & S_{LR0} \\ S_{RL0} & S_{RR0} \end{bmatrix} \tag{3.14}$$

where subscript 0 on the right-hand side of the matrix denotes the first entry S_0 of the SV.

The formulas of **M**s in Eq. (4.5) can be found in [LL10]- [LL12]. However, two issues are neglected in previous works when applying MC to CP LCD:

- Calculating the correct orientation of the polarized glasses.
- The rotation of light-propagation coordinate from the LCD to glasses.

We first elaborate the necessity of correct glasses orientation. The polarizing modules in the LCD panel and polarized glasses are anisotropic. Eq. (3.15) [YW06] shows the Mueller matrix of the wave retarder (WR), where γ is the phase delay between the orthogonal electrical fields of the light, and ψ is the orientation of the slow and fast axes of WR. Eq. (3.16) and (3.17) [YY09] show that both γ and ψ

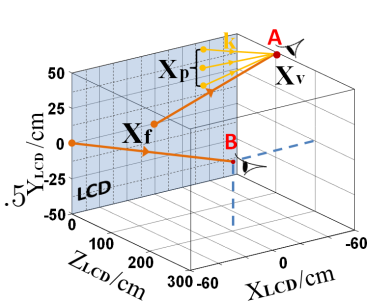

(a) Viewing location: $\mathbf{X}_v$. Viewer's focusing point on the screen: $\mathbf{X}_f$. Pixel location on the screen: $\mathbf{X}_p$. Viewer A with the focusing point at screen center. and viewer B with the focusing point at the left edge of the screen.

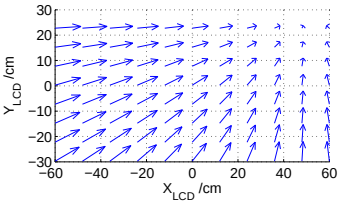

(b) **k**s in LCD coordinate, viewer A.

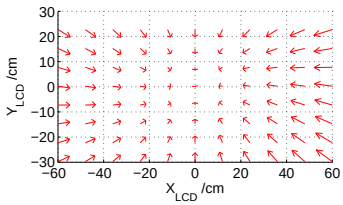

(c) **k**s in glasses coordinate, viewer A.

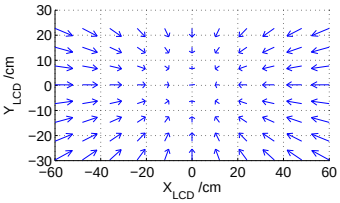

(d) **k**s in LCD coordinate, viewer B.

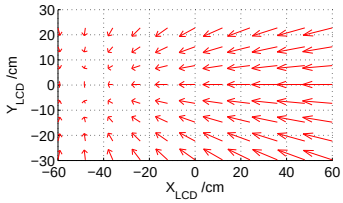

(e) **k**s in glasses coordinate, viewer B.

Figure 3.6: Light vector **k**s on screen in LCD and glasses coorindates resulted from two arbitrary viewing locations and the corresponding focusing points. The proposed LCD-to-glasses coordinate transformation is applied.

are functions of the incident light, where θ and ϕ denote the polar and azimuthal angles of the light in the WR frame respectively. Note that essentially both PR and QWP are WRs. In Eq. (3.16) and (3.17), ϕ_{WR} is the angle from x axis of the LCD or glasses coordinate to the slow axis of the WR; we set the refraction indices $n_x = 1.565$, $n_y = 1.479$, $n_z = 1.479$ for the LCD, and $n_x = 1.59$, $n_y = 1.58$, $n_z = 1.58$ for the glasses [LL10]. Therefore, **M**s in the LCD panel are determined by θ_{LCD} and ϕ_{LCD} as shown in Fig. 3.5(b), which are the polar angle and azimuthal angle of light in the LCD frame respectively. Similarly, **M**s in the glasses are determined by θ_{lens} and ϕ_{lens} as shown in Fig. 3.5(c), which are the polar angle and azimuthal angle of light in the glasses frame respectively.

θ_{LCD} and ϕ_{LCD} are determined by the viewing location $\mathbf{X}_v$ and pixel location $\mathbf{X}_p$ in the LCD coordinate, as illustrated in Fig. 3.6(a). Here, $\mathbf{k} = \mathbf{X}_v - \mathbf{X}_p$ is the light vector emitted from pixel $\mathbf{X}_p$ towards the viewing location $\mathbf{X}_v$ in the LCD coordinate. Then $\theta_{LCD} = \arctan\left(\frac{\mathbf{k}(3)}{(\mathbf{k}(1)^2+\mathbf{k}(2)^2)^{-1/2}}\right)$ and $\phi = \arccos\left(\frac{\mathbf{k}(3)}{(\mathbf{k}(1)^2+\mathbf{k}(2)^2)^{-1/2}}\right)$.

To calculate θ_{lens} and ϕ_{lens}, one needs to transform **k** from LCD to glasses

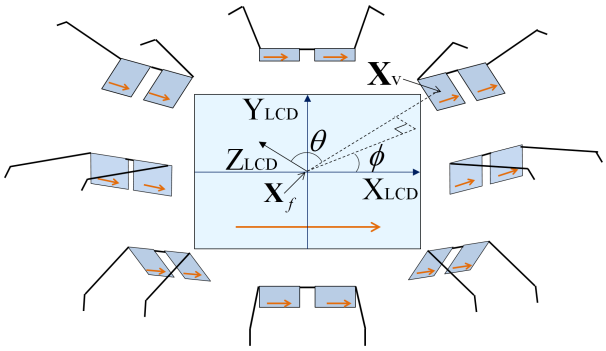

(a) Horizontal viewing glasses (for comfortable viewing).

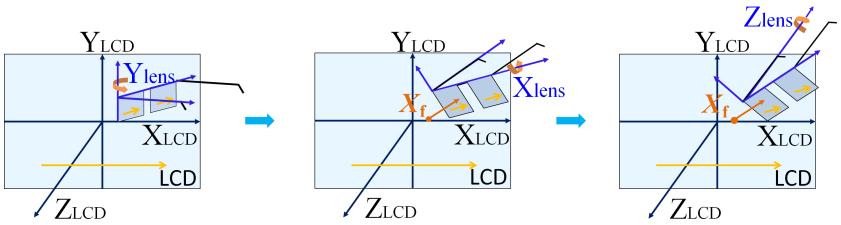

(b) Order of glasses rotation.

Figure 3.7: Comfortable viewing condition and the proposed LCD-to-glasses coordinate transformation.

$$\mathbf{M}_{WR}(\gamma,\psi) = \begin{bmatrix} 1 & 0 & 0 & 0 \\ 0 & \cos^2(2\psi)+\sin^2(2\psi)\cos\gamma & \sin(2\psi)\cos(2\psi)(\cos\gamma-1) & -\sin(2\psi)\sin\gamma \\ 0 & \sin(2\psi)\cos(2\psi)(\cos\gamma-1) & \sin^2(2\psi)+\cos^2(2\psi)\cos\gamma & -\cos(2\psi)\sin\gamma \\ 0 & \sin(2\psi)\sin\gamma & \cos(2\psi)\sin\gamma & \cos\gamma \end{bmatrix} \tag{3.15}$$

$$\gamma = \frac{2\pi(n_\xi - n_\eta)d}{\lambda\cos\theta}\cdot\left|\frac{(n_x-n_y)\sin 2(\phi-\phi_{WR})\cos\theta}{\sin 2\psi}\right| \tag{3.16}$$

$$\psi = -\frac{1}{2}\times \tan^{-1}\left(\frac{(n_x-n_y)\sin(2\phi-\phi_{WR})\cos\theta}{\frac{1}{2}\Delta(n_x-n_y)\cos(2\phi-\phi_{WR})(1+\cos^2\theta)+\left(n_z-\frac{1}{2}(n_x+n_y)\right)\sin^2\theta}\right) \tag{3.17}$$

coordinate. Since only angles are of our concern in this case, this LCD-to-glasses coordinate transformation can be simplified as rotation, where translation is omitted.

We define θ_x, θ_y and θ_z as the rotation angles around X_{lens}, Y_{lens} and Z_{lens} respectively. Thus, the coordinate transformation is the product of matrices $\mathbf{R}_x(\theta_x)$, $\mathbf{R}_y(\theta_y)$ and $\mathbf{R}_z(\theta_z)$, which are the rotation matrices in $\mathbb{R}^3$ around x, y, z axes respectively.

Glasses orientation determines the LCD-to-glasses coordinate transformation. However, the assumptions of the glasses orientation in previous works are not precise which affect the accuracy of optical modeling. No glasses orientation is specified in [WKL12]. In [LL12] and [LL12], glasses are assumed to be parallel to the screen at light's oblique incidence. This assumption is erroneous if the viewer rotates the glasses towards the screen to watch comfortably when he/she is at an oblique viewing location.

We impose the comfortable viewing constraint: horizontal viewing glasses (HVG) as illustrated in Fig. 3.7(a), which requires the horizontal axis of the glasses (X_{lens}) to be parallel to plane X_{LCD}-Z_{LCD} (or the floor) when the viewer doesn't deliberately tilt his/her head (or rotation around Z_{lens}).

If the glasses are initially parallel to the screen, then HVG can be achieved by rotating the glasses around Y_{lens} first and then around X_{lens} as shown in the left two figures of Fig. 3.7(b). The following is the short proof. Suppose the LCD-to-glasses coordinate transformation for HVG is $\mathbf{v}_{lens} = \mathbf{R}_x(\theta_x) \cdot \mathbf{R}_y(\theta_y) \cdot \mathbf{v}_{LCD}$, then, the glasses-to-LCD coordinate transformation becomes $\mathbf{v}_{LCD} = \mathbf{R}_y(-\theta_y) \cdot \mathbf{R}_x(-\theta_x) \cdot \mathbf{v}_{lens}$. By this expression, a horizontal vector in the glasses coordinate $[1, 0, 0]^T$ is transformed into LCD coordinate as $[\cos(\theta_y), 0, \sin(\theta_y)]^T$, which is parallel to plane X_{LCD}-Z_{LCD}. Consequently, the complete LCD-to-glasses coordinate transformation is shown in Eq. (3.18), where head tilt $\mathbf{R}_z(\theta_z)$ comes in the end, and θ_z is predefined by the viewer ($\theta_z = 0$ for head-tilt-free case).

$$\mathbf{k}_{lens} = \mathbf{R}_z(\theta_z)\mathbf{R}_x(\theta_x)\mathbf{R}_y(\theta_y)\mathbf{k} \tag{3.18}$$

Next, we solve for θ_x and θ_y given the viewing location $\mathbf{X}_v$, viewer's focusing point $\mathbf{X}_f$, and the HVG constraint. $\mathbf{X}_f$ is the point on the screen where light vector

$\mathbf{k}$ is normal to glasses surface (as shown in Fig. 3.5(a)). Note that θ_z in Eq. (3.18) is independent of $\mathbf{X}_v$ and $\mathbf{X}_f$. Eq. (3.19) shows that $\mathbf{X}_v - \mathbf{X}_f$ on the right-hand side is transformed into a normal vector in the glasses coordinate on the left-hand side. Notice the rotation order for HVG in Eq. (3.19).

$$[0,0,1]^T \|\mathbf{X}_v - \mathbf{X}_f\|_2 = \mathbf{R}_x(\theta_x)\mathbf{R}_y(\theta_y)\,(\mathbf{X}_v - \mathbf{X}_f) \tag{3.19}$$

Solve for θ_y and θ_x from Eq. (3.19), and the results are shown in Eq. (3.20) and (3.21), where X_{v1}, X_{v2}, X_{v3} are the 1^{st}-3^{rd} entries of $\mathbf{X}_v$ respectively, and X_{f1} and X_{f2} are the first two entries of $\mathbf{X}_f$.

$$\theta_y = \arctan\left(\frac{X_{f1} - X_{v1}}{X_{v3}}\right) \tag{3.20}$$

$$\theta_x = \arctan\left(\frac{X_{v2} - X_{f2}}{X_{f1} - X_{v1}}\sin\theta_y\right) \tag{3.21}$$

Figs. 3.6(b)-(e) demonstrate the proposed LCD-to-glasses transformation of light vector $\mathbf{k}$s. The 2 arbitrary viewing locations and the corresponding focusing points are shown in Fig. 3.6(a). As observed from Fig. 3.6(b) and (d), the light vectors in the LCD coordinate point towards the viewing location, whereas in Fig. 3.6(c) and (e) the light vectors in the glasses coordinate point towards the focusing point.

The other issue when applying MC in CP LCD is reflected by Fig. 3.5(a) and Eq. (4.5), where the Mueller rotation matrix $\mathbf{M}_{\text{Rot}}(\theta_{rot})$ rotates the SV output from the LCD by θ_{rot} before multiplication with the $\mathbf{M}$s in the polarized glasses. $\mathbf{M}_{\text{Rot}}$ is the Mueller rotation matrix [YW06]. This rotation, which is neglected in previous works [WKL12], [LL10] and [LL12] using Mueller calculus, arises from the LPC rotation between the LCD and glasses as shown in Fig. 3.5(b) and (c). Because Mueller calculus is computed in light-propagation coordinate (LPC), and if the LCD and glasses are oriented differently, the LPC is different by a rotation angle θ_{rot} around z_{LCD} (or z_{lens}) as shown in Fig. 3.5(c). θ_{rot} can be calculated as the angle between axes y_{LCD} and y_{lens} as:

$$\theta_{rot} = \arccos\left(\frac{\boldsymbol{y}_{\text{LCD}} \cdot \boldsymbol{y}_{\text{lens}}}{|\boldsymbol{y}_{\text{LCD}}||\boldsymbol{y}_{\text{lens}}|}\right) \tag{3.22}$$

where vector $\boldsymbol{y}_{LCD}$ is axis y_{LCD} in glasses coordinate (computed in Eq. (3.23)), and vector $\boldsymbol{y}_{lens}$ is axis y_{lens} in glasses coordinate (computed in Eq. (3.24)). $\mathbf{k}$ in Eq. (3.23) and (3.24) is light vector $\mathbf{X}_v - \mathbf{X}_p$.

$$\boldsymbol{y}_{LCD} = \mathbf{R}_x(\theta_x) \cdot \mathbf{R}_y(\theta_y) \cdot \left([0,0,1]^T \times \mathbf{k}\right) \tag{3.23}$$

$$\boldsymbol{y}_{lens} = [0,0,1]^T \times \left(\mathbf{R}_x\left(\theta_x\right) \cdot \mathbf{R}_y\left(\theta_y\right) \cdot \mathbf{k}\right) \tag{3.24}$$

3.2.4 Results of optical modeling of CP LCD

Note that with head tilt, CP LCD has sever crosstalk in the form of color bleeding which is addressed in our previous work [ZN14].

Assuming the viewer observe the screen from 9 different locations as shown in Fig. 3.8 where the 9 locations are respectively denoted as A-I, and the viewer has no head tilt ($\theta_z = 0$) [ZN14], the results of screen transmittance (at wavelength $550nm$) are shown in Fig. 3.9. Fig. 3.9(a) and (b) show results when the rotation of LPC is neglected. Fig. 3.9(c) and (d) are results when LPC rotation is considered, and the polarized glasses are assumed to be parallel to the screen. Fig. 3.9(e) and (f) are results when LPC rotation is also included, and the proposed glasses orientation as expressed in Eq. (3.22)-(3.24). Each subplot from Figs. 3.9(a)-(f) shows the screen transmittance resulted 9 viewing locations.

We can observe that in Fig. 3.9(a) and (b), without the rotation of LPC, the result shows erroneous transmission patterns at oblique viewing angles in ; the result assuming parallel glasses in Fig. 3.9(c) and (d) are similar to those applying the proposed glasses orientation in Fig. 3.9(e) and (f), but we can observe that the screen transmittance in Fig. 3.9(c) and (d) changes more significantly with the viewing location compared that in (Fig. 3.9(e) and (f). Thus, from the proposed screen simulation as shown in Fig. 3.9(e) and (f), the screen transmittance t_{LL} and t_{LR} (also t_{RR} and t_{RL}) does not vary significantly with the viewing angle. In addition, both

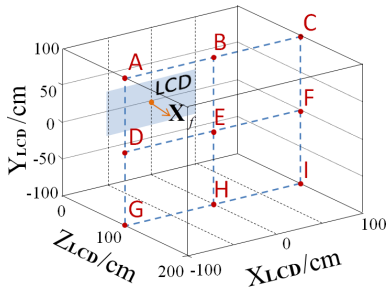

Figure 3.8: 9 viewing location with the focusing points used for simulations of screen transmittance in Fig. 3.9. The 9 viewing locations are denoted respectively as *A*-*I*. The focusing point of these 9 views is at the screen center.

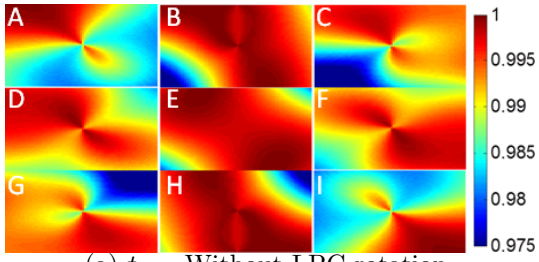

(a) t_{LL}. Without LPC rotation.

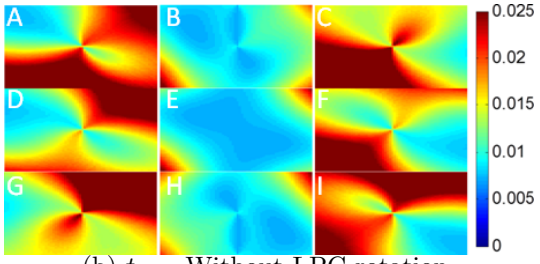

(b) t_{LR}. Without LPC rotation.

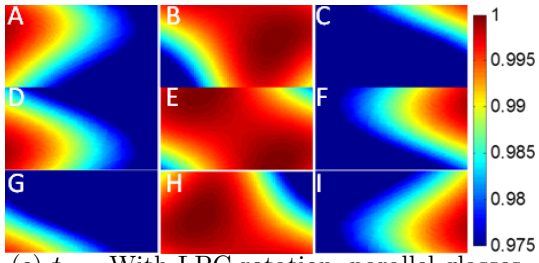

(c) t_{LL}. With LPC rotation, parallel glasses.

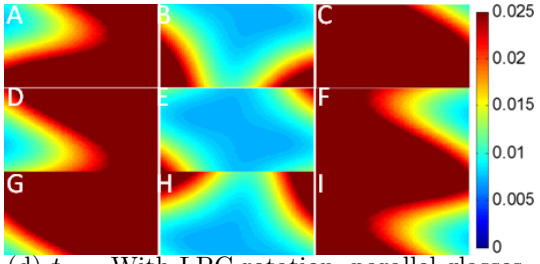

(d) t_{LR}. With LPC rotation, parallel glasses.

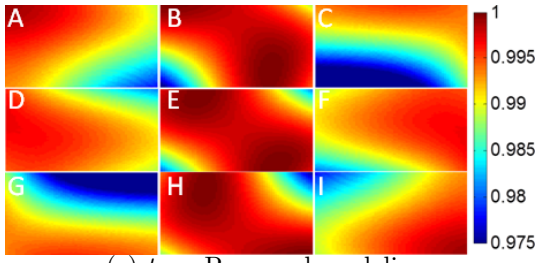

(e) t_{LL}. Proposed modeling.

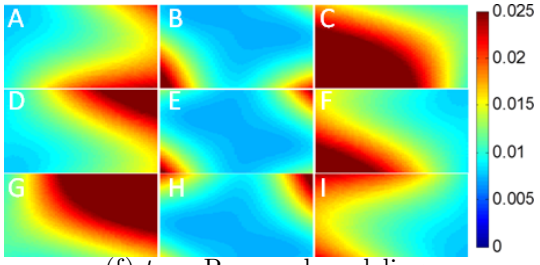

(f) t_{LR}. Proposed modeling.

Figure 3.9: Results of t_{LL} and t_{LR} of the screen using different modeling methods. Each screen is labeled with the viewing location as specified in Fig. 3.8.

the transmittance distribution and the range: $0.975 \leq t_{LL} \leq 1$, and $0 \leq t_{LR} \leq 0.025$ shown in Fig. 3.9(e) and (f) indicate that screen transmittance smoothly distributed across the screen.

Fig. 3.10 shows crosstalk (as defined in Eq. (4.3), (4.4)) across the screen

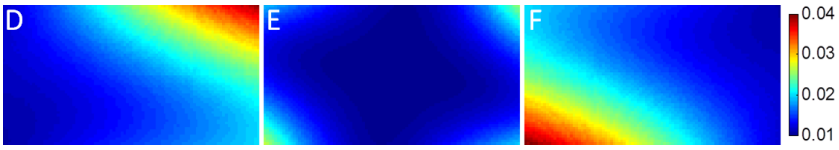

(a) Left-eye crosstalk.

(b) Right-eye crosstalk.

Figure 3.10: The result of crosstalk across the screen from viewing locations D, E and F as specified in Fig. 3.8. Crosstalk is calculated from Eq. (4.3) and (4.4).

resulted from the proposed glasses orientation (as shown in Fig. 3.9(e) and (f)). We can observe that the resulted crosstalk is limited with the maximum value of 4%. Furthermore, crosstalk changes smoothly across the screen varies insignificantly among different viewing angles. Note that the proposed modeling in Eq. (4.5) applies no phase compensation scheme to increase the viewing angle of the screen so that the screen transmittance of real CP LCD should be more viewing-location invariant compared with results in Fig. 3.9(d).

Fig. 3.11 shows results of natural images from our simulation as well as the real CP LCD [Cor09]. And the source of the input stereo images in Fig. 3.11 is [BWS05]. The simulations are resulted from Eq. (4.2) where the transmittance indices are calculated by the proposed method in Eq. (4.5). The images of the real CP LCD are photos taken at frontal viewing location. We can observe that our simulations match the real display correctly, and crosstalk is most visible in the enlarged areas in Fig. 3.11.

To validate the proposed modeling and glasses orientation, we had 10 subjects whose ages range from 20 to 30 observing the screen from viewing locations D-F as shown in Fig. 3.9(a). Each subject observed the CP LCD [Cor09] after the polarized lens of the preferred eye and with the other eye blocked. At each viewing location, the subject can adjust the glasses orientation according to his/her own comfort. As shown in Fig. 3.12(a), the stimuli in the blocked-eye LCD channel has white squares

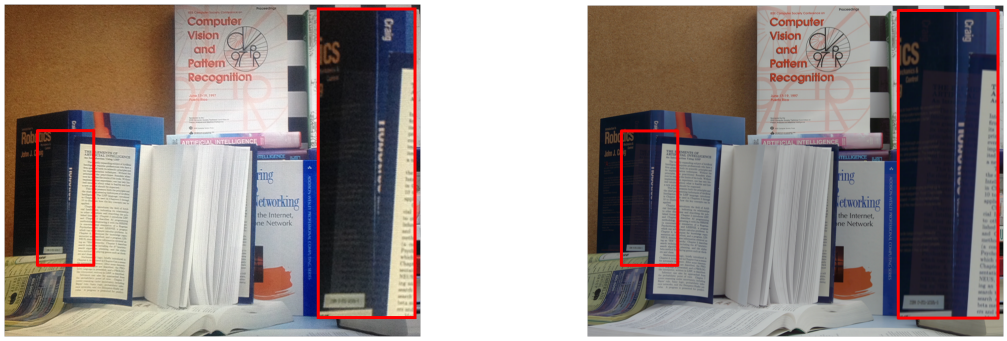

(a) Real display (b)Simulation

(c)Real display (d)Simulation

(e)Real display (f)Simulation

Figure 3.11: Comparison of real display with simulation results. (a) and (b): "Books" in the left view. (c) and (d): "Dwarves" in the right view. (e) and (f): "Dolls" (right column) in left view.

and that in the observing-eye LCD channel is black.

Figs. 3.12(c)-(e) show the simulated results of the observing-eye channel arising from neglecting the LPC rotation, polarized glasses parallel to LCD and the proposed glasses orientation respectively. The viewing locations are labeled by *D*-*F* at the top-left corners which are the same in Fig. 3.11. We can observe that Figs. 3.12(c)-(e) show the square pattern caused by crosstalk. However, Fig. 3.12(c) shows erroneous color bleeding because the rotation of LPC (Eq. (3.19)) is missing. Fig. 3.12(d), which

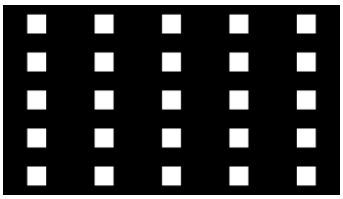

(a) Input image of the blocked eye.

(b) Input image of the observing eye.

(c) Without rotation of light-propagation coordinate (LPC).

(d)Polarized glasses are parallel to the screen.

(e) Proposed orientation of polarized glasses.

Figure 3.12: Input stereo images and simulations of the screen for subjective test for display model. (a, b) Input stereo images. (c)-(e) Simulations of the screen after the 3D lens for the observing eye.

is the result of parallel viewing glasses, shows brighter square pattern at side viewing locations compared with Fig. 3.12(e) which is from the proposed glasses orientation. In addition, we can observe from Fig. 3.12(c) - (e) that at viewing locations D and E, crosstalk is not symmetrical across the screen. The reason is that at an oblique viewing angle the incident angles of the lights across the screen are not symmetrically distributed towards the glasses, and that the WR is anisotropic. As a result, γs and ψs in Eq. 3.15 are not symmetrically distributed on the screen at oblique viewing angles. During the subjective test, 9 out of 10 subjects chose Fig. 3.12(d) to be the best match of their observation, and 1 chose Fig. 3.12(c). Viewing locations A-C and

(a) Photo. (b) Simulation.

Figure 3.13: Photo and simulation of the screen in the left-eye view when the head title is 90° [ZN14].

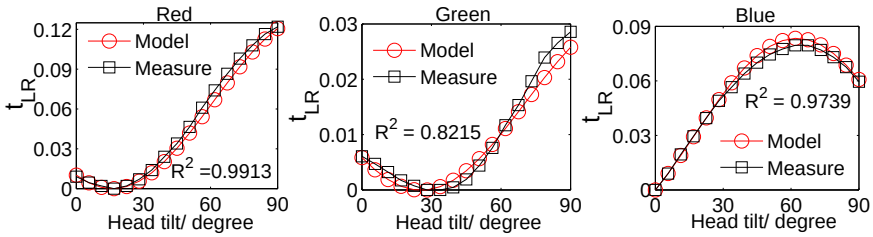

Figure 3.14: Measure and simulation of t_{LR} with head tilt. Left: red pixel. Middle: green pixel. Right: blue pixel. [ZN14]

G-I (in Fig. 3.9(a)) are omitted in this subjective test because vertical misalignment of the light rather than the polarizing system is the dominating factor of crosstalk at those viewing locations.

3.2.5 The case of head tilt

If there is no head tilt, crosstalk is very limited (less than 5%, [Zen]) even when the viewing angle (the angle between the screen normal and the ray from the screen center to the viewer) is very oblique (greater than 60°). However, if there is head tilt, crosstalk increases significantly in the form of "color bleeding". The effect of the head tilt in the CP LCD is shown in Fig. 3.13 where Fig. 3.13(a) is a photo of a real CP LCD and Fig. 3.13(b) shows the result from the proposed optical modeling after rotating the passive glasses by 90°. The input image for the left eye in Fig. 3.13 is black, and the input image for the right eye in Fig. 3.13 is white on the left half and is black on the right half. The CP LCD tested in this paper is LG 47LH55 [Cor09] (1080p) which is 58.5cm × 104.0cm (h×w). We can observe from Fig. 3.13 the left half of the screen turns from black into purple and this is caused by the severe leakage

from the red and blue pixels in the right-eye channel. To test the accuracy of the proposed optical model in terms of crosstalk induced by head tilt, we compare the measured and the simulated results.

Fig. 3.14 shows the data of t_{LR} of the red, green and the blue pixels from both the measuring and the simulation. For the measured data in Fig. 3.14, initially, the right-eye field of the screen is lit up; then, the luminance after the left-eye lens is measured rotating the glasses and is subtracted by the minimum luminance (dark pixel luminance); finally, the data is normalized by the luminance measured without the lens. The luminance is measured by power meter Newport 835. We observe from Fig. 3.14 as the head tilt increases, both the measured and the simulated data show that the increment in t_{LR} for the red and the blue pixels are much greater than that for the green pixel. The R^2 coefficients ($R^2 = 1$ indicates perfect fit) between the measured and the simulated data as shown in Fig. 3.14 verify the optical model is able to predict the crosstalk induced by head tilt accurately.

3.3 Crosstalk reduction

As demonstrated by both the modeling and real CP LCD in Section 3.2.4, the amount of crosstalk induced by the polarizing system is limited , and it depends insignificantly on the viewing location. Consequently, we can reduce polarizing-system-based crosstalk efficiently by preprocessing the image prior to displaying. In this section, we investigate how to combine both the device and image content to efficiently mitigate crosstalk.

Note that when the viewing location deviates vertically from the screen center significantly as discussed in [ZN14], severe crosstalk caused by another factor occurs. This factor is the vertical misalignment of light in CP LCD which result in crosstalk not only much more severe than that caused by the polarizing system but also whose distribution changes significantly with the viewing location in the vertical direction.

For the crosstalk caused by vertical misalignment of light, it's inefficient to cancel it through image-processing-based method. Thus, regarding the proposed crosstalk reduction method in this paper, we only consider the case when the viewing location does not deviates from the screen center significantly (which is practical that the viewer can always adjusts the viewing location to be aligned vertically to the screen center).

In this section, we reduce crosstalk from two perspectives: crosstalk concerning the display, and crosstalk considering the image content. A preliminary version of the proposed crosstalk reduction method from the display perspective can be found in [ZN13] where crosstalk is canceled while maximizing the image contrast. However, [ZN13] does not explain the reason why we rescale the image in luminance but not in grayscale level ([DN11] rescales images in grayscale domain to reduce crosstalk), while this paper validate that the former better preserves color by using CIE color difference metric [DKS12]. In addition, [ZN13] only provides the objective results showing that preprocessing the image in YCbCr color space gives rise to increased dynamic range in the output image comparing to preprocessing in RGB color space. In this paper, however, we consider the residual crosstalk in chrominance (which is ignored in [ZN13] and [DN11]), and show there is significant crosstalk visibility increment after switching from RGB to YCbCR. Regarding crosstalk reduction considering image content, our preliminary work can be found in [ZN14], where crosstalk visibility can be predicted by combining color difference as well as image texture estimation. In this paper, we extend [ZN14] by neglecting image texture in crosstalk reduction, and show that the output image contrast can be further increased while crosstalk visibility is hardly increased.

3.3.1 Crosstalk reduction concerning the display

We denote the transmission matrix in Eq. (4.2) at pixel p as $\mathbf{T}_p$, and $\mathbf{T}_p$ can be calculated from the modeling in Section 3.2. An intuitive way to cancel out crosstalk

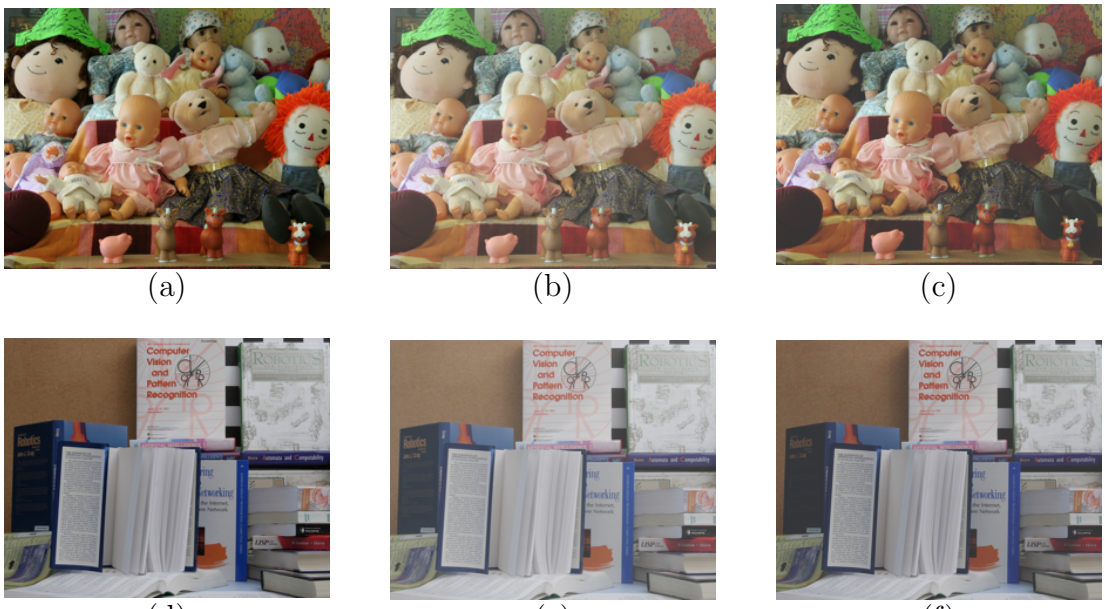

Figure 3.15: Results of rescaling the input image into a smaller dynamic range. Left column: original input images. Middle column: rescaling in grayscale level. Right column: rescaling in luminance (proposed). Top row: "Dolls". Bottom row: "Dwarves".

is to change luminance of the input image into $\mathbf{T}_p^{-1} \cdot [L_{in}, R_{in}]^T$ so that the output becomes $\mathbf{T}_p \cdot (\mathbf{T}^{-1} \cdot [L_{in}, R_{in}]^T)$. However, $\mathbf{T}_p^{-1} \cdot [L_{in}, R_{in}]^T$ as the input luminance may be unattainable. For example, when $t_{LL} = t_{RR} = 0.98$, $t_{LR} = t_{RL} = 0.02$, $L_{\text{in}} = 1$ and $R_{\text{in}} = 0$, the new luminance input in the LE and RE images become $L_{new,in} = 1.028$ and $R_{new,in} = -0.028$ respectively which fall outside the valid range (0 to 1). To achieve attainable input luminance, one needs to increase the black-level luminance and decrease the white-level luminance in the input images. We define the increment of black-level luminance in the LE and RE images as b_L and b_R respectively. Similarly, we define the decrement of the white-level luminance in the LE and RE images as w_L and w_R respectively.

Then we consider the problem of rescaling the luminance of the input image from the range of $[0, 1]$ to $[b_L, w_L]$ (or $[b_R, w_R]$). In [DN11], the input images are rescaled by shifting and rescaling in grayscale: $L'_{in} = 255 \times L_{in}^{\frac{1}{2.2}}(1 - b_L^{\frac{1}{2.2}} - w_L^{\frac{1}{2.2}}) + 255 \times b_L^{\frac{1}{2.2}}$ for the LE image, and $R'_{in} = 255 \times R_{in}^{\frac{1}{2.2}}(1 - b_R^{\frac{1}{2.2}} - w_R^{\frac{1}{2.2}}) + 255 \times b_R^{\frac{1}{2.2}}$ for the RE image. Note that the gamma-encoded grayscale level of b_L is $255 \times b_L^{\frac{1}{2.2}}$

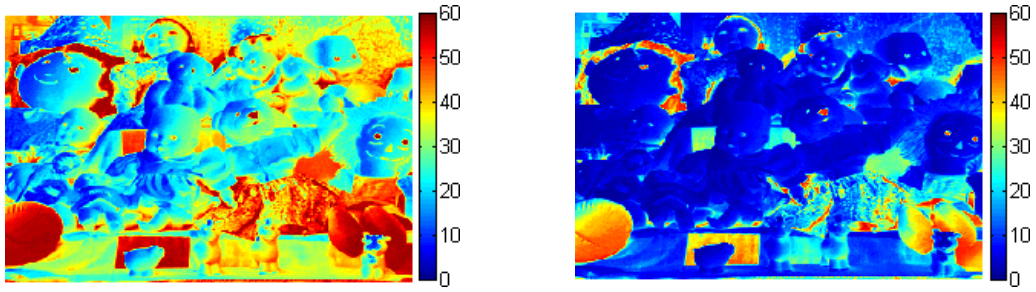

(a) (b)

Figure 3.16: Comparison of color difference between the original input image and the image rescaled into a smaller dynamic range. (a) Rescaling the input image in grayscale level. (b) Rescaling the input image in luminance (proposed).

where gamma is set as 2.2. However, rescaling in grayscale level induces significant color shift. We propose to linearly rescale the input image in luminance: $L'_{in} = L_{in} \times (1 - b_L - w_L) + b_L$, and $R'_{in} = R_{in} \times (1 - b_R - w_R) + b_R$. The comparison of the aforementioned rescaling methods are shown in Fig. 3.15 where we can observe better conservation of image contrast and color vibrancy obtained by the proposed rescaling. The source of input image in Fig. 3.15 is [BWS05]. Fig. 3.16 shows the results of color difference between the original image "Dolls" and the corresponding rescaled images. Note that in Fig. 3.16, the metric of color difference is CIE 94 [DKS12], and the source of the input image is [BWS05]. We apply color difference metric ΔE^*_{94} proposed by Commission on Illumination (CIE) defined in $L^*c^*h^*$ color space to obtain the results in Fig. 3.16. The calculation shows $\Delta E^*_{94} = 31.12$ per pixel after rescaling in grayscale level Fig. 3.16(a), and $\Delta E_{94} = 13.07$ per pixel in Fig. 3.16(b) (proposed method) which validates that the proposed rescaling in luminance results in less color shift. Consequently, the range of the luminance output $\mathbf{T}_p\left(\mathbf{T}_p^{-1}[L'_{in}, R'_{in}]\right)$ is $[b_L, 1 - w_L]$ in the LE channel and $[b_R, 1 - w_R]$ in the RE channel. Nevertheless, rescaling the luminance of the input images into a smaller dynamic range causes loss of image contrast. We propose minimizing b_L, w_L, b_R and w_R by a linear programming problem. Initially, $\mathbf{T}_p^{-1} \cdot [L_{in}, R_{in}]_p$ is calculated for the entire image where subscript p is the pixel index. Then, if negative luminance is resulted in the LE input image, we label the pixel having the smallest luminance with index $p_{min,L}$. Furthermore, if luminance that is greater than 1 exists, we label the pixel having the largest luminance

with index $p_{max,L}$. In the same manner, $p_{min,R}$ and $p_{max,R}$ are labeled in the RE input image.

Then b_L, w_L, b_R and w_R can be solved from:

$$\begin{aligned}
&\underset{b_L,b_R}{\text{minimize}}\, b_L + w_L + b_R + w_R \\
&\text{subject to} \\
&\begin{bmatrix} 0 \\ 0 \end{bmatrix} \preceq \mathbf{T}_p^{-1} \cdot \begin{bmatrix} L_{in} \cdot (1 - b_L - w_L) + b_L \\ R_{in} \cdot (1 - b_R + w_R) + b_R \end{bmatrix}_p \preceq \begin{bmatrix} 1 \\ 1 \end{bmatrix}, \qquad (3.25) \\
&p = p_{min,L}, p_{max,L}, p_{min,R}, p_{max,R}; \\
&0 \leq b_L, w_L, b_R, w_R \leq 1;
\end{aligned}$$

where the objective function minimizes the loss of dynamic range, the first constraint is to obtain attainable input signal, and the second constraint ensures legitimate values of b_L, w_L, b_R and w_R. To compare the proposed minimization method with the traditional method that only increases the black-level luminance without minimization, 17 stereo image pairs from [BWS05] are tested and the results can be found in [ZN13]. The results demonstrate that the dynamic range of the output images improves significantly for most tested images.

3.3.2 Crosstalk reduction concerning image content

Apart from the quality of CP LCD, image content is another important factor for crosstalk reduction. Many works [DKS12], [Woo12], [XYEP10] have shown image contrast is an important factor on crosstalk visibility. A more direct way of estimating the impact of image contrast on crosstalk visibility is proposed by Kang et al. [DKS12], where color difference between the original image and image with crosstalk is used as the metric for crosstalk visibility. Another significant factor is image texture, which is able to mitigate or facilitate crosstalk visibility through texture masking [WSM01]. In this section, we show that at high frequency, texture masking mitigates crosstalk visibility.

Concerning color difference

We apply color difference ΔE^*_{94} for the initial estimation of crosstalk visibility as proposed in [DKS12]. between the original image and the crosstalk image.

Eq. (3.26) calculates the color difference between the original LE image which is $L^*_l c^*_l h^*_l(i,i)$ and the LE crosstalk image $L^*_l c^*_l h^*_l(i,j)$. $L^*_l c^*_l h^*_l(i,j)$ in Eq. (3.26) denotes the $L^*_l c^*_l h^*$ representation of the LE output image when the input grayscale level in the LE channel is i and that in the RE channel is j. $L^*_l c^*_l h^*_l(i,i)$ in Eq. (3.26) denotes the LE output image when the input grayscale level is i and that in both the LE and RE channels. Similarly, Eq. (3.27) defines the initial estimation of RE crosstalk visibility.

$$\text{Crosstalk}_{l,\Delta E} = \Delta E^*_{94}\left\{L^*_l c^*_l h^*_l(i,j), L^*_l c^*_l h^*_l(i,i)\right\} \tag{3.26}$$

$$\text{Crosstalk}_{r,\Delta E} = \Delta E^*_{94}\left\{L^*_r c^*_r h^*_r(i,j), L^*_r c^*_r h^*_r(j,j)\right\} \tag{3.27}$$

Fig. 3.17(a), (b) show the simulated "Drumsticks" [BWS05] which are resulted from viewing location B as specified in Fig. 3.8. Fig. 3.17 (c) shows the initial binocular perceptual crosstalk obtained by averaging the initial LE crosstalk vsibility in Fig. 3.17(a) (calculated from Eq. (3.26)) and the initial RE crosstalk visibility in Fig. 3.17(b) (calculate from Eq. (3.27)). The proof of averaging crosstalk in the LE and RE views to acquire the binocular crosstalk can be found in [PSI05].

Concerning image texture

As can be observed in Fig. 3.17(c), the initial crosstalk visibility estimation based on color difference shows positive prediction on the fabric with square patterns in Fig. 3.17(a), (b) where crosstalk is hardly visible. Therefore, we propose to include image texture as a concealing factor in crosstalk perception: crosstalk in the area where the LE and the RE images are both highly-textured is hardly noticeable. Fig. 3.18 shows another example where crosstalk is salient when one of the channels is textured (Figs. 3.18(a)-(b)) whereas it is masked well when both channels have

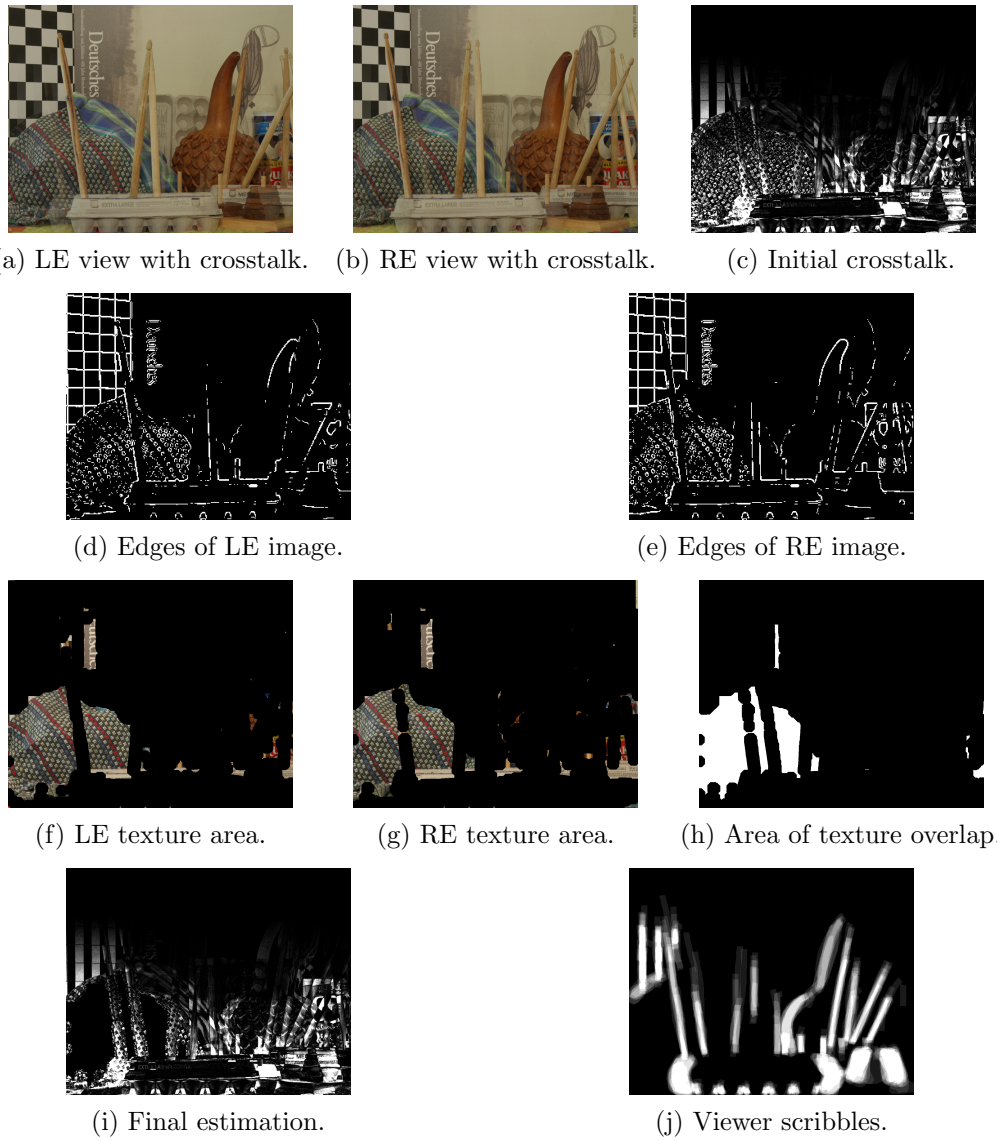

(a) LE view with crosstalk. (b) RE view with crosstalk. (c) Initial crosstalk.

(d) Edges of LE image. (e) Edges of RE image.

(f) LE texture area. (g) RE texture area. (h) Area of texture overlap.

(i) Final estimation. (j) Viewer scribbles.

Figure 3.17: Procedure for crosstalk visibility estimation. The source of input stereo image "Drumsticks" is [BWS05].

Figure 3.18: Crosstalk visibility influenced by image texture [ZN14]. (a) Textured image nontextured crosstalk, (b) Flat image with textured crosstalk. (c) Textured image textured crosstalk.

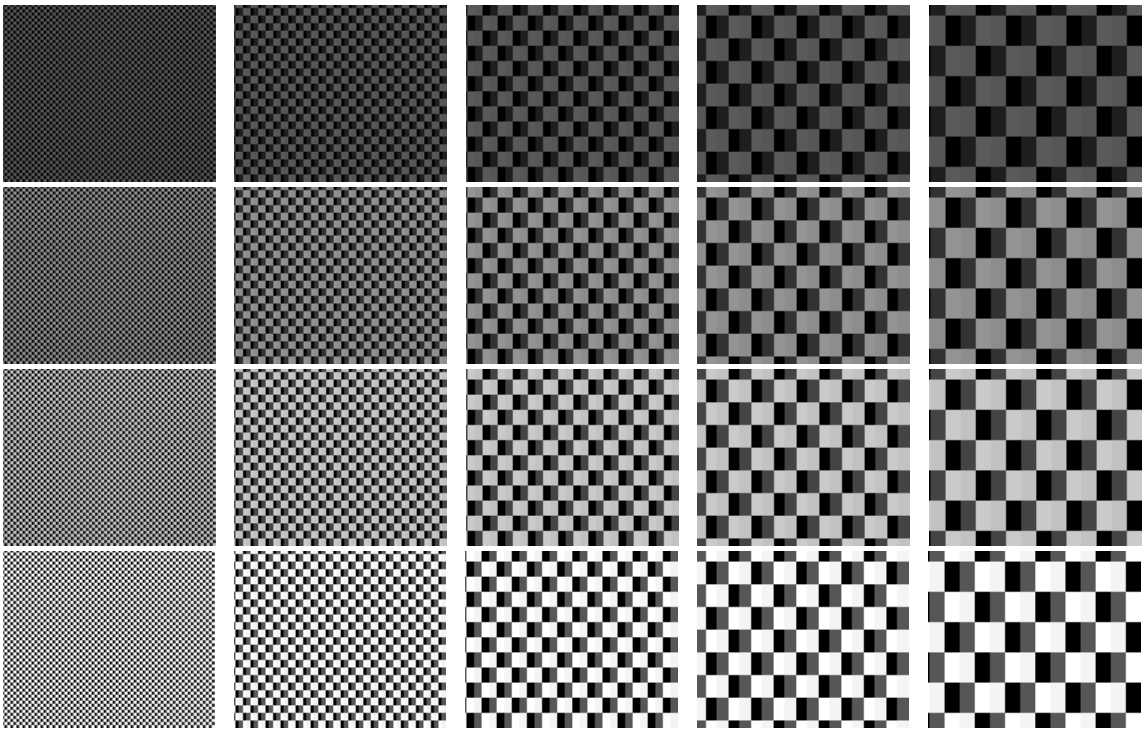

Figure 3.19: Influence of texture density and contrast on texture masking of crosstalk.

texture information (Fig. 3.18(c)). Therefore, areas in the LE and the RE images where textures are co-located can be excluded in crosstalk visibility estimation.

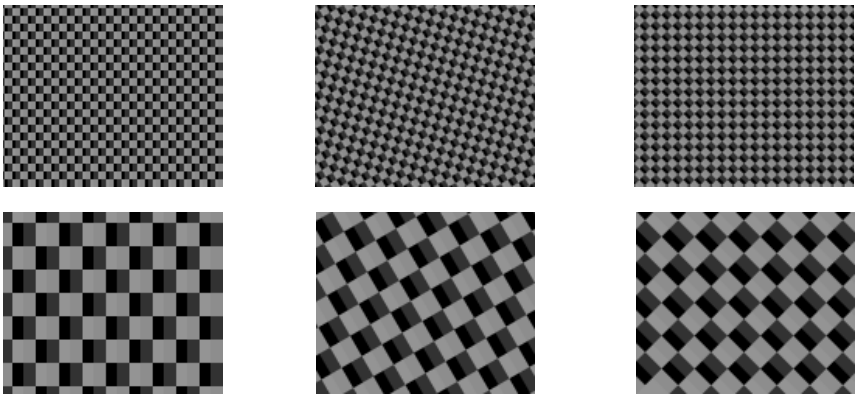

Figure 3.20: Examples showing orientation does not influence on how texture impacts crosstalk visibility. The density and contrast of the texture images within the top row and the bottom row image are respectively the same.

Based on this observation, we investigate how texture affects crosstalk visibility regarding texture density, contrast and orientation. Fig. 3.19 shows textures composed of checkerboards with different contrast and density. In each row of Fig. 3.19, the textures are of the same contrast while the density increases from left to

right. In each column of Fig. 3.19, the checkerboards are of the same density while the contrast increases from top to bottom. The crosstalk level for all subfigures in Fig. 3.19 is 10% according to Eq. (4.3) and (4.4). We can observe that with high texture density, as shown in the first two columns of Fig. 3.19, crosstalk is masked for all contrast. As density decrease in each row in Fig. 3.19, the visibility of crosstalk increases significantly. For each column in Fig. 3.19, the visibility of crosstalk also increases with contrast. However, fixing the density while changing contrast has smaller influence on crosstalk visibility than fixing contrast while change the density. As Section 3.3.2 has already considered the impact of contrast on crosstalk visibility through color difference, in this section, we mainly focus on the factor of texture density.

Regarding how the orientation of texture influences crosstalk visibility, we rotate the checkerboard image by different angles. The results of changing texture orientation in crosstalk image are shown in Fig. 3.20, where the crosstalk level for all subfigures is 10% according to Eq. (1.1) and (4.4). Note that the intended image and the crosstalk image have the same orientation because for most stero image pairs, the co-located areas have the same image texture. We can observe that there is no significant change of crosstalk visibility. Thus, in this paper, we do not take texture orientation into consideration for crosstalk visibility.

Fig. 3.17 shows the procedure of estimating crosstalk visibility considering both color difference (image contrast) and texture. Fig. 3.17(a) and (b) show the input LE and RE crosstalk images which are simulated from the proposed display model. The first step is to consider image contrast, and result of the initial crosstalk-visibility based on color difference is shown in Fig. 3.17(c). Then, Figs. 3.17(d) - (h) shows the procedure of detecting the co-located textured area in LE and RE images. Since texture contrast is spontaneously taken care of in the previous step through color difference, we only need to consider the density of texture. In Fig. 3.17(d) and (e), the edges in the input images are detected by Sobel filter. Then, to eliminate the sparsely-spaced edge, Fig. 3.17(d) and (e) are dilated and eroded, and this gives

(a) LE view of "Dwarves" .

(b) RE view of "Dwarves".

(c) Estimated crosstalk visibility.

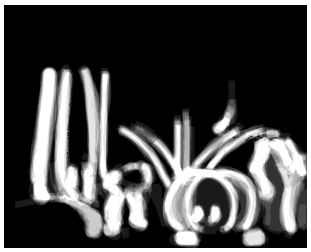

(d) Viewer scribbles of visible crosstalk.

(e) LE view of "Reindeer".

(f) RE view of "Reindeer".

(g) Estimated crosstalk visibility.

(h) Viewer scribbles of visible crosstalk.

Figure 3.21: Comparison of the proposed perceptual crosstalk estimation and crosstalk from viewer scribbles. (a), (b), (e) and (f) show the crosstalk image. The source of input stereo images is [BWS05].

rise to the texture area of the LE and RE images as shown in Fig. 3.17(f) and (g). The size of the structural element for the dilation is 1.0% of image height, and that for erosion is 1.5% of image height. Fig. 3.17(h) shows the co-located texture areas of the LE and RE input images as the white regions. After removing the textured areas (Fig. 3.17(h)) from the initial prediction (Fig. 3.17(c)), the final estimation for

perceptual crosstalk is shown in Fig. 3.17(i).

To evaluate the performance of the proposed crosstalk visibility estimation, subjective test is conducted among 10 participants. All the subjects observe the CP LCD wearing the polarized glasses with both eyes, and they scribble in regions where crosstalk is perceivable. The scribbled pixels are recorded as 255 in grayscale level. The viewing location is B as specified in Fig. 3.8. 3 stereo pairs: "Drumsticks", "Dwarves" and "Reindeer" [BWS05] containing prominent textured areas are tested. We show the averaged scribbles among the 10 subjects for each stereo pair. Fig. 3.17(j) shows the crosstalk scribble for "Drumsticks" compared with the result of the estimated crosstalk visibility as shown in Fig. 3.17(i). The results for "Dwarves" and "Reindeer" are shown in Fig. 3.21 where the simulated output images as well as our estimation of crosstalk visibility are also presented. As observed in Fig. 3.17 and Fig. 3.21, both subjective observations and our prediction suggest no perceptual crosstalk on the fabric with squares in "Drumsticks", the cloth with sunflowers in "Dwarves", and the textured fabric at the background of "Reindeer". Therefore, the accuracy of perceptual crosstalk prediction improves by excluding the textured areas.

To further minimize the loss of image contrast induced by crosstalk reduction, one can eliminate the textured areas in the stereo images when calculating b_L, w_L, b_R and w_L in Eq. (3.25). The reason is that the pixels with unattainable lumiance are likely to exist in the textured areas for the grayscale levels between the LE and RE images can be very different at the co-located textured areas). We demonstrate in the subjective test in Section 3.4 that excluding the textured areas in crosstalk reduction effectively increases the image contrast and does not cause the visibility of crosstalk to increase.

3.4 Experiment on crosstalk reduction and the results

For crosstalk reduction in color images, to reduce color shift, one can optimize b_L and b_R in the 3 color channels (red, green and blue) separately and select the maximum value to apply to all 3 colors. The alternative is to process the luma channel only, and keep the chroma channel unchanged as proposed in [SLF07] and [DN11]. Although color is preserved by setting the chroma channel aside, residual crosstalk exists in the chrominance. In this section, we apply the proposed crosstalk reduction algorithm as shown in Eq. (3.25) in both the RGB and YCbCr color spaces to investigate the impact of the choice of color space. In addition, to validate the proposed method of excluding the textured area for crosstalk reduction, results of the global method considering the entire image are compared with those resulted from excluding the texture areas. Consequently, the proposed crosstalk reduction algorithm in Eq. (3.25) is implemented in 4 different ways: in RGB color space considering the entire image, in RGB excluding the textured areas, in YCbCr considering the entire image, and in YCbCr excluding the textured areas. The aforementioned methods are respectively denoted as methods 1-4 in Table 3.1 and Fig. 3.23.

Fig. 3.22 shows the simulated output images of "computer" from [BWS05]. Fig. 3.22(a, b) show unprocessed image with crosstalk. Fig. 3.22(c, d) show crosstalk reduction in RGB, considering the entire image (method1). Fig. 3.22(e, f) show crosstalk reduction in RGB, excluding the textured areas (method2). Fig. 3.22(g, h) show crosstalk reduction in YCbCr, entire image (method3). Fig. 3.22(i, j) show crosstalk reduction in YCbCr, excluding the textured areas (method4). The source of the input stereo image "Computer" is [BWS05]. Without any preprocessing, we observe that crosstalk in Fig. 3.22(a) (LE image) appears as the faint marker in the red background, and as the ghosting of the keyboard in Fig. 3.22(b) (RE image). Figs. 3.22(c)-(i) show results of the proposed crosstalk reduction algorithm

(Eq. (3.25)) implemented by method 1-method4 respectively.

We conduct subjective test on 11 stereo pairs (listed in Table 3.1 from [BWS05]) resulted from methods 1-4 in terms of visibility of the residual crosstalk as well as image quality. For the subjective test, 16 subjects, 4 are females and 12 are males with ages ranging from 20 to 50, observe the stereo images with both eyes using the polarized glasses. The subjective test is conducted under home environment according to ITU recommendation.

Table 3.1 shows the mean opinion score (MOS) of subjective test. In Table 3.1, method1 denotes crosstalk reduction in RGB, considering the entire image; method2 denotes in RGB, excluding the textured areas; method3 denotes in YCbCr, entire image; method4 denotes in YCbCr and excluding the textured areas. Each subject score the visibility of crosstalk from 0 (no crosstalk perceived) to 4 (crosstalk is the same as the unprocessed stereo image with crosstalk). Image contrast is evaluated subjectively in terms of image contrast and color vibrancy. Each subject ranks the results of methods 1-4 from 1 (the worst quality) to 4 (the best quality). All the values in the table are averaged among the 16 subjects.

Regarding crosstalk visibility, we can observe from Table 3.1 that the results of methods 1-4 all suggest significant decreasing in crosstalk compared with the unprocessed stereo image. Additionally, most images suggest that RGB-based crosstalk reduction (methods 1, 2) has less residual crosstalk than YCbCr-based crosstalk reduction (methods 3, 4). Furthermore, 9 out of 11 images (except for "Aloe" and "Laundry") show that method 2, which is crosstalk reduction in RGB excluding the textured areas, leads to the least crosstalk visibility.

However, the MOS in Table 3.1 alone can not show if there is significant distinction among the 4 crosstalk-reduction methods. For this reason, we carry out t-test and as well as 2-way ANOVA test for the subjective test.

The t-test results of the subjective test regarding both crosstalk visibility and image contrast are shown in Table 3.2. Since there are 16 subjects, 11 images and 4

crosstalk-reduction methods, the degree of freedom is $(16-2)\times(11-1)\times(4-3) = 150$. We set $\alpha = 0.05$ when computing the p values. As shown in Table 3.2, regarding crosstalk visibility, methods 1 and 2 are significantly different, methods 3 and 4 are insignificantly different, methods 1 and 3 are insignificantly different, and methods 2 and 4 are significantly different. Thus, for the performance of crosstalk reduction, only method 2 is considerably different from the other methods. For image contrast, there exists considerable difference between methods 1 and 2, as well as between methods 3 and 4. However, there is no significant difference between methods 1 and 3, and also between methods 2 and 4. In addition, to further validate significant variation among the performance of methods 1-4 in terms of crosstalk visibility and image contrast, and also to investigate if there is considerable interaction between the crosstalk-reduction methods and the images used for the subjective test, we carry out the 2-way ANOVA test. The replicate of this test is 16 from the observations of 16 subjects. Table 3.3 shows 2-way ANOVA test of the 11 images ($DoF = 10$) processed by 4 different crosstalk-reduction methods ($DoF = 3$) respectively, and they are observed by 16 subjects (replicate is 16). We set $\alpha = 0.05$ for p value. As shown in Table 3.3, concerning crosstalk visibility, $p = 0.018$ resulted from methods 1-4, $p = 0.00$ resulted from the images used, and $p = 0.52$ for interaction between methods 1-4 and the images. These values show that methods 1-4 as well as the images have significant impact on the result of crosstalk visibility, and there is no synergistic between methods 1-4 and the images for crosstalk reduction. Concerning image contrast in Table 3.3, $p = 0.00$ resulted from methods 1-4, $p = 0.98$ concerning the images, and $p = 0.55$ for the interaction between methods 1-4 and the images. The results of ANOVA test indicate that, concerning image contrast, the cross-talk reduction methods have a considerable impact, while the images do not have significant impact. Furthermore, there is no interaction between crosstalk-reduction methods and the images regarding the results of image contrast. Therefore, the 2-way ANOVA test further verifies the significant variation caused by methods 1-4 on

the subjective test independent of the images used for the subjective test.

Fig. 3.23 shows the subjective test results of crosstalk visibility and images contrast of 11 images after being processed by crosstalk-reduction methods 1-4. Each data point in Fig. 3.23 are averaged values among the 16 subjects. Fig. 3.23(1) shows that for most images (except for "Books"), the results of crosstalk visibility change similarly among methods 1-4. Furthermore, method 2: crosstalk reduction in RGB excluding the textured areas gives rise to most significant reduction in crosstalk visibility. From Fig. 3.23 (2), which is the results of images, due to the large variations, there is no significant evidence about which method is superior than the other, namely, the performances of methods 1-4 are similar in terms of images contrast.

Consequently, considering crosstalk visibility as well as image contrast, the subjective test shows that the combination of reducing crosstalk in RGB and excluding the co-located texture (method 2) areas gives rise to the best crossralk-reduction results by significantly reducing crosstalk while preserving image contrast.

From the results above, we conclude that:

- The proposed crosstalk reduction algorithm as shown in Eq. (3.25) reduces crosstalk induced by the polarizing system of CP LCD efficiently.
- Crosstalk reduction implemented in the RGB color space outperforms that in the YCbCr color space in terms of perception of the residual crosstalk.
- Excluding the textured areas for crosstalk reduction not only further boosts the image contrast and color vibrancy but also lowers crosstalk perception.

3.5 Conclusion

We develop an accurate model for CP LCD which captures the attributes of crosstalk caused by the polarizing system. The optical modeling of the polarizing system employs Mueller calculus (MC) [YW06] where a more reasonable and

precise glasses orientation estimation is proposed. Furthermore, the rotation of light-propagation coordinate from the LCD frame to the glasses frame in MC which is missing in previous works is calculated. The simulation results suggest that limited crosstalk is induced by the polarizing system. In addition, the distribution of crosstalk on the screen changes insignificantly with the viewing location. The simulations of CP LCD from the proposed modeling method match human observations of the real display [Cor09]. Regarding crosstalk reduction, we propose minimizing the contrast lost by solving a linear programming problem. We also demonstrate that rescaling the input image to a smaller dynamic range in luminance demain results in less color shift. In addition, we propose to exclude the textured areas in crosstalk reduction. The subjective result validates that crosstalk reduction in RGB color space where textures areas are not processed, yields the best crosstalk reduction that preserves image's contrast and color vibrancy.

3.6 Acknowledgment

Chapter 3, in full, is a reorganized composition of the materials as they appear in International Conference on Acoustics, Speech and Signal Processing (ICASSP), IEEE, 2012, Menglin Zeng, Truong Nguyen, and, International Conference on Image Processing (ICIP), IEEE, 2014, Menglin Zeng, Haleh Azartash, and Truong Nguyen, and IEEE Transactions on Image Processing, Vol. 24, Number 12, 2015, Menglin Zeng, Alan Robinson, and Truong Nguyen. The dissertation author was the primary investigator and author of these papers.

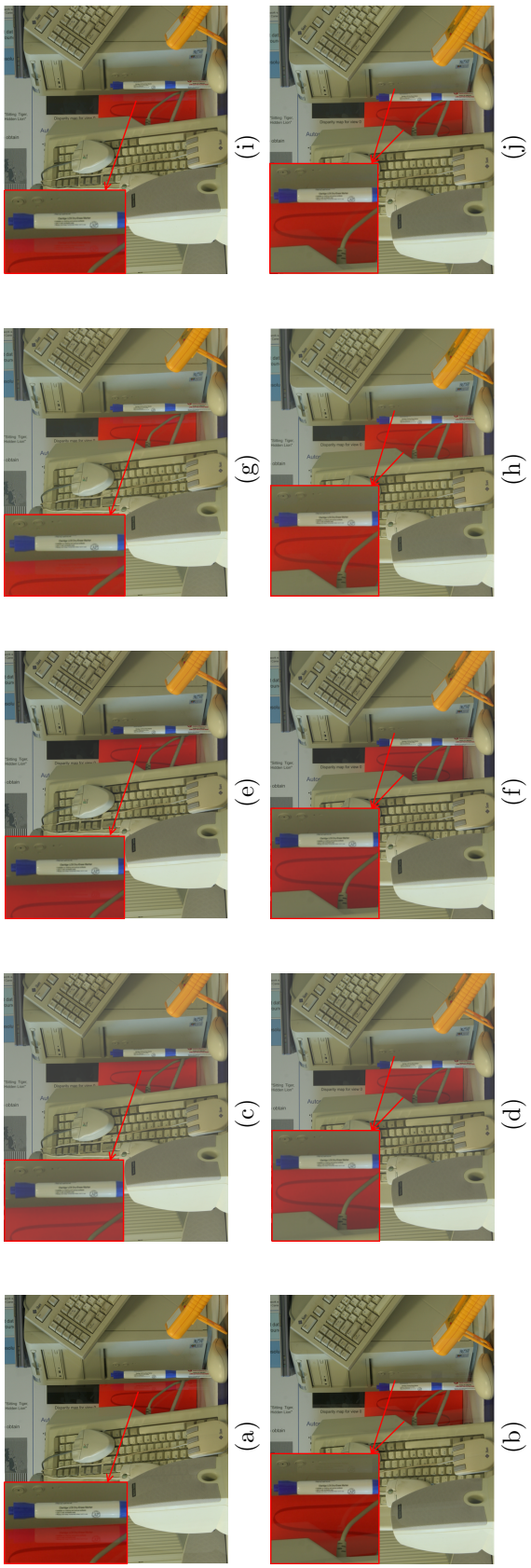

Figure 3.22: Results of crosstalk reduction using different methods. Top row: LE view. Bottom row: RE view.

Table 3.1: Mean opinion score (MOS) of subjective-test results for crosstalk reduction in two aspects: crosstalk visibility and image quality.

Image	Crosstalk visibility				Image contrast			
names	method1	method2	method3	method4	method1	method2	method3	method4
Aloe	0.63	0.66	0.66	0.66	1.94	2.25	2.94	3.50
Art	0.72	0.69	1.19	1.03	1.44	2.06	2.81	3.56
Books	1.44	1.40	1.22	1.25	2.50	3.13	2.94	2.69
Computer	0.59	0.44	0.97	0.91	3.25	3.38	1.94	1.44
Dolls	0.69	0.59	0.78	0.84	1.44	3.56	1.75	3.25
Drumsticks	1.34	0.91	1.03	0.97	3.31	2.13	1.69	2.88
Dwarves	0.91	0.50	0.85	0.94	2.00	1.06	3.13	3.63
Laundry	0.59	0.69	0.84	1.03	1.44	2.25	3.38	3.19
Moebius	0.94	0.84	1.09	1.03	1.44	1.69	3.19	3.56
Reindeer	0.75	0.69	0.97	0.88	3.75	2.69	2.38	1.19
Rocks	0.59	0.41	0.63	0.50	1.94	2.69	3.63	2.00

Table 3.2: T-test of subjective-test results comparing methods 1-4 for crosstalk reduction. The degree of freedom (DoF) is $(16-1)\times(11-1)=150$, for 16 subjectss and 11 images. We set $\alpha=0.05$ for p value.

t-test results	Crosstalk Visibility			
	method1&2	method3&4	method1&3	method2&4
h	1	0	0	1
p	0.004	0.86	0.13	3.85×10^{-4}
DoF	150	150	150	150
t-test results	Image Contrast			
	method1&2	method3&4	method1&3	method2&4
h	1	1	0	0
p	6.12×10^{-4}	0.01	0.06	0.42
DoF	150	150	150	150

Table 3.3: 2-way ANOVA test of crosstalk visibility and images contrast from the subjective test concerning factors of the crosstalk-reduction methods 1-4 and images.

Source of variation	Crosstalk Visibility				
	SS	DoF	MS	F	p-value
Images	5.00	3	1.67	3.39	0.018
Methods1-4	99.11	10	9.91	20.17	0.00
Interaction	14.28	30	0.477	0.97	0.52
Within	324.33	660	0.49		
Total	442.718	703			
Source of variation	Image Contrast				
	SS	DoF	MS	F	p-value
Images	36.78	3	12.26	9.08	0.00
Methods1-4	3.96	10	0.40	0.29	0.98
Interaction	38.46	30	1.28	0.95	0.55
Within	891.44	660	1.35		
Total	970.64	703			

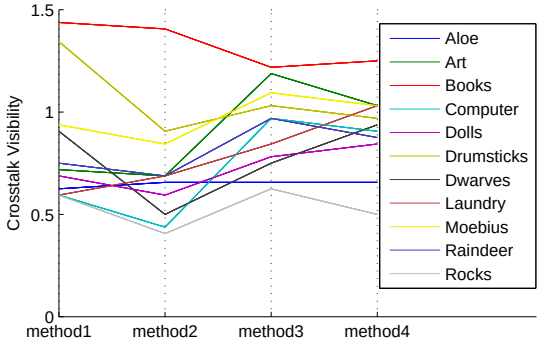

(a) Crosstalk visibility.

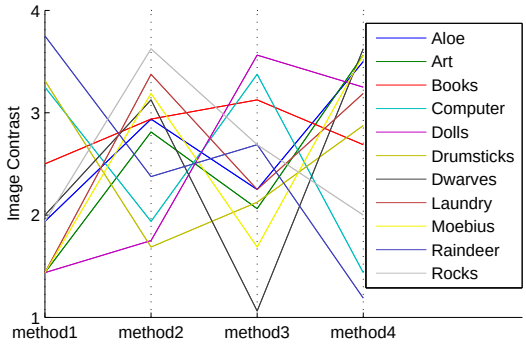

(b) Image contrast.

Figure 3.23: Subjective test of 11 images in terms of crosstalk visibility and image contrast resulted from methods 1-4. The source of the images is [BWS05]

Chapter 4

Analysis of Crosstalk in 3D Circularly Polarized LCDs Depending on the Vertical Viewing Location

Crosstalk in Circularly Polarized (CP) liquid crystal display (LCD) with polarized glasses (passive 3D glasses) is mainly caused by two factors: the polarizing system including wave retarders and the vertical misalignment (VM) of light between the liquid crystal (LC) module, and patterned retarder (PR). We show that the latter, which is highly dependent on the vertical viewing location, is a much more significant factor of crosstalk in CP LCD than the former. There are 3 contributions in this paper. Initially, a display model for CP LCD which accurately characterizes VM is proposed. A novel display calibration method for VM characterization which only requires pictures of the screen taken at 4 viewing locations. In addition, we prove that VM-based crosstalk can not be efficiently reduced by either preprocessing the input images or by optimizing the polarizing system. Furthermore, we derive the analytic solution for the viewing zone where the entire screen does not have VM-based crosstalk.

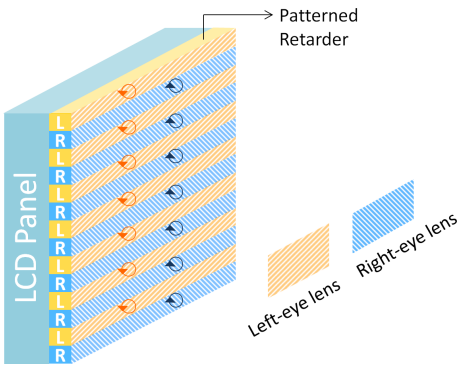

Figure 4.1: Schematic set up of CP LCD with passive glasses.

4.1 Introduction

4.1.1 Achieving 3D in circularly polarized LCD

With the development of the technology in film-type patterned retarder (PR) [LL12], circularly polarized (CP) LCDs with passive glasses are prospering in the 3D market. As illustrated in Fig. 4.1, CP LCD shows the LE and RE images in the odd-row pixels (the LE field of LCD) and the even-row pixels (the RE field of LCD) respectively. On top of every LE pixel row, covers the LE-field PR, which comprises the quarter-wave retarders (QWR) for the LE view. Similarly, on top of every RE pixel row, covers the RE-field PR, which comprises the QWRs for the RE view. The interlacing of the LE and RE QWRs gives rise to PR. The light transmitted through the LE-field PR becomes left-hand (LH) circularly polarized. The light transmitted through the RE-field PR becomes right-hand (RH) circularly polarized. In the passive glasses, the LE lens only transmits light of LH polarization, and the RE lens only transmits light of RE polarization. Thus, the PR and passive glasses are the most critical factors in achieving the separation of LE and RE views in CP LCD. Any issue that causes the light to deviate from the desired polarization will lead to light leakage from the undesired view.

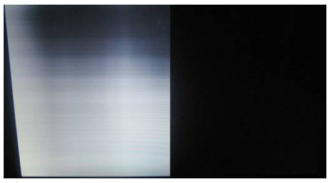

(a) Vertical-misalignment crosstalk.

(b) Polarizing-system crosstalk.

Figure 4.2: Comparison of VM-based crosstalk and the crosstalk induced by the polarizing system, where the level of crosstalk is indicated by the brightness of the screen on the left half.

4.1.2 Vertical misalignment vs. polarizing system in CP LCD

The reason why, in this paper, we focus on vertical misalignment (VM) as the main factor causing crosstalk in CP LCD, is that compared to the other factors, including the polarizing system of CP LCD, VM is the dominant factor that causes very severe crosstalk. The polarizing system of CP LCD which comprises PR and the wave retarder in the passive glasses, has been extensively investigated in [LL12], [HWZ+05], [LL10], [HLW05], [WKL12] concerning crosstalk in CP LCD, while VM is only addressed by a few works [ZN14] and [ZN13].

In [MZN15], it is proved that, even without any phase-compensation scheme, the amount of crosstalk caused by the polarizing system is less than 4%. Furthermore, within low level of crosstalk ($< 5\%$ in [LWH11]), the human visual system (HVS) is still able to fuse the LE and RE images to perceive depth. Thus the crosstalk caused by the polarizing system of CP LCD is rather a type of "3D noise" [BPJ+11] appearing as faint shadows from the other view. However, an increasing level of crosstalk, which is the case of VM-based crosstalk as shown in this paper, hinders the HVS to find the correct correspondences between the LE and RE images [Pat07]. In this case, stereo images are not fused by the HSV [YS90] and objects appear to be double-contoured, as shown in Fig. 1.1. As a result, VM-based crosstalk prevents the perception of depth.

Fig. 4.2 compares the VM-based crosstalk with the crosstalk caused by the

polarizing system in a real CP LCD [Cor09]. In Fig. 4.2, the screen is captured after the left-eye polarized lens; the left-eye input image is black, the right-eye input image is white on the left half and is black on the right half. Thus, the bright areas shown on the left-half screen in Fig. 4.2 (a) and (b) are caused by crosstalk. The right-half screens in Fig. 4.2 (a) and (b) have no crosstalk because the input images in LE and RE channels are black. Fig. 4.2 (a) is resulted from shifting the viewing location vertically with respect to the screen center to induce vertical misalignment of light, and Fig. 4.2 (b) is captured at the viewing location aligned to the screen center (frontal parallel). From Fig. 4.2, we can observe that the crosstalk caused VM is much brighter than the crosstalk caused by the polarizing system.

4.1.3 Related works and organization

So far, not a significant number of works have been done to investigate the issue of VM. [Woo12] only addresses VM by qualitative description. The optical designs in [LL12] and [LL10] can mainly target on reducing crosstalk caused by the polarizing system. The modeling of VM can also be found in [ZN13]. However, [ZN13] requires preknowledge of many intrinsic display parameters. In this paper, we propose a novel calibration method based on least square, which takes only a few pictures of the screen taken at 4 locations, and then solves for CP LCD's intrinsic parameters. A preliminary version of the proposed calibration method can be found in [ZN14] where the calibration method is presented. [ZN14] requires users' input for the calibration which affects the result by the subjective evaluations. This paper changes the users' input into image processing. In addition, this paper provides the detailed derivation of the calibration method, proves mathematically that VM-based crosstalk can not be effectively reduced by the polarizing system, and also presents analytic solution for the viewing zone that is free from the severe crosstalk caused by VM. In [BLBC10], P.B. et al. proposed calibrating CP LCD by using Fourier-optics based device. Compared to the proposed calibration method, the Fourier-optics based device is costly as well

as requiring measurements at many locations.

The remainder of this paper is organized in 5 sections. In Section 4.2, a display model for CP LCD considering VM is proposed. In Section 4.3, the calibration method for the intrinsic parameters of CP LCD is presented with the validation of subjective test. We discuss the cancellation of VM-based crosstalk through the display system in Section 4.4. In Section 4.5, the analytic solution of the VM-free viewing zone is derived. Section 4.7 concludes this work.

4.2 Display model considering VM

4.2.1 VM characterization

The mechanism of VM is shown in Fig. 4.3(a). Before light is transmitted through PR, the LE-field and RE-field lights have the same polarization. It is PR that turns the LE-field and RE-field lights into orthogonal polarization. However, as shown in Fig. 4.3(a), due to the spacing between the LC panel and PR for modules such as color filter (CF), glass substrate and LP, when the incident angle shifts vertically, some portion of the light is transmitted through the undesired field of PR. Fig. 4.3(a) shows that, at normal incident angle, the LE-field light ray (emitted from the LC unit labeled with "L"), which is completely transmitted through the LE PR (PR unit labeled with "L"), is in LH circular polarization. If some portion of the light ray is transmitted through the RE PR (PR unit labeled with "R"), the addition of the LH and RH polarization leads to partially polarized light or unpolarized light. If the LE-field light is transmitted completely through the RE PR, it turns into RH circular polarization. VM occurs in the RE field in a similar way. To characterize VM, we define indices hit and $miss$ in Eq. (4.1), as the percentage of light transmitted in the desired and undesired PR respectively. Note that $hit + miss = 1$.

$$\begin{bmatrix} hit \\ miss \end{bmatrix} = \frac{1}{emitted\ light} \cdot \begin{bmatrix} light\ from\ the\ desired\ PR \\ light\ from\ the\ undesired\ PR \end{bmatrix} \tag{4.1}$$

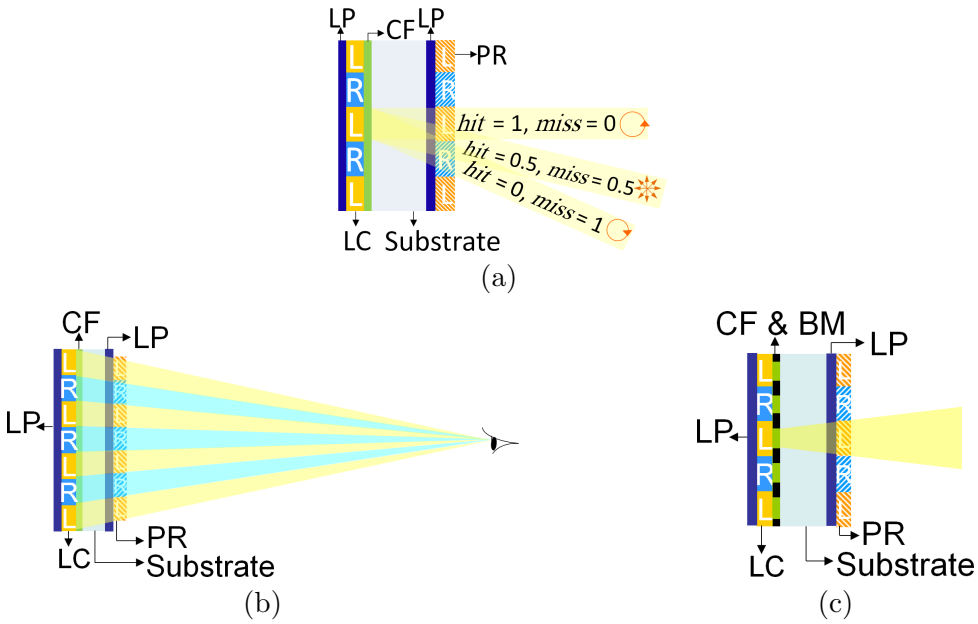

Figure 4.3: Issue of vertical misalignment (VM) of light in CP LCD and its mitigations.

Two methods are widely adopted to mitigate VM:

- Reduce the size of the PR module and shift it w.r.t the LC panel, such that the entire screen is VM-free within certain viewing zone [Woo12] (Fig. 4.3(b)).
- Insert black matrix (BM), comprised of horizontal black strips, in the CF layer to absorb some portion of the vertically misaligned light ray [YUT08] (Fig. 4.3(c)).

Nevertheless, severe VM-based crosstalk still presents in CP LCD especially when the viewing location deviates vertically away from the screen center. Fig. 4.2 compares crosstalk induced by the polarizing system of CP LCD, which is shown in Fig. 4.2(a), and crosstalk resulted from VM in CP LCD, which is shown in Fig. 4.2(b). The input images in Fig. 4.2(a), (b) are the same (see the caption of Fig. 4.2 for details). All the real-display demonstrations in this paper are on LG 47LH55 (1080p) [Cor09], which is $58.5cm \times 104.0cm$ ($h \times w$). The viewing location in Fig. 4.2(a) is vertically aligned to the screen center to eliminate VM-based crosstalk. The viewing location in Fig. 4.2(b) is aligned to the upper edge of the screen such that VM-based

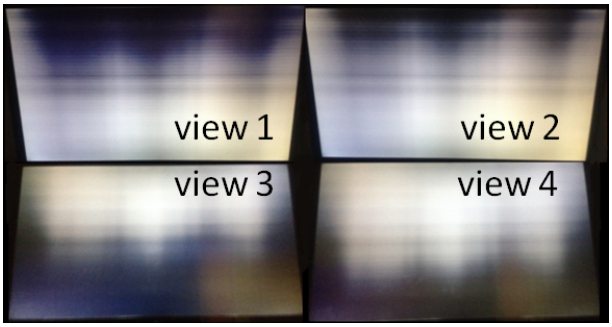

Figure 4.4: Real CP LCD [Cor09] at different viewing locations: *view*1-*view*4. The screen is captured after the left-eye lens. The left-eye input image is black and the right-eye input image is white.

crosstalk shows. The viewing distance in Fig. 4.2(a), (b) is $1m$. The brightness shown on the left half of the screen in Fig. 4.2 is resulted from crosstalk, and it increases with crosstalk. We can observe from Fig. 4.2 that when VM-based crosstalk is present, it's much more dominant than that caused by the polarizing system. Besides, the dark area shown in Fig. 4.2(b) is the result of the absorption of light from the black matrix. Apart from the severity of VM-based crosstalk, its spatial distribution on the screen is sensitive to the viewing location along the vertical direction. Fig. 4.4 shows images of a real CP LCD [Cor09] observed from 4 different viewing locations denoted as *view*1-*view*4. *view*1: aligned to screen top edge at distance $1m$, *view*2: aligned to screen top edge at distance $0.8m$, *view*3:aligned to screen bottom edge at distance $1m$, *view*4: aligned to screen bottom edge at distance $0.8m$. The bright areas shown on the screen in Fig. 4.4 indicate crosstalk caused by VM, and the dark areas arise from the absorption of light by BM. We can observe from Fig. 4.4 that the crosstalk-prominent area moves with the viewing location. Due to the severity and mobility of VM-based crosstalk, the comfortable viewing zone where no severe crosstalk presents is significantly limited in the vertical direction.

4.2.2 The display model

The relationship between the luminance input and output of CP LCD can be expressed as:

$$\begin{bmatrix} L_o(i,j) \\ R_o(i,j) \end{bmatrix} = \begin{bmatrix} t_{LL} & t_{LR} \\ t_{RL} & t_{RR} \end{bmatrix} \begin{bmatrix} L_{in}(i) \\ R_{in}(j) \end{bmatrix} \tag{4.2}$$

In Eq. (4.2) [ZN14], $L_{in}(i)$ and $R_{in}(j)$ are the luminance in the input images in the LE and RE channels respectively, $L_o(i,j)$ and $R_o(i,j)$ are the luminance after the polarized glasses in the LE and RE channels respectively. i and j in Eq. (4.2) are the grayscale levels of the LE and RE input images respectively. The 2x2 matrix on the RHS in Eq. (4.2) is the display transmittance matrix (TM). t_{LL} in TM is the transmittance of the LE pixel in the LE view, t_{LR} in TM denotes the transmittance of the RE pixel in the LE view. Similarly, the entries t_{LR} and t_{RL} in TM are defined. The entries of transmittance in TM in Eq. (4.2) range from 0 to 1. Eq. (4.2) shows that the display has no crosstalk if TM is diagonal. Extending from Eq. (1.1), to combine the display model in Eq. (4.2), the LE and RE crosstalk can be expressed as [MZN15]:

$$crosstalk_L = \frac{t_{LR}}{t_{LL}} = \frac{S_{LL0} \times miss + S_{LR0} \times hit}{S_{LL0} \times hit + S_{LR0} \times miss} \tag{4.3}$$

$$crosstalk_R = \frac{t_{RL}}{t_{RR}} = \frac{S_{RL0} \times hit + S_{RR0} \times miss}{S_{RL0} \times miss + S_{RR0} \times hit} \tag{4.4}$$

Let us first consider the simplified display which has no issue of VM. Fig. 4.5 shows the 4 possible light paths considering the polarizing system of CP LCD only. We use Mueller calculus (MC) [YW06] to model CP LCD's polarizing system as illustrated in Fig. 4.5. In MC, the polarization state of light is characterized by the 4x1 Stokes vector [YW06], denoted as $\mathbf{S}$, where the first entry S_0 is intensity (normalized luminance in this paper). The optical modules (such as LP and wave retarder) are characterized by the 4x4 Muller matrix, denoted as $\mathbf{M}$. The details of the $\mathbf{M}$s for LP, LC and PR can be found in [LL10] and [YW06]. When light is transmitted through

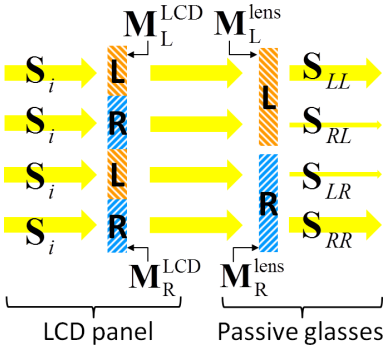

Figure 4.5: 4 types of light paths in the polarizing system of CP LCD.

an optical module, the Stokes vector of the light is left multiplied with the corresponding Mueller matrix. The left-most "LCD panel" in Fig. 4.5 is the composition of all the optical modules in CP LCD before PR. Components such as LC, the back and front LPs are included in "LCD panel". Since lights from the LE and RE fields of the monitor have the same polarization before they are transmitted through the PR, we can denote their Stokes vectors as $\mathbf{S}_i$ (as shown in Fig. 4.5). Furthermore, we assume $\mathbf{S}_i = [1, 1, 0, 0]^T$, which is horizontally polarized with luminance 1 (normalized intensity). Consequently, the minor changes in luminance and polarization after the LCD panel [ZGW06] are ignored, and the resulted output luminance after the polarized glasses is by definition the transmittance of the display. As shown in Fig. 4.5, the Stokes vector of the light signal from the LE field of the monitor transmitted after the LE lens is denoted as S_{LL}, and that from the LE field of the monitor transmitted after the RE lens is denoted as $\mathbf{S}_{RL}$. In the same way, we define $\mathbf{S}_{LR}$ and $\mathbf{S}_{RR}$.

$$\begin{pmatrix} \mathbf{S}_{LL} \\ \mathbf{S}_{LR} \\ \mathbf{S}_{RL} \\ \mathbf{S}_{RR} \end{pmatrix} = \begin{pmatrix} \mathbf{M}_L^{lens} \\ \mathbf{M}_L^{lens} \\ \mathbf{M}_R^{lens} \\ \mathbf{M}_R^{lens} \end{pmatrix} \mathbf{M}_{Rot}(\theta_{rot}) \begin{pmatrix} \mathbf{M}_L^{PR} \\ \mathbf{M}_R^{PR} \\ \mathbf{M}_L^{PR} \\ \mathbf{M}_R^{PR} \end{pmatrix} \mathbf{S}_{in} \tag{4.5}$$

$$\begin{bmatrix} t_{LL} & t_{LR} \\ t_{RL} & t_{RR} \end{bmatrix} = \begin{bmatrix} S_{LL0} & S_{LR0} \\ S_{RL0} & S_{RR0} \end{bmatrix} \begin{bmatrix} hit & miss \\ miss & hit \end{bmatrix} \tag{4.6}$$

The next step is to include VM into the display model. Considering a light ray emitted from the LE field of the monitor before this transmission through the PR. By the definition of *hit* and *miss* in Eq. (4.1), the portion of this light ray transmitted through the LE PR first and then transmitted after the LE lens has the Stokes vector (SV): $hit \times \mathbf{M}_L^{PR}\mathbf{M}_L^{lens}\mathbf{S}_{in} = hit \times S_{LL}$. Similarly, the portion of this light ray that's misaligned to the RE PR and then transmitted through the LE lens has the Stokes vector: $hit \times \mathbf{M}_L^{PR}\mathbf{M}_R^{lens}\mathbf{S}_{in} = hit \times S_{LR}$. Therefore, the Stokes vector of this LE-field light ray transmitted through the LE lens becomes $hit \times \mathbf{S}_{LL} + miss \times \mathbf{S}_{LR}$. In the same way, the SV of a LE-field light ray transmitted through the RE lens is $hit \times \mathbf{S}_{RL} + miss \times \mathbf{S}_{RR}$; the SV of a RE-field light transmitted through the LE lens is $hit \times \mathbf{S}_{LR} + miss \times \mathbf{S}_{LL}$; the SV of a RE-field light transmitted through the RE lens is $hit \times \mathbf{S}_{RR} + miss \times \mathbf{S}_{RL}$. Writing the aforementioned the SV outputs into matrix form, the transmittance matrix of the display can be expressed as shown in Eq. (4.6). Since only luminance is concerned in transmittance, only the first entries of the SVs are used in Eq. (4.6).

We can observe from Eq. (4.6) that even when the polarizing system is ideal, crosstalk increases significantly with *miss*. Since RHS matrices in Eq. (4.6) are constrained to have non-negative entries: entries in the left matrix quantity are luminance and those in the right matrix quantity are ratios between 0 and 1, to result in a crosstalk-free TM, the two RHS matrices have to be both diagonal.

4.3 Display Calibration for VM

To calculate *hit* and *miss*, the intrinsic display parameters which are shown in Fig. 4.6 need to be calibrated. h_p in Fig. 4.6 is pixel height, which can be calculated from the screen size and display resolution. For LG 47LH55 [Cor09], $h_p = 58.5cm/1080 \approx 541.9\mu m$. h_{BM} in Fig. 4.6 is BM unit's height. Estimated under the magnifier, $h_{BM} = \frac{1}{3}h_p = 180.6\mu m$ [Cor09]. The other display parameters

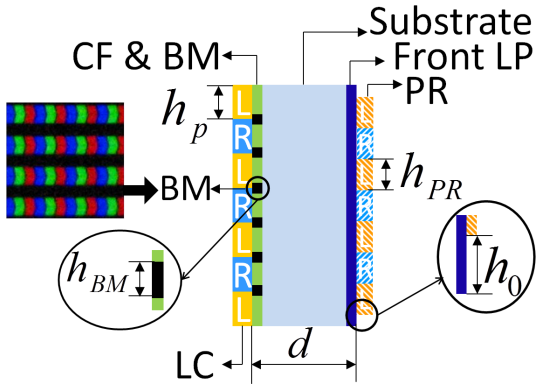

Figure 4.6: Illustration of the intrinsic display parameters to characterize vertical misalignment in CP LCD.

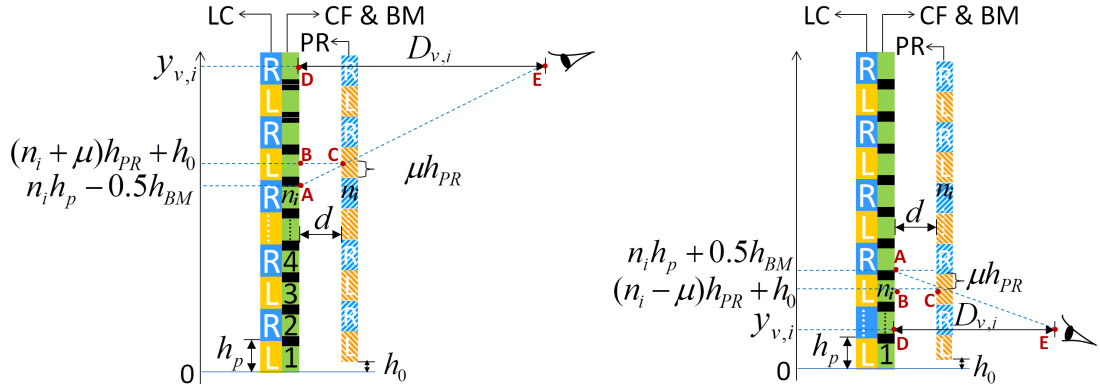

(a) Viewing from high position.

(b) Viewing from low position.

Figure 4.7: Schematic cross section of LC panel, CF and BM layer, PR with different viewing locations.

shown in Fig. 4.6 are h_{PR}: the PR unit's height, h_0: the vertical shift between the LC and PR modules, and d: the spacing between the LC and PR. However, h_{PR}, h_0 and d are difficult to acquire, and no previous work has been done in calibrating the intrinsic display parameters of CP LCD to model VM. In the remainder of this section, we propose a novel calibration method to estimate these unknown parameters. The preliminary version of this method can be found in our published work [ZN14].

Assume the LE input image is black and the RE input image is white, and the screen is observed after the LE lens, Fig. 4.7(a) illustrates the viewing condition where the screen is observed from a high position (above the screen center). In this case, the RE (white) pixels, whose indices are greater than n_i, are transmitted through

the RE-field (desired) PR (or $miss = 0$), and thus in RH polarized, whereas, the RE pixels, whose indices are smaller than n_i, have positive overlap with the LE-field (undesired) PR (or $miss > 0$), and they deviate from RH polarization. Subscript i of n_i denotes the i^{th} observation used for display calibration (will be explained later). As demonstrated in $view1$ and $view2$ of Fig. 4.4, the black-channel view of the real CP LCD (1080p) [Cor09] is dark (VM-free) in the upper part and bright (VM-present) in the lower part observed from high viewing locations. Another viewing condition is illustrated in Fig. 4.7(b), where the screen is observed from a low position (below the screen center) in the LE channel. In this case, the RE (white) pixels, whose pixel indices are smaller than n_i, are transmitted through the RE-field (desired) PR ($miss = 0$), and thus in RH polarization, whereas, the RE pixels, whose indices are greater than n_i, have positive overlap with the LE-field (undesired) PR ($miss > 0$), and they deviate from RH polarization. In $view3$ and $view4$ in Fig. 4.4, the black-channel view of the real CP LCD is dark (VM-free) in the lower part and bright (VM-present) in the upper part observed from low viewing locations.

Consequently, by setting the input image for one eye black and that for the other eye white, the screen observation in the black-image channel is highly dependent on the display's intrinsic parameters and the viewing location. Therefore, we can calculate h_{PR}, h_0 and d from screen observation. As shown in Fig. 4.7(a), A is the starting point of VM, E is the viewing location, the light from A transmits PR toward the viewer through C, B and D are respectively projections of C and E on the $CF\&BM$ layer, and $D_{v,i}$ is the viewing distance of the i^{th} observation for display calibration. By definition, $BC = d$, and $DE = D_{v,i}$. Because $BC \parallel DE$, we have $\triangle ABC \sim \triangle ADE$. Similarly, $\triangle ABC \sim \triangle ADE$ also holds in Fig. 4.7(b). With the expressions of Y-axis values of A-E as shown in Fig. 4.7, we can write the relationship $\frac{BC}{AB} = \frac{DE}{AD}$ as shown in Fig. 4.7, into:

$$\frac{d}{(\mu \pm n_i)h_{PR} \mp n_i h_p \pm h_0 + 0.5h_{BM}} = \frac{D_{v,i}}{\pm y_{v,i} \mp n_i h_p + 0.5h_{BM}} \tag{4.7}$$

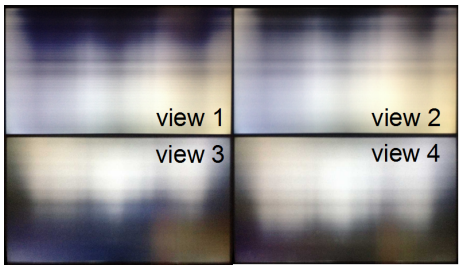

(a) Pictures of the screen.

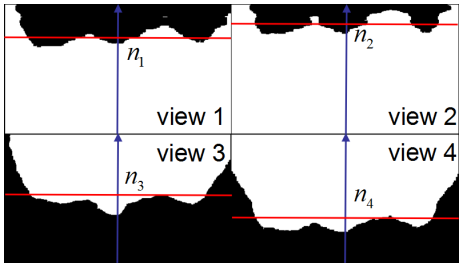

(b) Binarized screen pictures with dividing lines.

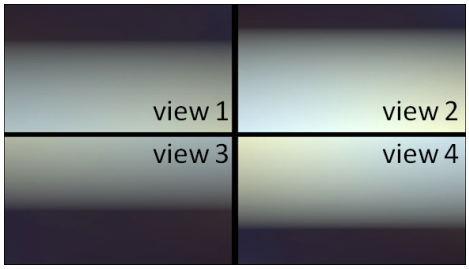

(c) Simulations of the screen.

Figure 4.8: Proposed calibration method for the display intrinsic parameters and simulation results.

where $y_{v,i}$ is location of the viewer measured vertically. In Eq. (4.7), $\pm$ takes $+$, and $\mp$ takes $-$ if the VM-present area appears at the lower part of the screen ($view1$ and $view2$ in Fig. 4.4, also Fig. 4.7(a)), and vice versa if the VM-present area is at the upper part of the screen ($view3$ and $view4$ in Fig. 4.4, also Fig. 4.7(b)). To solve for the 3 unknowns (h_{PR}, h_0 and d), we need at least 3 of Eq. (4.7) resulted from 3 distinct viewing locations. To improve the accuracy, 4 viewing locations are used in this paper. The procedure of the calibration method based on Eq. (4.7) is as follows:

(1) Set the input image in the LE channel black RE channel white. Then screen photos are taken after the LE lens from 4 (or more) distinct viewing locations, and record the vertical position $y_{v,i}$ and the distance $D_{v,i}$ of each viewing location. Note that at each viewing location, both the bright and dark regions must appear on the screen (like Fig. 4.4). Then transform these images into orthographic views by Homography transform [Ma04] as shown in Fig. 4.8(a).

(2) Binarize the screen images. As shown in Fig. 4.8(b), the white region is classified by white pixels and the dark region is classified by black pixels. This binary

classification is achieved by k-means method (where k=2) implemented in the histogram of the gray image. Furthermore, to get rid of the noise, we operate imageclose.

(3) Find the dividing lines of the dark and bright regions. For the case where the dark region is above the bright region (view 1 and 2 in Fig. 4.8), the dividing line is found by averaging the vertical location of the black pixels with the maximum column index (lowest location) in all pixel columns. For the case where the dark region is below the bright region (view 3 and 4 in Fig. 4.8), the dividing line is found by averaging the vertical location of the black pixels with the minimum column index (highest location) in all pixel columns. However, due to manufacture defects, the left and the right edges of the screen is significantly inconsistent with central main part of the screen, and this affects the accuracy of the dividing line. To mitigate this, initially, we calculate the initial location of the dividing line. Furthermore, for the case where the dark region is above the bright region, we measure the distance between the lowest black pixel and the dividing line. Moreover, for the case where the dark region is below the bright region, we measure the distance between the highest black pixel and the dividing line. Finally, we average the black pixel location again by neglecting the pixels that exceed the aforementioned distance. We denote the pixel indices of the 4 dividing lines in Fig. 4.8(b) by n_i, where $i = 1, 2, 3, 4$.

(4) Plug into Eq. (4.7) the values of $D_{v,i}$, $y_{v,i}$ and n_i, where $i = 1, 2, 3, 4$, to obtain 4 equations. Then, by formulating these 4 equations into matrix form, the unknown parameters can be solved from the following least-square (LS) problem:

$$\mathbf{p} = \left(\mathbf{A}^T\mathbf{A}\right)^{-1}\mathbf{A}^T\mathbf{b} \tag{4.8}$$

where $\mathbf{p}$ is the vector of the unknown parameters:

$$\mathbf{p} = [h_{\mathrm{PR}}, \quad h_0, \quad d]^T \tag{4.9}$$

Matrix $\mathbf{A}$ in Eq. (4.8) is:

$$\mathbf{A} = \begin{bmatrix} (\mu \pm n_1)\, D_{v,1} & \pm D_{v,1} & \pm n_1 \mp y_{v,1} - 0.5 h_{BM} \\ (\mu \pm n_2)\, D_{v,2} & \pm D_{v,2} & \pm n_2 \mp y_{v,2} - 0.5 h_{BM} \\ (\mu \pm n_3)\, D_{v,3} & \pm D_{v,3} & \pm n_3 \mp y_{v,3} - 0.5 h_{BM} \\ (\mu \pm n_4)\, D_{v,4} & \pm D_{v,4} & \pm n_4 \mp y_{v,4} - 0.5 h_{BM} \end{bmatrix} \tag{4.10}$$

where each row is resulted from one screen observation. Vector $\mathbf{b}$ in Eq. (4.8) is:

$$\mathbf{b} = \begin{bmatrix} \pm n_1 h_p D_{v,1} - 0.5 h_{BM} D_{v,1} \\ \pm n_2 h_p D_{v,2} - 0.5 h_{BM} D_{v,2} \\ \pm n_3 h_p D_{v,3} - 0.5 h_{BM} D_{v,3} \\ \pm n_4 h_p D_{v,4} - 0.5 h_{BM} D_{v,4} \end{bmatrix} \tag{4.11}$$

For each row of $\mathbf{A}$ (Eq. (4.10)) and $\mathbf{b}$ (Eq. (4.11)), $\pm$ takes $+$ and $\mp$ takes $-$ if the bright area is below the dark area in the screen observation ($view1$ and $view2$ in Fig. 4.4, also Fig. 4.7(a)), and vice versa if the bright area is above the dark area ($view3$ and $view4$ in Fig. 4.4, also Fig. 4.7(b)).

After display calibration, hit and $miss$ can be computed by projecting the light ray emitted from the $CF\&BM$ layer on the PR plane, and calculating the overlapping portions of the light with the desired and undesired field of PR respectively. Note that the pixels in the same row have the same values of hit and $miss$. Fig. 4.8(b) shows the simulation results compared with the real CP LCD [Cor09] as shown in Fig. 4.8(a). We can observe that the brightness patterns of the simulation match correctly with those in the real CP LCD, except that the nonsmooth brightness in the real CP LCD which is caused by the manufacturing deficiency (we ignore this in the VM modeling). In addition, Fig. 4.7 shows that the blue and orange shades in the real CP LCD are also captured by the simulation. This color shift is caused by the polarizing system of CP LCD, whose modeling can be found in [MZN15]. From the calibration shown in Fig. 4.3(b), the resulted display parameters are $h_{\mathrm{PR}} = 541.82\mu m$, $h_0 = 40.6\mu m$, and $d = 384.7\mu m$. Fig. 4.9 demonstrates the robustness of the proposed

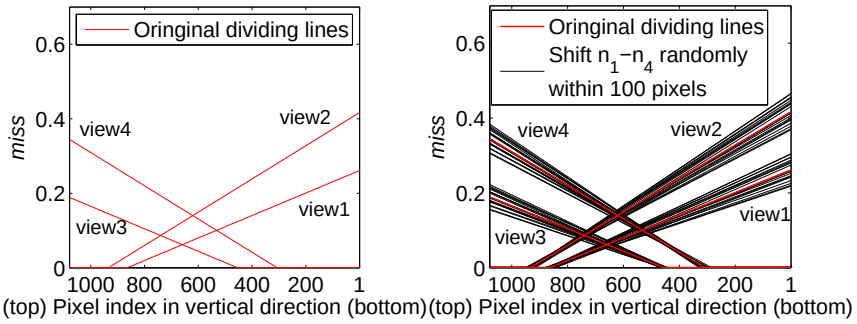

Figure 4.9: Test of robustness of the proposed calibration method. Left: *miss* resulted from the original input n_1-n_4 in Fig. 4.8. Right: 20 cases of *miss* after shifting n_1-n_4 randomly together within 100 pixels.

(a) Observing-eye image. (b) Blocked-eye image.

Figure 4.10: Subjective test on crosstalk caused by vertical misalignment (VM) of light in CP LCD. (a) and (b) are input images.

calibration method by showing the simulated *miss* after inducing variations in the original dividing lines. The x-axis values of the red crosses in (a) show n_1-n_4 from Fig. 4.8(b). The horizontal axis in Fig. 4.9 increases with the vertical pixel index. Note that the column-wise *miss* in Fig. 4.9 is sufficient to represent the entire screen. We can observe that the results change insignificantly against the input variation. In fact, increasing the accuracy of the estimated intrinsic display parameter will be further improved by increasing the number of distinct screen observations.

Fig. B.1 (in **Appendix B**) shows the comparison between the screen pictures at another ground of viewing locations and the corresponding simulations where the aforementioned intrinsic display parameters calculated by the proposed calibration method are used. We can observe from Fig. B.1 that, apart from the uneven brightness due to manufacture defects, the real display and the simulation are consistent with each other. This indicates that the calculated intrinsic display parameters result in valid output.

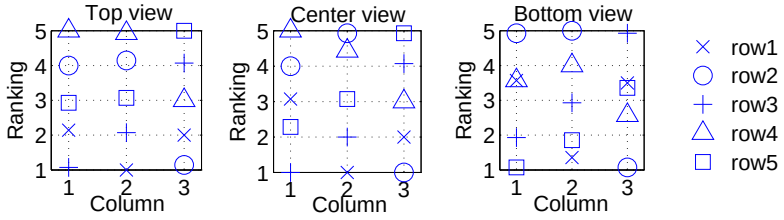

(a) Subjective rankings of the square sequences.

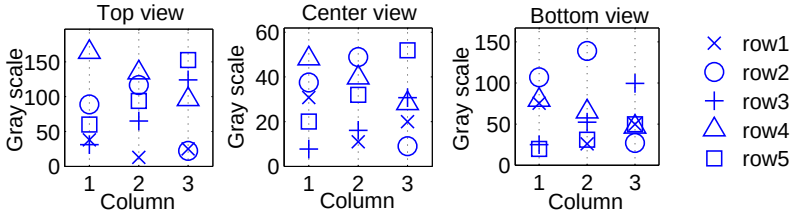

(b) Simulated grayscale levels of the square sequences.

Figure 4.11: Results of subjects' rankings of the crosstalk intensity compared with simulation results from the proposed modeling. The simulation results of crosstalk intensity are represented by graylevel scales.

Furthermore, to validate the proposed calibration method in a quantitative way, we carry out subjective test among 16 participants. The ages of the subjects range from 20 to 50, and 3 are females, 13 are males. During the test, each subject observes the CP LCD with his/her preferred eye after the corresponding 3D lens, and the other eye of the viewer is blocked. Fig. 4.10(a) and (b) show the input images, where the observing-eye input image is black (excluding the aiding text), and the block-eye input image has 3 columns of squares. The grayscale levels of the squares in the blocked-eye image (as shown in Fig. 4.10(b)) are random. From $row1$ to $row5$, these grayscale levels are:

- column 1: 150, 200, 50, 255, 100.
- column 2: 100, 50, 250, 100, 200.
- column 3: 100, 50, 200, 150, 255.

Because of crosstalk, the squares in the blocked-eye image also appears in the observing-eye view. Moreover, since spatial distribution of the crosstalk induced by VM changes with the vertical location of the viewer (as shown in Fig. 4.4), the brightness of the

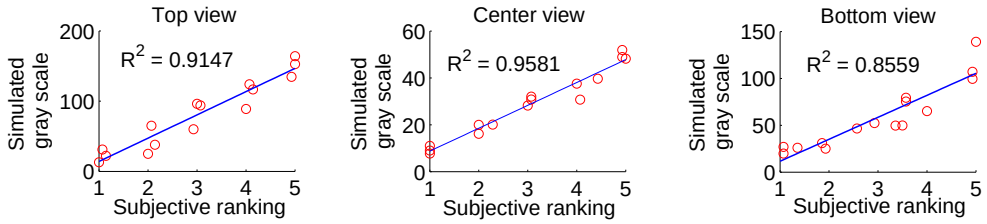

Figure 4.12: Correlation between subjective ranking and simulation results measured by R^2 coefficient of determinanation.

squares perceived in the observing-eye channel also changes as the viewing location shifts up and down. Consequently, the accuracy of our VM model can be validated by comparing the subjects' perception of brightness with the grayscale level predicted from the model.

During the subjective test, each subject observes the screen [Cor09] from 3 viewing locations: vertically aligned to the screen top edge (top view), vertically aligned to the screen center (center view), and vertically aligned to the screen bottom edge (bottom view). The viewing distance for these 3 views is $1m$. At each viewing location, the subject ranks within every column sequence from the brightest square (rank 5) to the darkest (rank 1) square. Fig. 4.11 show the results of the subjective rankings and our prediction in terms of grayscale levels respectively. The input stereo images for subjective test are shown in Fig. 4.10. Fig. 4.11(a) shows subjective rankings of brightness for each column sequence (rank $5-1$: brightest through darkest) averaged among the 16 subjects. Fig. 4.11(b) shows simulated grayscale levels of each sequence resulted from the proposed calibration method. We observe from the subjective rankings in Fig. 4.11(c) that within each column sequence, the order of the perceived brightness among the squares varies when the vertical viewing level changes. In addition, this change of order is also predicted in the simulated grayscale levels of the squares. As shown in Fig. 4.11(a) and (b), the orderings of grayscale levels in each column from model prediction mostly matches the orderings of the perceived brightness from human observation. However, the latter shows greater brightness distinctions than the former. One of the reasons is that the subjects only make 5

rankings which highly quantized the brightness perception. The other reason can be the manufacturing deficiency which caused nonuniform light distribution as shown in Fig.4.4. In Fig. 4.12, the subjective rankings and model predictions are plotted in the same graph with their linear fittings (from least square). The R^2 coefficients ($R^2 = 1$ when observation and model prediction is totally correlated) in Fig. 4.12 suggest better that the model predictions for the top and center views agree better with human observations than those for the bottom view. One reason for this is that from the bottom view, the squares have similar brightness: $row1$, $row4$ and $row5$ in $column3$ at bottom view, the effect of quantization (and even error) in the subjective ranking is more significant.

Fig. B.2 (in **Appendix B**) shows the LE-view simulations of natural images at two different viewing locations compared with the real CP LCD [Cor09]. We can observe that the proposed display model accurately predicts the display output in terms of the visibility and spatial distribution of crosstalk. It shows in both simulation and the real display that crosstalk in the top view appears mainly in the lower half of the image, while crosstalk in the bottom view is more visible in the upper half of the image caused by VM. Consider "Books" [SP07] in Fig. B.2 for example, the book entitled with "Computer Vision" shows limited crosstalk along its left edge in the top view while a prominent white shadow is observed in the bottom view.

4.4 Crosstalk Reduction considering VM

Since severe crosstalk occurs with VM, crosstalk reduction methods based on luminance compensation [LW94] will induce significant contrast loss. Moreover, because VM-based crosstalk changes with the viewing location, head tracking is required to update the compensation parameters (and this method fails for multiple viewers scenario). In this section, the reduction of VM-based crosstalk is discussed for both the conventional and unconventional display systems.

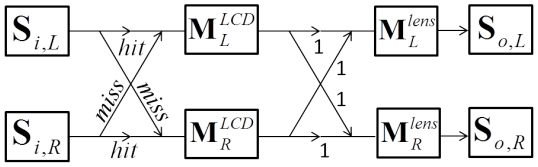

Figure 4.13: System diagram of the display with the issue of vertical misalignment.

Fig. 4.13 shows the system diagram of the display with the issue of VM where the upper and the lower channels are LE and RE respectively, where the upper band is left-eye channel; Lower band is right-eye channel; Left crossed path is vertical misalignment in the LCD panel; Right crossed path is light propagation from the undesired eye channels to 3D glasses. In Fig. 4.13, $\mathbf{S}_{i,L}$ and $\mathbf{S}_{i,R}$ denote the Stokes vectors (SV) of the light in the LE and RE channels respectively before VM occurs; $\mathbf{M}_L^{LCD}$ and $\mathbf{M}_L^{LCD}$ denote the Muller matrices (MM) of all optical modules after VM occurs. Consider the conventional display configuration in Fig. 4.3, $\mathbf{M}_L^{LCD} = \mathbf{M}_L^{PR}$, and $\mathbf{M}_L^{LCD} = \mathbf{M}_R^{PR}$. $\mathbf{M}_L^{lens}$ and $\mathbf{M}_R^{lens}$ are MMs of LE and RE lenses respectively. The upper band and lower band of Fig. 4.13 are the LE and RE light paths without crosstalk. The two crossed paths in Fig. 4.13 induces crosstalk. The left crossed path in Fig. 4.13 with coefficient $miss$ represents the vertically misaligned light signal. The right crossed path with coefficient 1 represents the light signal that propagates from the unintended channel of the monitor to the 3D lens (such as the RE pixel viewed after the LE lens). Notice that without the VM crossed path, the system in Fig. 4.13 reduces to the polarizing system of CP LCD in Fig. 4.5.

We apply crosstalk definition in Eq. (1.1) in the following analysis. From Fig. 4.13, the LE *signal* can be calculated by tracing all light paths starting from $\mathbf{S}_{i,L}$ ending at $\mathbf{M}_L^{lens}$, and the LE *leakage* can be calculated by tracing all light paths that start from $\mathbf{S}_{i,R}$ and end at $\mathbf{M}_L^{lens}$. Eq. (4.12), (4.13) show the expressions of LE *signal* and *leakage* respectively:

$$hit \cdot \mathbf{M}_L^{\text{lens}} \cdot \mathbf{M}_L^{LCD} \cdot \mathbf{S}_{i,L} + miss \cdot \mathbf{M}_L^{lens} \cdot \mathbf{M}_R^{LCD} \cdot \mathbf{S}_{i,L} \tag{4.12}$$

$$miss \cdot \mathbf{M}_L^{lens} \cdot \mathbf{M}_L^{LCD} \cdot \mathbf{S}_{i,R} + hit \cdot \mathbf{M}_L^{lens} \cdot \mathbf{M}_R^{LCD} \cdot \mathbf{S}_{i,R} \tag{4.13}$$

Similarly, the RE *signal* and *leakage* in Fig. 4.13 are shown in Eq. (4.14), (4.15) respectively:

$$hit \cdot \mathbf{M}_R^{\text{lens}} \cdot \mathbf{M}_R^{LCD} \cdot \mathbf{S}_{i,R} + miss \cdot \mathbf{M}_R^{lens} \cdot \mathbf{M}_L^{LCD} \cdot \mathbf{S}_{i,R} \tag{4.14}$$

$$miss \cdot \mathbf{M}_R^{lens} \cdot \mathbf{M}_R^{LCD} \cdot \mathbf{S}_{i,L} + hit \cdot \mathbf{M}_R^{lens} \cdot \mathbf{M}_L^{LCD} \cdot \mathbf{S}_{i,L} \tag{4.15}$$

In the conventional CP LCD configuration as shown in Fig. 4.3, the LE and the RE signals are in the same polarization before VM occurs, namely, $\mathbf{S}_{i,L} = \mathbf{S}_{i,R} = \mathbf{S}_i$. To simplify the expression, let $\mathbf{S}_{LL} = \mathbf{M}_L^{lens}\mathbf{M}_L^{LCD}\mathbf{S}_i$, and $\mathbf{S}_{LR} = \mathbf{M}_L^{lens}\mathbf{M}_R^{LCD}\mathbf{S}_i$. Consequently, the problem of reducing the LE-view *crosstalk* can be formulated as:

$$\begin{aligned} \underset{S_{LL},S_{LR}}{\text{minimize}} \frac{miss \cdot (\mathbf{S}_{LL})_1 + hit \cdot (\mathbf{S}_{LR})_1}{hit \cdot (\mathbf{S}_{LL})_1 + miss \cdot (\mathbf{S}_{LR})_1} \\ = \frac{miss}{hit}, \text{when } \mathbf{S}_{LR} = \mathbf{0} \end{aligned} \tag{4.16}$$

where subscript 1 denotes the first entry of the resulted SV. The optimal value of Eq. (4.16) is $\frac{miss}{hit}$ acquired at $\mathbf{S}_{LR} = \mathbf{0}$ (and $\mathbf{S}_{LL} \neq \mathbf{0}$). In other words, when VM occurs, the minimum crosstalk in the conventional CP LCD configuration is achieved when the transmission of the RE-field light in the LE lens is 0. Similarly, from Fig. 4.13, the minimum *crosstalk* in the RE channel is also $\frac{miss}{hit}$ when the RE lens entirely blocks lights from the LE field: $\mathbf{S}_{RL} = \mathbf{0}$. Many methods [LL12], [HHS10], [ZN14], [MZN15] have been proposed to minimize $\mathbf{S}_{LR}$ and $\mathbf{S}_{RL}$. However, as shown in Fig. 4.9, the value of $\frac{miss}{hit}$ is large when VM occurs. Therefore, optimizing the polarizing system in conventional CP LCD can not efficiently reduce VM-based crosstalk.

Consequently, let's consider the case of unconventional CP LCD, where $\mathbf{S}_{i,L} \neq \mathbf{S}_{i,R}$. In other words, lights in the LE and the RE channels are in different polarization status before VM occurs. Note that this does not hold for the currently available CP LCDs.

Eq. (4.17a)-(4.17h) are obtained from minimizing *crosstalk* in Eq. (4.3), (4.4). Eq. (4.17a), (4.17b) are resulted from maximizing the LE *signal* as shown in Eq. (4.12), while Eq. (4.17c), (4.17d) are resulted from maximizing the RE *signal* as shown in

Eq. (4.14). Eq. (4.17e), (4.17f) arise from minimizing the LE *leakage* as shown in Eq. (4.13)), while Eq. (4.17g), (4.17h) arise from minimizing the RE *leakage* as shown in Eq. (4.15). In Eq. (4.17a)-(4.17d), the SVs on the LHS are in the range space of the corresponding matrices on the RHS, whereas the SVs on the LHS of Eq. (4.17e)-(4.17h) are in the null space of the corresponding matrices on the RHS.

$$\mathbf{S}_{i,L} \in \mathcal{R}\left(\mathbf{M}_L^{lens}\mathbf{M}_L^{LCD}\right) \tag{4.17a}$$

$$\mathbf{S}_{i,L} \in \mathcal{R}\left(\mathbf{M}_L^{lens}\mathbf{M}_R^{LCD}\right) \tag{4.17b}$$

$$\mathbf{S}_{i,R} \in \mathcal{R}\left(\mathbf{M}_R^{lens}\mathbf{M}_R^{LCD}\right) \tag{4.17c}$$

$$\mathbf{S}_{i,R} \in \mathcal{R}\left(\mathbf{M}_R^{lens}\mathbf{M}_L^{LCD}\right) \tag{4.17d}$$

$$\mathbf{S}_{i,L} \in \mathcal{N}\left(\mathbf{M}_R^{lens}\mathbf{M}_L^{LCD}\right) \tag{4.17e}$$

$$\mathbf{S}_{i,L} \in \mathcal{N}\left(\mathbf{M}_R^{lens}\mathbf{M}_R^{LCD}\right) \tag{4.17f}$$

$$\mathbf{S}_{i,R} \in \mathcal{N}\left(\mathbf{M}_L^{lens}\mathbf{M}_R^{LCD}\right) \tag{4.17g}$$

$$\mathbf{S}_{i,R} \in \mathcal{N}\left(\mathbf{M}_L^{lens}\mathbf{M}_L^{LCD}\right) \tag{4.17h}$$

As a brief review of MM, the MM of LP is rank-1 matrix [YW06], and the MM for wave retarder is rank-4 matrix (wave retarder only modulates the polarization but not the intensity of light). In fact, in CP LCD, at least one LP is required in the LE and RE channels, because otherwise the display becomes nondiscriminative of the LE and RE images. Subsequently, the results of the matrix multiplications on the RHS of Eq. (4.17a)-(4.17h) are rank-1 matrices.

Next, we analyze the SVs in Eq. (4.17a)-(4.17h). Considering Eq. (4.17a), (4.17h), in order that $S_{i,L}$ and $S_{i,R}$ are in the range space and the null space of $\mathbf{M}_L^{lens}\mathbf{M}_L^{LCD}$ respectively, $\mathbf{S}_{i,L}$ must be orthogonal to $\mathbf{S}_{i,R}$ (or $\mathbf{S}_{i,L}^T\mathbf{S}_{i,R} = 0$). Let $\mathbf{S}_{i,L} = [1, \mathbf{x}]^T$ and $\mathbf{S}_{i,L} = [1, \mathbf{y}]^T$, where $\mathbf{x}$ and $\mathbf{y}$ are 3×1 vectors. In addition, $||\mathbf{x}|| = ||\mathbf{y}|| = 1$, such that $[1, \mathbf{x}]^T$ and $[1, \mathbf{y}]^T$ are totally-polarized SVs with normalized intensity. Then, by assuming $[1, \mathbf{x}][1, \mathbf{y}]^T = 0$, one can derive $\mathbf{x} = -\mathbf{y}$. This implies that lights in the LE and the RE channels are in the opposite polarizations, i.e.,

horizontal linear polarization versus vertical linear polarization, left-hand circular polarization versus right-hand circular polarization etc.

Then, considering Eq. (4.17a), (4.17c), because $\mathbf{S}_{i,L}^T\mathbf{S}_{i,R} = 0$, $\mathbf{M}_L^{lens}\mathbf{M}_L^{LCD}$ and $\mathbf{M}_R^{lens}\mathbf{M}_R^{LCD}$ are rank-1 matrices, we have $\mathbf{M}_L^{lens}\mathbf{M}_L^{LCD} \perp \mathbf{M}_R^{lens}\mathbf{M}_R^{LCD}$. Similarly, considering Eq. (4.17a), (4.17d), we have $\mathbf{M}_L^{lens}\mathbf{M}_L^{LCD} \perp \mathbf{M}_R^{lens}\mathbf{M}_L^{LCD}$. From the above, we have $\mathbf{M}_L^{lens} \perp \mathbf{M}_R^{lens}$. Subsequently, as long as $\mathbf{S}_{i,L}^T\mathbf{S}_{i,R} = 0$, and $\mathbf{M}_L^{lens} \perp \mathbf{M}_R^{lens}$, such unconventional CP LCD does not have crosstalk even when VM occurs. However, the realization of $\mathbf{S}_{i,L}^T\mathbf{S}_{i,R} = 0$ before VM takes place is no less difficult than shortening the spacing between the LC and the PR to reduce VM. In conclusion, VM-based crosstalk can not be efficiently reduced through image processing, or the conventional and unconventional CP LCD display systems.

4.5 Analytic solution of VM-free viewing zone

Because VM causes severe crosstalk in CP LCD at oblique viewing angles, it's desirable to find the viewing zone where the entire screen does not have the issue of VM.

Recall that VM is measured by $miss$, and being VM-free is equivalent to $miss = 0$. Fig. 4.14 shows $miss$ of a pixel column ($miss$ is uniform row-wisely) changing with the viewing location. In Fig. 4.14, the viewing distance in the subplots in the left column, middle column and right column are $0.5m$, $1m$, $1.5m$ respectively. The vertical viewing level for subplots from the first row to the bottom row are respectively aligned to the screen top, 1/4 of screen height from the screen top, screen center, 3/4 of screen height from the screen top, and screen bottom. The blue regions indicates the VM-free viewing zone ($miss = 0$). We can observe that when fixing the vertical viewing level, $miss$ decreases as the viewing distance increases. In addition, the VM-free area shifts with the vertical viewing level. Eq. (4.18) calculates the locations of the upper and lower bounds on the screen where $miss = 0$, and

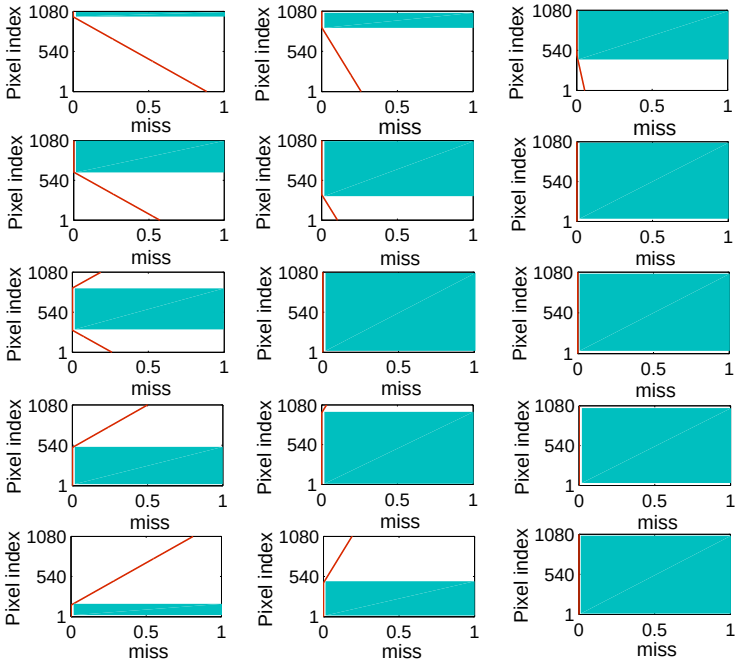

Figure 4.14: Vertical misalignment of the screen measured by $miss$ at different viewing locations.

it's a function of viewing distance D_v, the vertical viewing level y_v, and the intrinsic parameters of the display d, h_{PR}, h_0, h_{BM} and h_p:

$$y_{bnd} = \frac{D_v \cdot \left(h_0 \pm \frac{1}{2} h_{BM} \pm \kappa \cdot h_{PR}\right) + d \cdot y_v}{d - D_v \cdot \left(1 - \frac{h_{PR}}{h_p}\right)} \tag{4.18}$$

The derivation of Eq. (4.18) can be found in [Zen]. The LHS of Eq. (4.18) becomes $y_{bnd,up}$ (upper bound) and $y_{bnd,low}$ (lower bound) when taking $+$ and $-$ respectively. κ in Eq. (4.18) is still set as 0.02. If y_v is fixed at the screen center, the results of $y_{bnd,up}$ and $y_{bnd,low}$ changing with D_v are shown in Fig. 4.15(a). We can observe in Fig. 4.15(a) that the vertical expansion of the VM-free region increases with D_v, $y_{bnd,up}$ exceeds the screen top edge when $D_v \geq 0.75m$, and $y_{bnd,low}$ drops beyond the screen bottom edge when $D_v \geq 0.78m$. In order for the entire screen to be VM-free, it requires $y_{bnd,up} \geq H_{\mathrm{top}}$, where H_{top} denotes the Y coordinate of the screen top, and also $y_{bnd,up} \leq H_{\mathrm{bot}}$, where H_{bot} denotes the Y coordinate of screen bottom. From

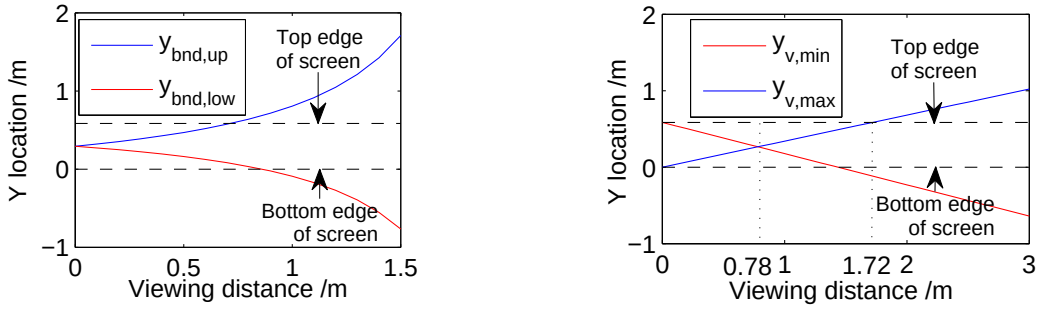

(a) Photo. (b) Simulation.

Figure 4.15: Analysis of vertical misalignment (VM). (a) The upper and the lower bounds of the VM-free screen area. (b) VM-free viewing zone.

Eq. (4.18), the former requirement becomes:

$$y_v \geq \frac{D_v}{d}\left[h_0 - \frac{1}{2}h_{BM} - \kappa h_{PR} + H_{\text{top}}\left(\frac{h_{PR}}{h_p} - 1\right)\right] + H_{\text{top}} \\ = y_{v,min} \tag{4.19}$$

where $y_{v,min}$ is the lowest vertical viewing level at viewing distance D_v. Similarly, Eq. (4.20) calculates the highest vertical viewing level $y_{v,max}$ at D_v:

$$y_v \leq \frac{D_v}{d}\left[h_0 + \frac{1}{2}h_{BM} + \kappa h_{PR} + H_{\text{bot}}\left(\frac{h_{PR}}{h_p} - 1\right)\right] + H_{\text{bot}} \\ = y_{v,max} \tag{4.20}$$

Fig. 4.15(b) shows how $y_{v,min}$ and $y_{v,max}$ change with D_v. Notice that the VM-free viewing zone: $y_{v,min} \leq y_v \leq y_{v,max}$ does not exist if D_v is too small. By forcing $y_{v,max} \geq y_{v,min}$ in Eq. (4.20) and (4.19), we obtain the smallest viewing distance $D_{v,min}$ beyond which the entire screen is VM-free:

$$D_{v,min} \geq \frac{d \cdot H_{\text{LCD}}}{h_{BM} + 2\kappa h_{PR} + H_{\text{LCD}}\left(1 - \frac{h_{PR}}{h_p}\right)} \tag{4.21}$$

where H_{LCD} is the screen height. By plugging the aforementioned intrinsic display parameters into Eq. (4.21), one can also acquire $D_{v,min} = 0.78m$. In summary, having the calibrated intrinsic display parameters, the VM-free viewing zone can be computed from Eq. (4.19)-(4.21). Assuming the screen bottom is $1m$ above the floor, and the viewer's height is less than $1.9m$, from Fig. 4.15(b), VM can hardly occur as long as the viewing distance is greater than $2.5m$.

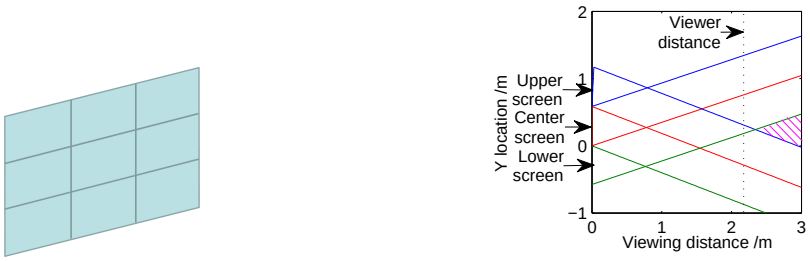

(a) (b)

Figure 4.16: The flat-grid formation of immersive display and its VM-free viewing zone. (a) Flat-grid screen formation. (b) Side view of the overlapped VM-free viewing zone highlighted by magenta shade.

4.6 VM-free viewing zone for multi-screen displays

In this section, we extend the analysis of VM-free viewing zone from a single-screen display to multi-screen immersive CP LCDs. The overall VM-free viewing zone of the multi-screen CP LCD is determined by the overlapping VM-free viewing zones of individual screens. Therefore, the objective in this section is to find the screen formation of the multi-screen CP LCD such that the overlapping VM-free viewing zone of all the screens is maximized.

There are various ways to align the screens to form an immersive 3D display. A simple screen formation is shown in Fig. 4.16(a) where the screens form a flat grid. However, this type of screen formation results in limited overlapped VM-free viewing zone as shown in Fig. 4.16(b). The vertical line segments denote the side views of the screen, and the rays of the same color denote the bounds of corresponding VM-free viewing zones. The dashed line marks the comfortable viewing distance. In Fig. 4.16(b), we assume that the VM-free viewing zones of the screen are identical, having the same parameters as shown in Fig. 4.15 (b). Consequently, it is desirable to "bend" the screen formation which will give rise to an enlarged overlap of the VM-free viewing zones at the desired viewing distance. Furthermore, for the sake of display continuity, it is necessary to constrain the screen formation to be seamless, that is, for all the interior screens, their bezels are seamlessly connected to the neighboring

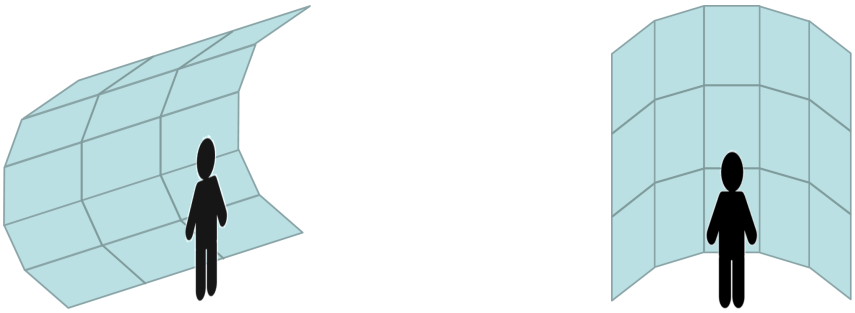

(a) Horizontal formation. (b) Vertical formation.

Figure 4.17: Two ways of screens formation for seamless immersive 3D display. (a) The screens are oriented horizontally. (b) The screens are oriented vertically (rotated by 90 degrees).

screens. To be seamless, the screens formation can not be bended both vertically and horizontally. In addition, as proved in Section 4.3, VM-induced crosstalk changes significantly along the screen's vertical direction but insignificantly along the screen's horizontal direction. As a results, it is much more meaningful to tilt the screens along their vertical axes than horizontal axes. Fig. 4.17 shows two screen formations where the screens are tilted along their vertical axes. In Fig. 4.17 (a), the screens are horizontal with respect to the floor, while in Fig. 4.17 (b), the screens are rotated by 90°. The VM-free viewing zone of the horizontal screen formation as shown in Fig. 4.17 (a) has span unlimitedly in the horizontal direction, and thus the audience can be spread out horizontally. For the vertical screen formation as shown in Fig. 4.17 (b), the horizontal span of the VM-free viewing zone is bounded by $y_{v,min}$ and $y_{v,max}$ (Fig. 4.15 (b)). The rest of this section focuses on the maximization of the overlapped VM-free viewing zone of the two screen formations as shown in Fig. 4.17. Assuming that the screens are identical, having the same parameters of the screen as shown in Fig. 4.15, and that the viewers are standing in the vicinity of the comfortable viewing distance, our objective is to maximize the vertical span of the VM-free viewing zone at the comfortable viewing distance (VSCVD). For LG 47LH55 (1080p), the comfortable viewing distance for 3D is 86 inches (2.18 m) [Vie]. Beginning from the single-screen case, Fig. 4.18 (a) shows the side view of the VM-free viewing zone of the center screen,

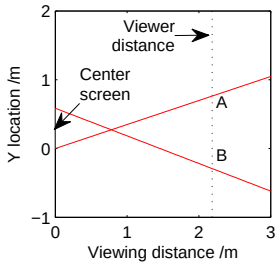

(a) Center screen.

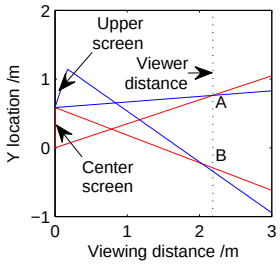

(b) Near convergence.

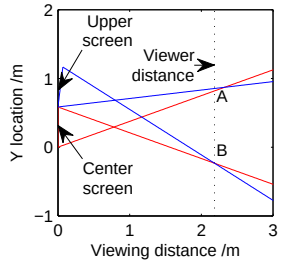

(c) Far convergence.

Figure 4.18: Side view of the screens showing maximizing the vertical span of VM-free viewing zone at comfortable viewing distance with near and far convergence.

where the upper bound and lower bound of the VM-free viewing zone intersect with the comfortable viewing distance at point A and B respectively. In Fig. 4.18, the length of line segment AB, which is the intersection of the VM-free viewing zone of the center screen with the line at the comfortable viewing distance, is the VSCVD of the center screen. By adding other screens, VSCVD can only be equal or smaller than that of the center screen. Consequently, to maintain the maximum value of VSCVD we need to adjust the off-centered screens such that the intersections of their VM-free viewing zones at the comfortable viewing distance do not fall inside line segment AB in Fig. 4.18 (a). Fig. 4.18 (b) and (c) show two extreme cases of tilting the upper screen while maintaining the maximum VSCVD. In Fig. 4.18 (b), the upper bounds of the VM-free viewing zones of the center and upper screens intersect at the same point A at the comfortable viewing distance. Fig. 4.18 (c) is the case where the lower bounds of the VM-free viewing zones of the center and upper screens intersect at the same point B at the comfortable viewing distance. These two extremes as shown in Fig. 4.11 (b) and (c) are denoted as "near convergence" and "far convergence" respectively. Therefore, to obtain maximum VSCVD, one needs to

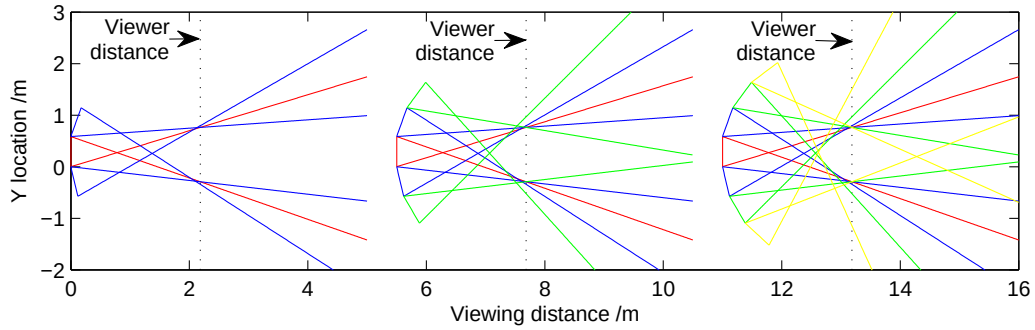

(a) Near-convergence screen formation.

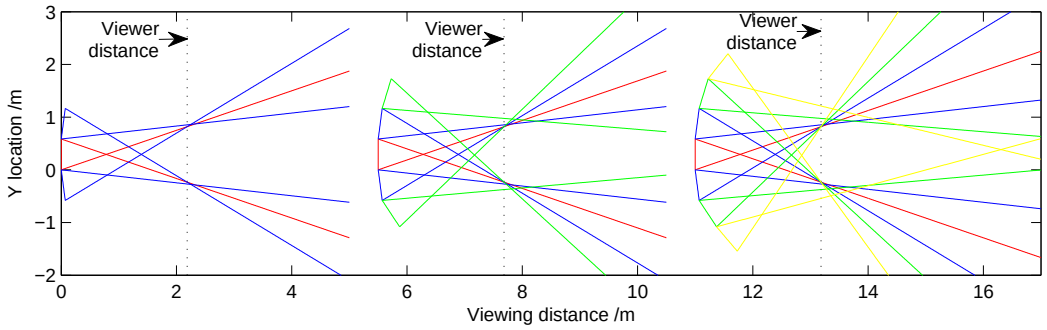

(a) Far-convergence screen formation.

Figure 4.19: Side views of maximized VM-free viewing zone for 3-screen, 5-screen, and 7-screen cases. (a) Side view of the VM-free viewing zone of near-convergence screen formation. (b) Side views of the VM-free viewing zone of far-convergence screen formation.

confine the tilting of all screens between the near convergence and far convergence. Applying near convergence to all the screens gives rise to the result as shown in Fig. 4.19 (a), and far convergence Fig. 4.19 (b). In Fig. 4.19, we also assume that all the screens are identical, having the same parameters of VM-free viewing zone as those those in Fig. 4.15. Comparing Fig. 4.19 (a) and (b), we can observe that the overlapping VM-free viewing zone of near-convergence case extends more towards the screens, while that of far-convergence case prolongs further from the screens. The near-convergence formation can be applied to the scenario where the viewers desire to have the freedom to move closer to the screen. On the other hand, the far-convergence formation can be applied to the vertical screen formation as shown in Fig. 4.17 (b), whose horizontal span of the VM-free viewing zone is bounded, to increase the depth span.

4.7 Conclusion

This paper focuses on the issue of crosstalk caused by vertical misalignment (VM) of light in circularly polarize (CP) LCD. The contributions of this paper are 3 folds: the modeling, the proof that VM-based crosstalk cancellation is not possible, and analytic solution of VM-free viewing zone.

The modeling of CP LCD considers two major factors that causes crosstalk: the polarizing system including patterned retarder (PR) and the passive glasses, and VM. The modeling of the former can be found in [MZN15]. We show that crosstalk induced by VM is much more severe than that caused by the polarizing system. Moreover, the spatial distribution of VM-based crosstalk is sensitive to the vertical position of the viewer. However, some intrinsic display parameter which are difficult to acquire is required in the modeling of VM. We propose a novel display calibration method which only requires pictures of the screen taken at 4 locations to solve for these intrinsic parameters. The display model is validated by human observations with changing the viewing locations. Additionally, simulations of the output natural images match the real CP LCD (1080p) [Cor09].

Due to the severity and mobility of VM-based crosstalk, preprocessing the input image using methods based on the luminance compensation scheme in [LW94] is impractical. We then discuss under two assumptions that when VM exists, whether the polarizing system of CP LCD is able to reduce VM-based crosstalk efficiently. The first assumption is true to the existing CP LCDs where lights from the left-eye (LE) and right-eye (RE) fields in the CP LCD panel are in the same polarization before the PR. The second assumption allows different polarizations in the LE and RE fields before light passes through PR. However, we show that the least crosstalk can be achieved in the first assumption equals to the percentage of VM of light, which can be significant at vertically oblique viewing angles. Moreover, we also show that the second assumption achieves crosstalk cancellation in a technically-challenging way.

Based on the intrinsic display parameters, we derive analytic solution of the VM-free viewing zone where no severe crosstalk appears on the entire screen. Finally, we apply the VM-free solution to multi-screen CP LCD and maximize the overall VM-free viewing zone.

4.8 Acknowledgment

Chapter 4, in full, is a reorganized composition of the materials as they appear in International Conference on Image Processing (ICIP), IEEE, 2014, Menglin Zeng, Haleh Azartash, and Truong Nguyen, and, IEEE Transactions on Image Processing, Vol. 25, Number 3, 2016, Menglin Zeng, Truong Nguyen. The dissertation author was the primary investigator and author of these papers.

Chapter 5

Motion vs. Crosstalk Visibility

Our future work will extend the results on crosstalk analysis and reduction from images to videos. It is important to study the effect of motion on crosstalk in video. This chapter summarizes the experimental study on how horizontal motion affects crosstalk visibility.

5.1 Motion Blur

Motion blur can be caused by various factors. In the video capturing stage, due to rapid movement of the object or the long exposure of a single capture, motion blur can be recorded in the video source [BBZ96]. In the displaying stage, commonly in LCDs [PFD05], where it takes time (liquid crystal response time) for a dark pixel to rise to the intended brightness or for a bright pixel to be darkened fully, motion blur can be so significant that the trajectory of a moving object becomes visible. An example is displaying the soccer ball being passed across the field in an LCD TV. Furthermore, motion blur can also occur in the human visual system (HSV) [Ham97]. Because of retinal persistence, it takes time for the retina to capture the change of brightness, thus, the displacement of the objects takes place before the retina captures it. A good example of this is that fireworks appear to have tails at night time. The last category of motion blur is computer-graph-induced motion blur in animations

and video games [PC83]. To cater to how motion blurs in HSV, videos appear more natural if motion blur is manually induced to fast-moving objects.

5.2 Motion and Crosstalk Visibility

Since motion blurs the images along the direction of the motion, we are interested in knowing whether the visibility of crosstalk decreases because of motion blur. For instance, crosstalk can be easily identifiable in still images, but if the object with crosstalk moves in videos, it is possible that, due to the blurriness caused by motion as well as the limited appearance time of the objects in videos, crosstalk becomes less identifiable to the observer. If motion decreases the visibility of crosstalk, then in crosstalk reduction in 3D video we can assign less weighting on objects where crosstalk is less identifiable because of motion, and thus further preserving the video quality.

However, because crosstalk is horizontally attached to the object, only horizontal motion affects the visibility of crosstalk. Consequently, for the rest of this chapter we only focus on the relationship between horizontal motion and crosstalk. For arbitrary motion, one can always project the motion vector onto the horizontal direction.

Furthermore, since the motion blur caused by the capturing devices and displaying monitors varies, we only consider how motion blur induced by HSV affects crosstalk visibility.

5.3 Subjective Test

In order to find out the relationship between horizontal motion and the visibility of crosstalk, we conduct a subjective test from which we quantify the range of moving speed and crosstalk where crosstalk becomes indistinguishable.

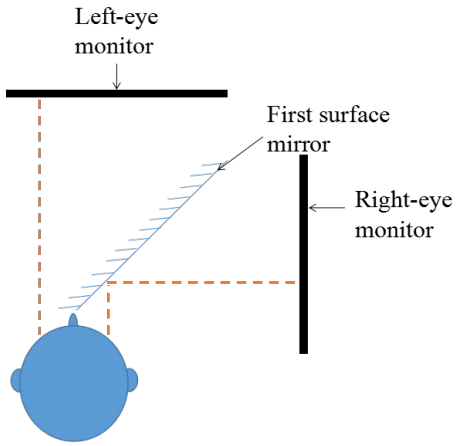

Figure 5.1: The set up of stereoscopic display for the subjective test. Two CRT monitors are used where one shows the image to the left eye, and the other monitor shows the image to the right eye.

5.3.1 Stereoscopic display set up

The set up of the stereoscopic display for the subjective test is shown in Fig. 5.1, which is composed of two CRT monitors and a first-surface mirror. The subject's left eye looks directly at the left CRT, and the right eye looks at the right CRT through the reflection of the first-surface mirror. The left-eye (LE) and right-eye (RE) CRT monitors are at right angle, and the first-surface mirror is at 45° equally spaced between the two monitors such that the LE and RE observations of the two monitors are strictly parallel and also vertically aligned. We use a chin rest to stabilize the head location of the subjects. The distance between the mirror and the chin rest should be close enough that the left eye can only see the LE monitor and vice versa for the right eye. Additionally, the height of the chin rest is adjusted for all subjects accordingly to ensure that they can see the entire LE and RE monitors.

Note that in this experiment, we are only interested in the relation between motion blur caused by human visual system and crosstalk visibility. Therefore, it is necessary to rule out factors in the device that cause motion blur. Compared with LCDs, CRT monitors have the advantage of much less motion blur due to significantly faster pixel rising and falling response and faster frame-refreshing rate. In addition, unlike the commonly used second-surface mirror, which induces crosstalk because of

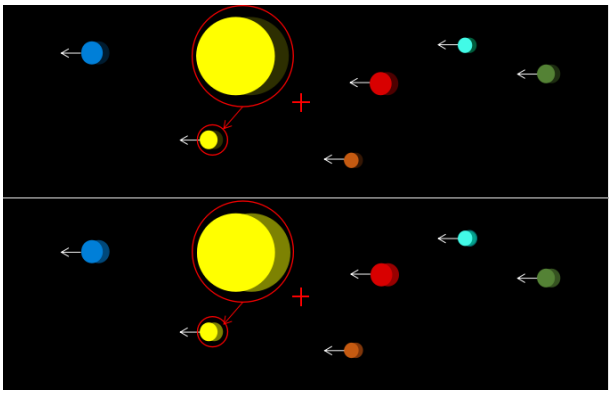

(a) Before matching of crosstalk.

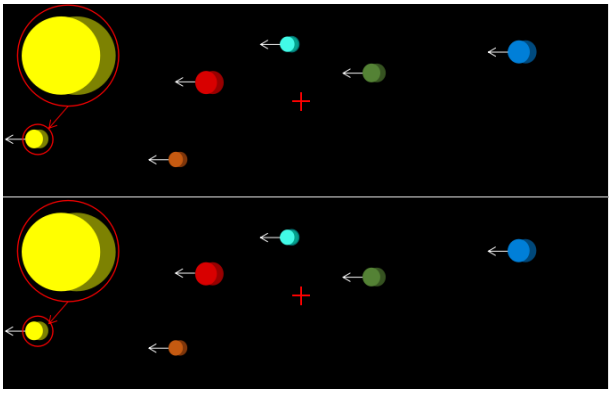

(b) After matching of crosstalk.

Figure 5.2: The video content of the subjective test. The top half and the bottom half of the video are test and reference videos respectively.

the reflection on the glasses, the reflection of the first-surface mirror is crosstalk-free. Therefore, we can accurately control the amount of crosstalk in the subjective test.

5.3.2 Stimuli

The content of the video for the subjective test is randomly colored dots moving in one direction on a black background as shown in Fig. 5.2. Because, additional factors other than motion, such as the direction of motion, texture of the foreground and background objects, can also affect crosstalk visibility, we simplify the test video to only focus on how horizontal motion influences crosstalk visibility. As shown in Fig. 5.2, the video for the subjective test is divided into the top half and the bottom half, where the top half is the test video and the bottom half is the reference video.

The test video is where the subjects can increase and decrease the level of crosstalk by using an x-box controller, and the reference video is where the crosstalk level is fixed. The goal for the subjects is to match the level of crosstalk from the test video to the reference video while observing the stereoscopic display.

Fig. 5.2 shows an example of the matching process. Initially, crosstalk in the test video is random and different from the crosstalk in the reference video, as shown in Fig. 5.2(a). Fig. 5.2(b) shows the situation when the subject increases the level of crosstalk in the test video to match the crosstalk in the reference video. Note that all the dots in the test video have the corresponding dots in the reference video with the same brightness, color, size, disparity, motion direction, and horizontal position. The only difference between two corresponding dots in the test and reference videos is crosstalk level. Furthermore, the amount of crosstalk is the same for all the dots in the test video, as well as for all the dots in the reference video. When subjects adjust crosstalk in the test video, crosstalk levels change simultaneously for all the dots in the video .

The subjects observe 54 individual video segments encompassing six levels of reference crosstalk ranging from 0% - 50% moving at nine different speeds ranging from $0°/sec$ - $40°/sec$, respectively. The randomized initial crosstalk in each test video segment are different for all subjects. The order of the reference video segments are randomized and different among the subjects as well. Regarding the range of crosstalk level, for 3D LCD with shutter glasses, if the frame-refresh rate is greater than $120Hz$, and has perfect synchronization, crosstalk is less than 10%. However, crosstalk can increase significantly if these conditions fail as well as when the shutter glasses are not horizontally aligned with the LCD. For CP LCD, as our previous work shows, crosstalk is also less than 10% if the viewer is within the VM-free viewing zone with no head rotation. However, crosstalk increases drastically ($> 50\%$) once the viewer deviates from the frontal parallel viewing position. Considering the range of motion speed, most objects moves within the speed of $30°/sec$. Moreover, it is difficult for

HSV to track the objects with speed beyond $40°/sec$. Note that the subjects are instructed to track the moving dots the best they can during the test.

5.3.3 Training before test

All subjects are provided with training before the real subjective test for them to familiarize them with the system and to produce reliable results. Initially, the subjects are informed of what crosstalk is and its appearance through examples on the monitor. Then, the subjects are shown six video segments with motion speed at $0°/sec$ (still images) and six video segments with motion speed at $5°/sec$. While the subjects are performing the matching of crosstalk in the training stage, we (experiment conductors) inform the subjects whether they are approaching or deviating from the target crosstalk in the reference video until they reach the true crosstalk. Slow motion speeds are chosen at the training stage so that the subjects can better observe the appearance and the change of crosstalk levels as they press the controller. External aid from the test conductor is to train the subjects to be as accurate as possible in the real test. Note that during the real test stage, the subjects perform the matching independently with no information from the test conductors.

5.3.4 Control of the system

We limit the duration of each video segment to 10 *sec*, during which the dots cross the screen multiple times. We impose this time limitation because in a real-world scenario, it is unlikely that the appearance of a moving object lasts for more than 10 *sec*. Moreover, it causes discomfort and even nausea if the subjects track fast-moving objects for a long time. Note that all subjects are informed of this time limitation before the test begins. Also, the subjects can choose to move on to the next video segment before it reaches 10 *sec* once they think they finish matching. During the test, the subjects can observe the real-time change of crosstalk in the test video as they perform matching. Within each video segment, all the dots in both the

test video and the reference video move in one direction. The direction of motion alternates from video segment to video segment. A 3-sec black video is inserted between the neighboring video segments for the purpose of relaxing the eyes. The entire time of the subjective test, including training, is less than 20 *min* to prevent the eyes from getting tired.

We record the crosstalk level in the test video as the subjects press the increase and decrease control keys. For each video segment designed for a certain reference crosstalk at a certain moving speed, beginning with the initial randomized crosstalk in the test video, until the end of the video segment (or when the subject presses the control key to move on to the next video segment), a sequence of crosstalk level is recorded. We regard the last recorded crosstalk level of this sequence as the final matching result for the video segment. Note that in the training stage, we inform the subjects when the crosstalk level in the test video reaches zero. Moreover, crosstalk less than 0% can not be shown in reality (but crosstalk greater than 100% can be shown). However, during the test, we allow the subjects to continue to press the decrease control key when crosstalk reaches zero, and the system continues to record negative crosstalk. There are two reasons why we allow negative crosstalk to be recorded. First, since crosstalk can go above 100%, the matching results will be biased to greater crosstalk if no negative crosstalk is recorded. Second, negative crosstalk better reflects the subjects' real judgment: they think crosstalk should be further decreased.

5.3.5 Subjective test results

Eighty-one subjects participated in this test. All the subjects are under the age of 30, having normal vision, and able to see the images on the monitors clearly. Fig. 5.3 shows the raw results of their matching compared with the true reference crosstalk. The subplots in Fig. 5.3 show the results at six reference crosstalk levels from 0 to 0.5 in increment of 0.1 respectively. The subplots in Fig. 5.3 show the re-

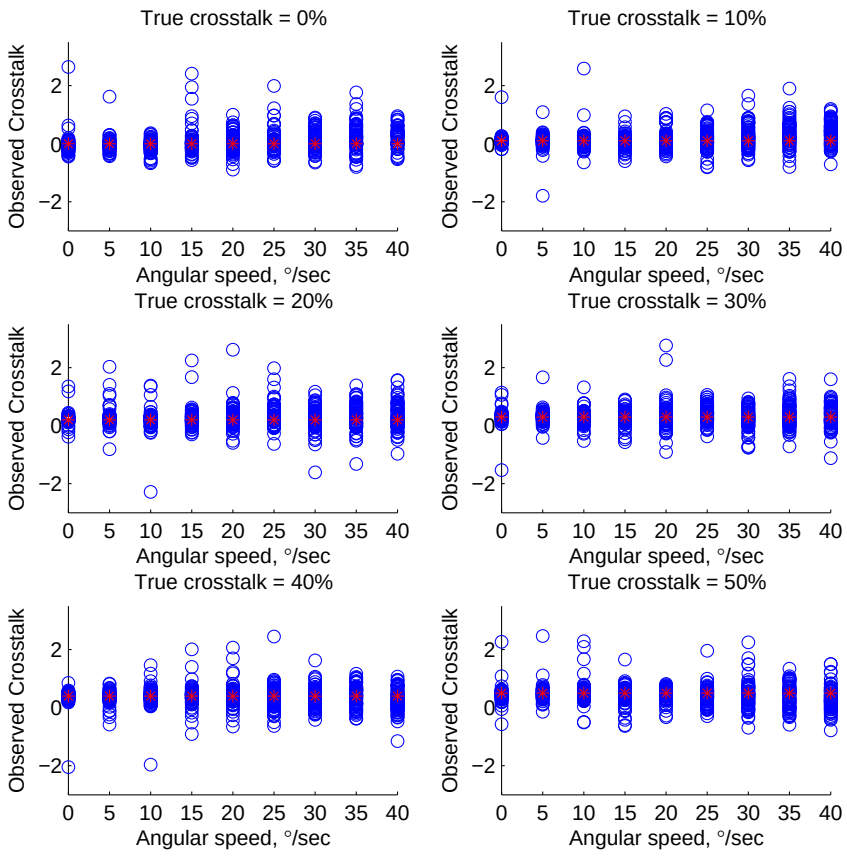

Figure 5.3: Crosstalk resulted from the matching of 81 subjects.

sults tested at nine moving speeds, respectively from $0°/sec$ to $40°/sec$ in increment of $5°/sec$. The x axes in Fig. 5.3 mark out the moving speeds, and the y axes show the observed crosstalk resulted from the subjects' matching attempts. Each blue circle in Fig. 5.3 represents an observed crosstalk level resulted from a subject's matching at a certain speed for a certain reference crosstalk. The red stars in Fig. 5.3 denote the true reference crosstalk. We can see from Fig. 5.3 that the observed crosstalk results are most centered at the true crosstalk level when the video is still (moving speed $= 0°/sec$), and the results become increasingly spread out as the moving speed increases. This indicates that as the moving speed increases, it becomes more difficult for the subjects to accurately match the crosstalk from the test video to the reference video. Note that, as mentioned in the previous section, because we record negative crosstalk resulted from subjects' continuing to decrease crosstalk when the displayed

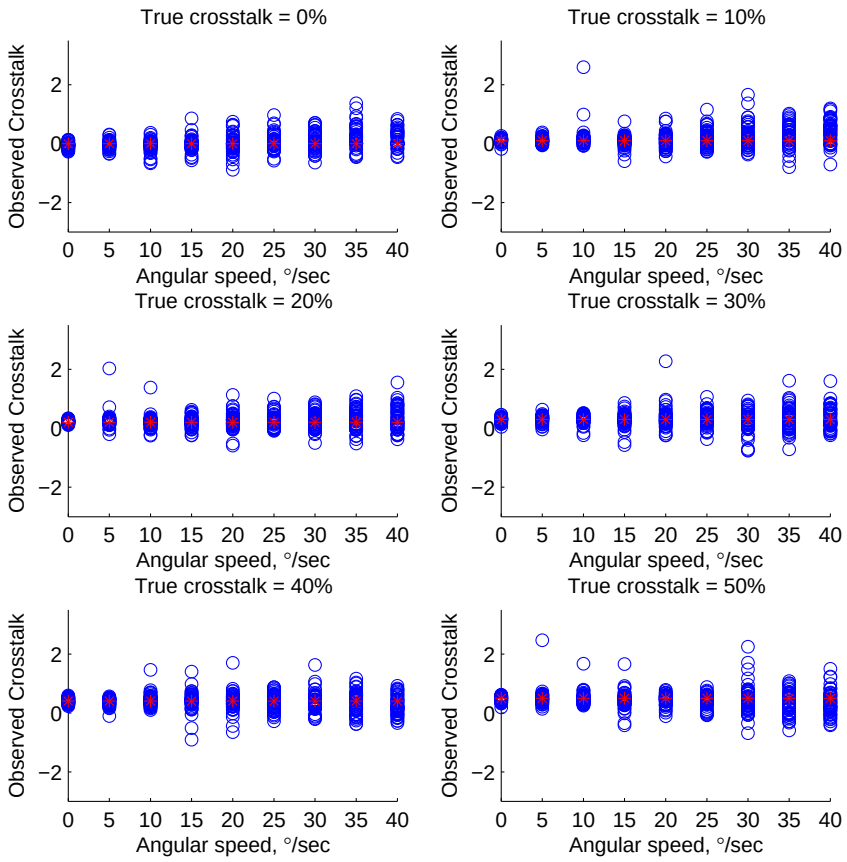

Figure 5.4: Crosstalk resulted from the matching test of 53 subjects after thresholding at speed $0°/sec$.

crosstalk in the test video has reached zero, some of the crosstalk observation results are negative. Even as the results of the 81 subjects in Fig. 5.3 show the increasing error in matching as the moving speed increases, we observe that some resulted crosstalk at moving speed $0°/sec$ deviates significantly from the true crosstalk. Because matching is easiest at speed $= 0°/sec$, if a subject shows considerable error at speed $= 0°/sec$, it is unlikely that this subject's matchings are reliable at the other speeds. Therefore, it is desirable to set a threshold at speed $= 0°/sec$ that rules out the subjects whose error is significant. We calculate each subject's error by taking the difference between the observed crosstalk and true crosstalk at speed $= 0°/sec$ tested at the six reference crosstalk levels and sum them up. If the error of a subject at speed $= 0°/sec$ is greater than $0.1 \times 6 = 0.6$, we discard all the matching results

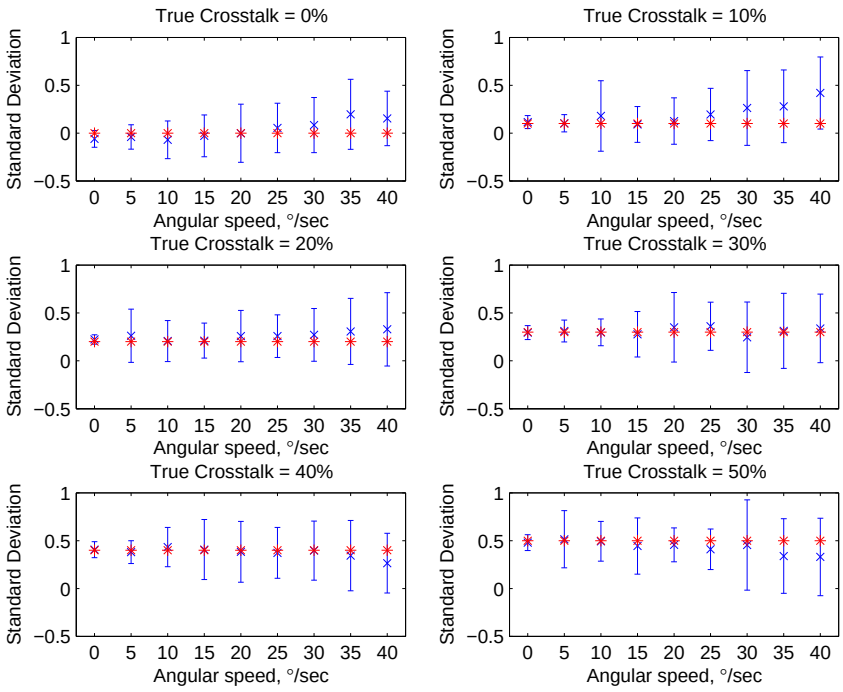

Figure 5.5: Mean and standard deviation of the matching results of the 53 subjects. Mean is marked by the blue stars; standard deviation is marked by the blue bars, and the red stars denote the true crosstalk.

of that subject. After the thresholding at speed = $0°/sec$, 53 subjects remained and their results are reliable for the remaining analysis.

The results after thresholding at speed = $0°/sec$ are shown in Fig. 5.4, where we can see that the observed crosstalk at speed = $0°/sec$ become more centered at the true crosstalk, and the tendency to spread out as the speed increases becomes more significant. Fig. 5.5 shows the mean and standard deviation (STD) of the matching results of the 53 subjects, where the mean and STD are calculated from the crosstalk resulted from the matching of the 53 subjects for a certain reference crosstalk level at a certain moving speed. The red stars in Fig. 5.5 mark the true reference crosstalk level. Regarding STD, we can observe from Fig. 5.5 that at each reference crosstalk level, STD increases as the moving speed increases, which again confirms our observation from Fig. 5.4 that the matching becomes more difficult when the moving speed rises. Regarding the mean, the mean values of the observed crosstalk

are close to the true crosstalk when the moving speed is less than $25°/sec$, but start to deviate from the true crosstalk at speeds over $25°/sec$. This again proves that the visibility of crosstalk degrades as the moving speed increases.

To further verify in the subjective test that crosstalk becomes less identifiable as the moving speed increases, we calculate Spearman's rank correlation coefficient denoted as ρ between the observed crosstalk and the true reference crosstalk as the moving speed increases. Spearman's rank correlation coefficient ρ is a measurement of how much the two variables are monotonically related. $\rho = 1$ when the relationship between the two variables can be characterized by a monotonically increasing function; $\rho = -1$ when characterized by a monotonically decreasing function; and $\rho = 0$ indicates no correlation.

It seems reasonable that crosstalk is more visible as crosstalk level increases. However, Fig. 5.6 shows that this correlation weakens when the moving speed increases. We can observe in Fig. 5.6(a) that in the speed range of $0°/sec$ - $10°/sec$ where $\rho \geq 0.8$, the monotonically increasing relationship between the observed crosstalk and true crosstalk is very strong. This shows that when the moving speed is small, the level of crosstalk is the dominant factor determining how distinguishable crosstalk is. At speed $15°/sec$ where $\rho = 0.67$, the monotonically increasing relationship is still strong. Than, in the following speed range of $20°/sec$ - $25°/sec$ where $0.4 \leq \rho \geq 0.6$, this relationship becomes moderate. At speed $30°/sec$ where $\rho = 0.33$, the monotonic relationship between crosstalk visibility and crosstalk is weak. This indicates that at speed $30°/sec$, crosstalk level is no longer the dominant factor in determining the visibility of crosstalk. Finally, in the speed range of $35°/sec$ - $40°/sec$, where $\rho \leq 0.2$, crosstalk visibility is very weakly related to the level of crosstalk, which means at such high moving speed, objects with different amounts of crosstalk appear almost the same according to the subjects' observations. Consequently, we can conclude that when the moving speed increases to a certain point ($30°/sec$), the observer can not distinguish different levels of crosstalk.

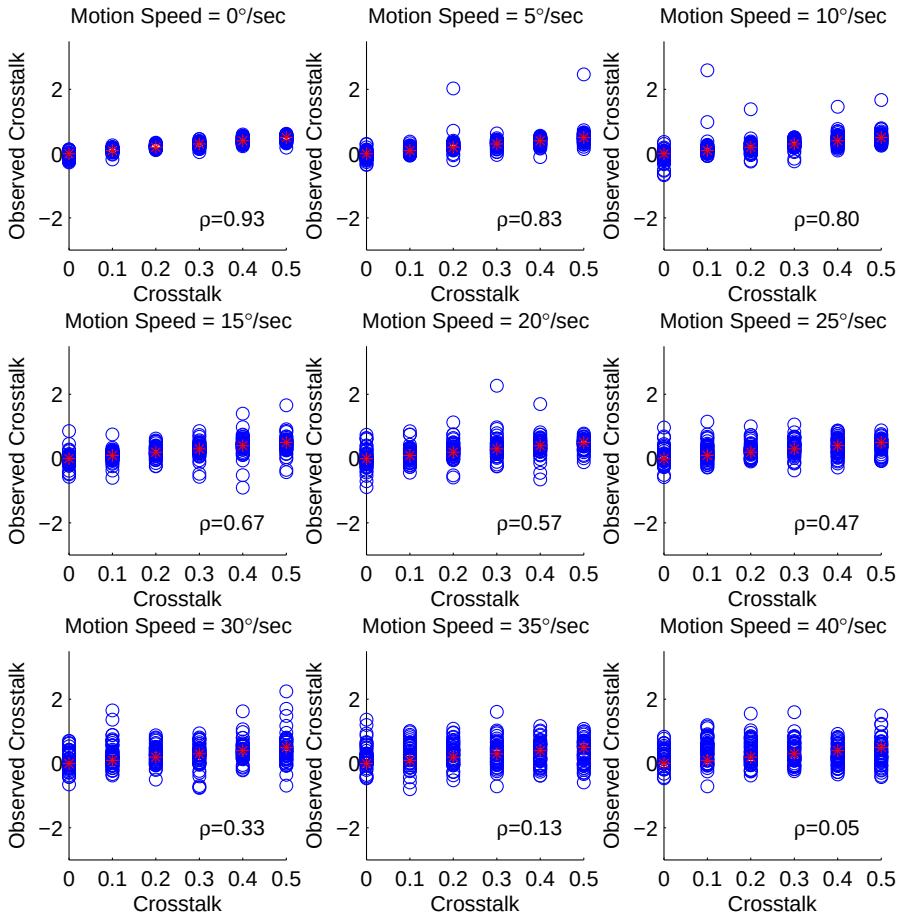

(a) Spearman rank correlation coefficient ρ.

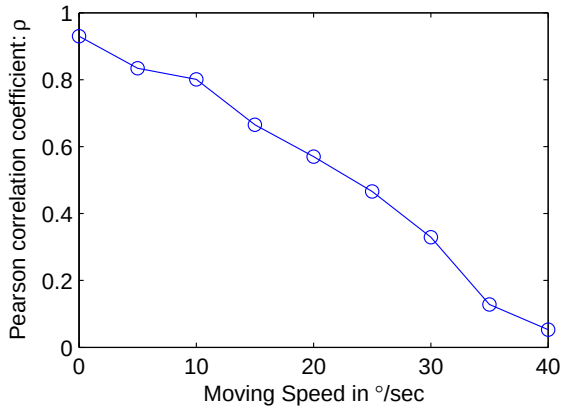

(b) ρ vs. moving speed.

Figure 5.6: Spearman's rank correlation coefficient ρ of the observed crosstalk resulted from matching by the subjects and the true reference crosstalk.

The curve of Spearman's rank coefficient in Fig. 5.6(b) directly shows the weakening of the relationship between crosstalk visibility and crosstalk as the moving speed increases.

5.3.6 Quantifying relationship between crosstalk visibility and moving speed

Even though we have shown that when crosstalk becomes decreasingly identifiable when the moving speed increases, it is desirable to find out quantitatively the range of moving speed at which a certain crosstalk becomes indistinguishable. We first calculate the mean absolute error between the crosstalk from the subjects' matching and the true reference crosstalk among the 53 subjects. Before the calculation of this matching error, we convert the normalized crosstalk into gray scale levels. Eq. 5.1 converts display luminance into the 8-bit gray-scale level, where I is the normalized display luminance and G is the gray-scale level. The reason for this conversion is that according to the luminance sensitivity function, HSV is more sensitive to low luminance than high luminance, that is, the same amount of luminance difference appears more visible in the lower luminance range than in the higher luminance range. Consequently, measuring the matching error in gray-scale level can better characterize visually how much the matching results deviate from the true reference crosstalk.

$$G = 255 \times I^{\frac{1}{2.2}} \tag{5.1}$$

After converting the observed crosstalk and reference crosstalk into gray-scale levels, we calculate the absolute error between them and take the average among the 53 subjects. The results of the mean absolute error (MAE) between the observed crosstalk and the true reference cross talk are shown in Fig. 5.7(a), where we can observe how the matching error changes with both crosstalk and moving speed. Note that the crosstalk axis in Fig. 5.7(a) is the true reference crosstalk. For better illustration, we show in 2D plots how matching error changes with crosstalk at different

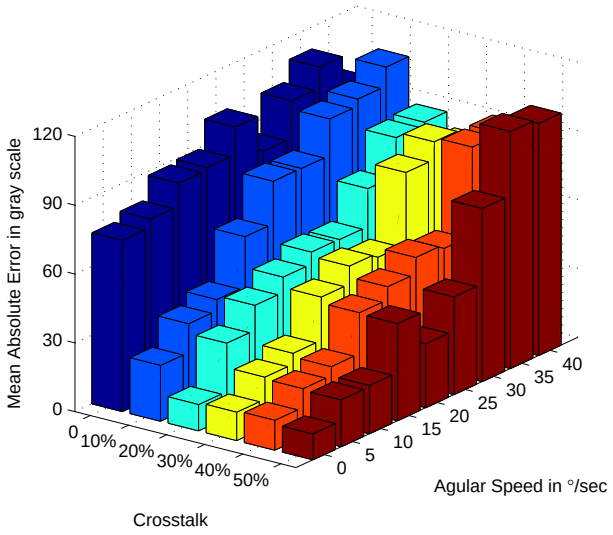

(a) 3D plot of crosstalk matching error.

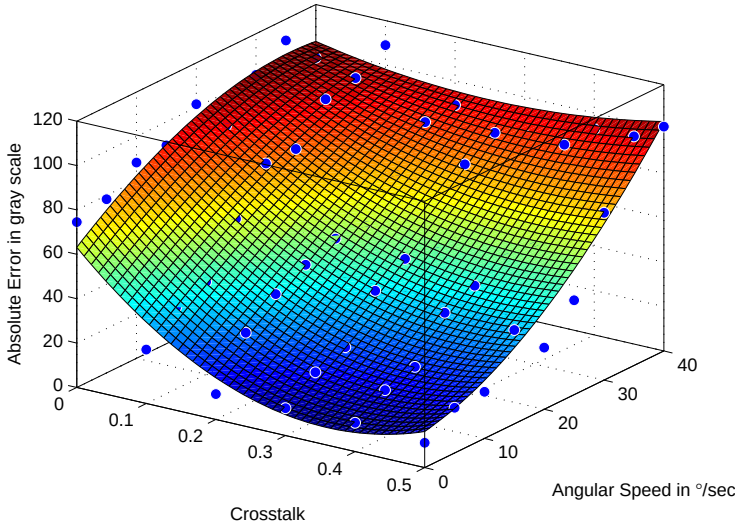

(b) Surface fitting of crosstalk matching error in (a). Blue denotes data used for fitting.

Figure 5.7: 3D plots of crosstalk matching error measured in gray-scale level with respect to crosstalk and moving speed.

moving speeds in Fig. 5.8(a), as well as how the error varies with moving speeds at different reference crosstalk levels in Fig. 5.8(b). From Fig. 5.8(a), we observe that, within the speed range of $0°/sec$ - $25°/sec$, the matching error decreases and crosstalk increases, whereas in the range of $30°/sec$ - $40°/sec$, the matching error remains high for all the crosstalk levels. This confirms our previous conclusion that, within the low speed range crosstalk, becomes more visibly identifiable as crosstalk

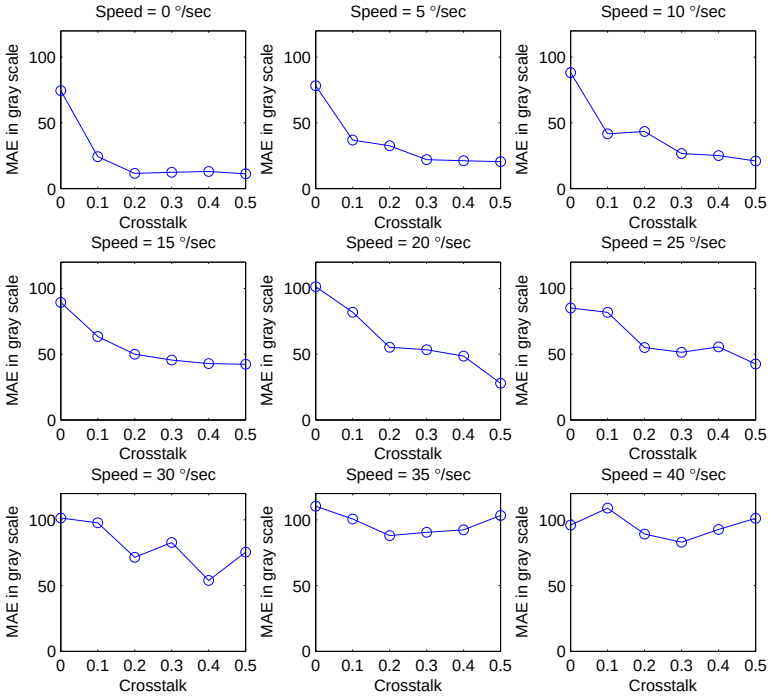

(a) Matching error vs. moving speed at different crosstalk levels.

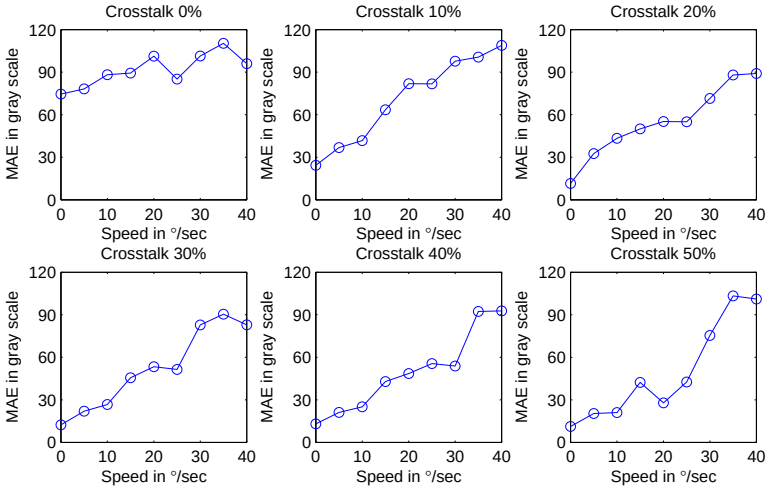

(b) Matching error vs. crosstalk at different moving speeds.

Figure 5.8: How crosstalk matching error changes with crosstalk and moving speeds.

level increases, while in the high speed range, crosstalk becomes less visible, and different levels of crosstalk are insignificantly distinguishable. Fig. 5.8(b) shows that for all crosstalk levels, the matching error increases as the moving speed increases. However, when crosstalk is 0%, this increment is the least significant, which explains why

the appearance of crosstalk-free objects does not change significantly as their moving speed increases. Furthermore, as crosstalk increases in Fig. 5.8(b), the difference of matching error between the low and high moving speeds also enlarges. This indicates that the change of the visibility of crosstalk as the moving speed increases is more significant for objects with greater amounts of crosstalk.

After applying polynomial fitting up to the 3rd order to the matching error in Fig. 5.7(a), the resulted surface is shown in Fig. 5.7(b). The resulted surface is able to characterize the increasing matching error as the moving speed is increasing, as well as the decreasing matching error when crosstalk is increasing. We can observe from Fig. 5.7(b) that the least matching error takes place at the maximum crosstalk level at moving speed $0°/sec$ (highest level of crosstalk in still image is most distinguishable). Furthermore, the surface in Fig. 5.7(b) shows that as the moving speed increases, different levels of crosstalk become less distinguishable. In order to quantify the range of moving speed and crosstalk level where crosstalk is indistinguishable, we insert a plane in the surface in Fig. 5.7(b) at the matching error which is chosen as the threshold. Crosstalk is distinguishable below this error threshold, and above this threshold, crosstalk is indistinguishable. We set the threshold at the matching error when crosstalk is 0 at moving speed $0°/sec$ as shown in Fig. 5.9(b). The inserted plane cuts out a curve in the surface. Fig. 5.9(a) and (c) show this curve resulted from setting a lower and higher error thresholds respectively. If we set a lower error threshold as Fig. 5.9(a) shows, the resulted curve indicates that at zero moving speed, crosstalk below certain a level is indistinguishable. It is possible that, for some observers some low-level crosstalk is not identifiable in still images. However, because this work is related to crosstalk reduction, it is safer to assume that at zero moving speed all levels of crosstalk are distinguishable. On the other hand, if we choose a higher error threshold, as Fig. 5.9(c) shows, the resulted curve infers that, even at some positive moving speeds all crosstalk levels are distinguishable. This, however, contradicts with the results from the subjective test which shows that the visibility

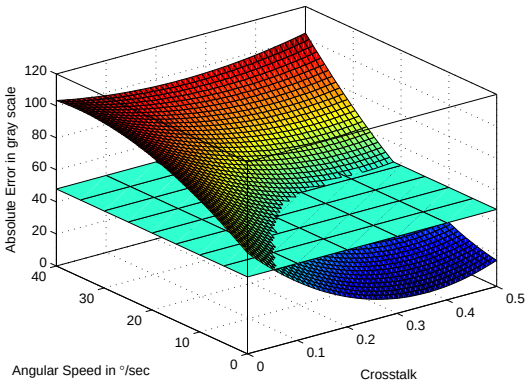

(a)Low threshold.

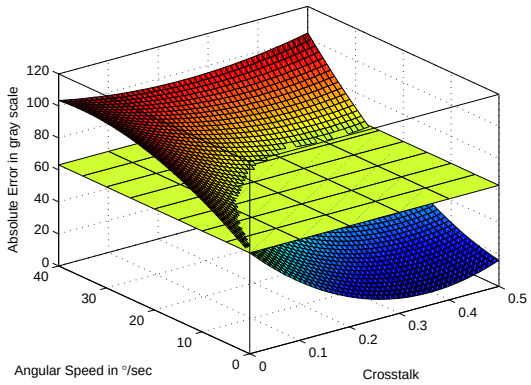

(b)Threshold at origin.

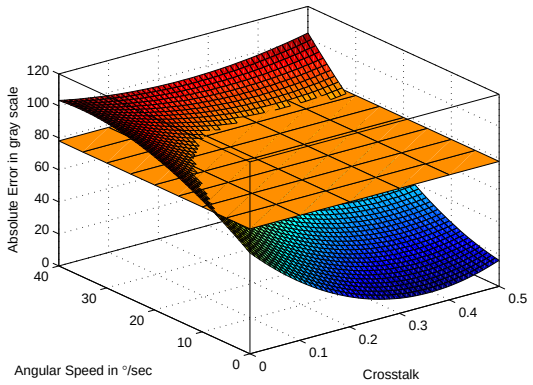

(c)High threshold.

Figure 5.9: Choosing the error threshold from the surface fitting in Fig. 5.7(b), above which crosstalk is induistinguishable.

of the same level of crosstalk drops if the moving speed increases. Therefore, the error threshold of zero crosstalk at zero moving speed is the most reasonable choice.

By equating the surface function in Fig. 5.7(b) to the threshold matching error as shown in Fig. 5.10(a), we obtain the curve in Fig. 5.10(b) that quantifies the range of crosstalk and moving speed where crosstalk is distinguishable and indistinguishable. Fixing the crosstalk level in Fig. 5.10(b) (by drawing a vertical line crossing a crosstalk value on the horizontal axis), objects whose moving speed is below the curve have distinguishable crosstalk, and above the curve indistinguishable. Similarly, when the moving speed is fixed (by drawing a horizontal line crossing a moving speed on the vertical axis), crosstalk that falls on the left side of the curve is indistin-

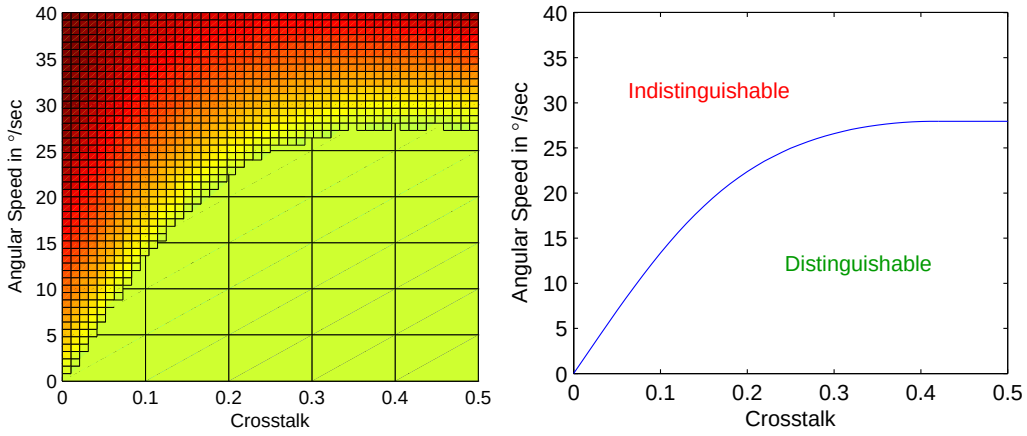

(a)Top view of Fig. 5.9(b). The threshold curve resulted (a).

Figure 5.10: The threshold curve resulted from Fig. 5.9(b), above which crosstalk is indistinguishable.

guishable, and crosstalk that falls on the right side distinguishable. We can observe from Fig. 5.10(b) that when the moving speed increases to approximately $28°/sec$ and beyond, all crosstalk levels becomes indistinguishable. We can apply this result to crosstalk reduction in 3D videos by assigning less or no weight to objects whose crosstalk and moving speed fall in the range of the crosstalk-indistinguishable region in Fig. 5.10(b).

5.4 Conclusion

In this chapter we conducted a subjective test to find out the relationship between crosstalk visibility and horizontal motion. The subjective test was conducted on a stereoscopic display consisting of two CRT displays. Fifty-four video segments that showed horizontally moving dots with six levels of crosstalk at nine moving speeds were displayed to 81 volunteer subjects. While watching the videos, the subjects were able to change the level of crosstalk in the test video to match the level of crosstalk in the reference video.Eighty-one subjects initially participated in the test. The results of 28 subjects who made significant errors when the moving speed was zero were removed, and the results of the remaining subjects were used for the analysis.

From the results of the subjective test, our analysis is as follows:

- For all crosstalk levels, the standard deviation of the matching results increases as the moving speed increases, which indicates that crosstalk becomes less identifiable as moving speed increases.

- The Spearman rank correlation coefficient shows strong increasing monotonic correlation between the matching results and true reference crosstalk when the angular speed is under $15°/sec$, and moderate increasing monotonic correlation in the speed range of $20°/sec$ - $25°/sec$, but weak correlation when the speed increases beyond $30°/sec$. We can infer from this result that at low speed, the observers are able to distinguish different levels of crosstalk, but as the speed increases, all levels of crosstalk visibly appear indistinguishable.

- We measure the crosstalk matching error by calculating the absolute difference between the crosstalk matched by the subjects and the true reference crosstalk after converting crosstalk luminance into gray-scale level. We plot the matching error in 3D with respect to the six crosstalk levels and nine moving speeds and fit a polynomial surface to the data. Then, we obtain a curve by inserting a plane at the error at zero crosstalk and zero speed in the fitted surface. The resulted curve quantifies the range of crosstalk and moving speed where crosstalk is indistinguishable and distinguishable. We can apply this result to crosstalk reduction in 3D in which less or no weight can be assigned to objects whose crosstalk and moving speed fall in the range of crosstalk-indistinguishable region and thus further preserve the video quality.

5.5 Acknowledgment

Chapter 5, in part is currently being prepared for submission for publication of the material, Menglin Zeng, Alan Robinson, and Truong Nguyen. The dissertation author is the primary investigator and author of this material.

Chapter 6

Conclusion and Future Work

6.1 Conclusions

In this work, we build models for active 3D LCD with shutter glasses and circularly-polarized LCD (CP LCD) with passive glasses, respectively. The model for active 3D LCD characterizes the temporal change of the display. Through the analysis of crosstalk in active 3D LCD, we find out that decreasing the rise and fall time of LCD response, decreasing the fall response of the glasses, but increasing the rise time of glasses results in reduced crosstalk. The modeling for CP LCD is composed of two parts: the modeling of the polarizing system, including linear polarizer and wave retarder by Mueller calculus method, and vertical misalignment (VM) between the LCD panel and pattered wave retarder. In the modeling of polarizing system, we improve the accuracy by applying coordinate transformation from the LCD to glasses. As a result, the erroneous "color bleeding" seen in previous related work disappears. Furthermore, in the modeling of VM, we propose a novel and robust display calibration method that only requires the observation of the display from four different locations. The simulation of our models are verified by measurement of real displays.

We prove that crosstalk caused by the polarizing system is approximately evenly distributed across the screen and is insignificant ($< 10\%$). For this type of

crosstalk, we formulate a linear-programming problem that maximizes the dynamic range of the image. Furthermore, we propose to carry out the reduction method in display luminance rather than gray-scaled level to better preserve color. In addition, we further preserve the dynamic range of the image by neglecting areas that have a texture image co-located in the left-eye and right-eye images.

We also find out that VM-based crosstalk is much more severe ($> 10\%$) than that which is caused by the polarizing system. Moreover, the spatial distribution of VM-based crosstalk changes significantly with vertical viewing location. Thus, it is inefficient to reduce VM-based crosstalk by image-processing methods which lead to considerable trade off in the image quality. In addition, we prove mathematically that VM-based crosstalk can not be canceled by the polarizing system. Therefore, we provide an analytic solution of the VM-free viewing zone of CP LCD from the calibration parameters. Extending the solution to the case of multiple displays, we propose a method to maximize the overlapping VM-free viewing zone.

To extend our work from image to video, we analyze how horizontal motion affects the visibility of crosstalk by conducting a subjective test. From the result, we obtain a curve that shows the range of crosstalk and moving speed within which crosstalk is distinguishable or indistinguishable. This can be applied to crosstalk reduction in 3D videos with less or no weight assigned to objects whose crosstalk and horizontal moving speed fall within the crosstalk-indistinguishable range.

6.2 Future Works

Our future work is to quantify crosstalk visibility in videos considering contrast, texture and motion and to design a crosstalk reduction algorithm for 3D video that reduces crosstalk while preserving the original video quality. In addition, temporal consistency of crosstalk reduction in video is a factor we should consider in the algorithm.

Appendix A

Modeling of wave retarders in circularly-polarized LCD

A.1 Details of applying Mueller matrix method to modeling CP LCD

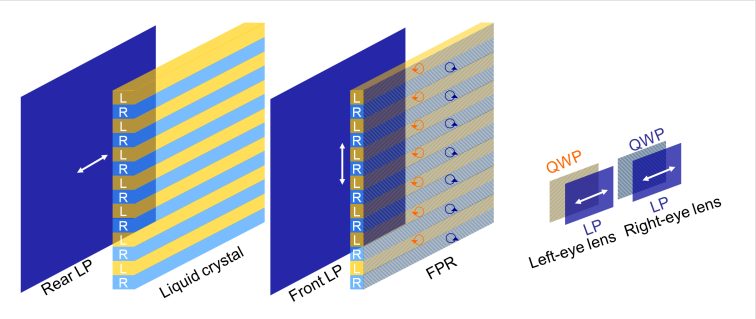

Figure A.1: Structure of circular 3D LCD with passive glasses

Fig. A.1 shows the schematic structure of a CPLCD with passive glasses where lights propagate from the left to the right. We can see in the Fig. A.1 that the LC module is divided into the left-eye and the right-eye fields with the left-eye field consisting of all even-row pixels that display the left-eye images and vice versa for the right-eye field.

In Fig. A.1, the rear and the front LPs polarize the light horizontally and vertically respectively. The LC module between the LPs acts as a wave retarder that

modulates the amount of light transmitted after the front LP. FPR in Fig. A.1 consists of patterned QWP that polarizes the left-eye image into left-hand polarization and the right-eye image into right-hand polarization. The passive glasses have a layer of QWP and LP as shown in Fig. A.1 where the left-eye lens transmits lights of left-hand polarization only and vice versa for the right-eye lens.

There are different optical modeling methods to calculate the state of the light such as 4x4 method [YW06], extended Jones matrix [YW06] and MM method. In this paper, we use MM method which works for partially polarized and unpolarized light and is able to model both uniaxial and biaxial wave plates.

MM method uses Stokes parameters to characterize the state of the light. Stokes parameters are represented as a 4x1 vector: $\mathbf{S} = [S_0, S_1, S_3, S_3]^T$, where S_0 is the intensity of the light, S_1, S_2 and S_3 are respectively the intensity difference between the horizontally and vertically polarized light, $+45°$ and $-45°$ polarized light, left-hand and right-hand circularly polarized light.

$$\mathbf{M}_p(\psi) = \frac{1}{2}\begin{bmatrix} 1 & \cos(2\psi) & \sin(2\psi) & 0 \\ \cos(2\psi) & \cos^2(2\psi) & \sin(2\psi)\cos(2\psi) & 0 \\ \sin(2\psi) & \sin(2\psi)\cos(2\psi) & \sin^2(2\psi) & 0 \\ 0 & 0 & 0 & 0 \end{bmatrix} \tag{A.1}$$

$$\psi_p = \arctan\left(\frac{\cos(\phi - \phi_P - \pi/2)}{\sin(\phi - \phi_P - \pi/2)\cos\theta}\right) \tag{A.2}$$

$$\mathbf{M}_{wp}(\Gamma, \psi) = \begin{bmatrix} 1 & 0 & 0 & 0 \\ 0 & \cos^2(2\psi) + \sin^2(2\psi)\cos\Gamma & \sin(2\psi)\cos(2\psi)(1-\cos\Gamma) & \sin(2\psi)\sin\Gamma \\ 0 & \sin(2\psi)\cos(2\psi)(1-\cos\Gamma) & \sin^2(2\psi) + \cos^2(2\psi)\cos\Gamma & -\cos(2\psi)\sin\Gamma \\ 0 & -\sin(2\psi)\sin\Gamma & \cos(2\psi)\sin\Gamma & \cos\Gamma \end{bmatrix} \tag{A.3}$$

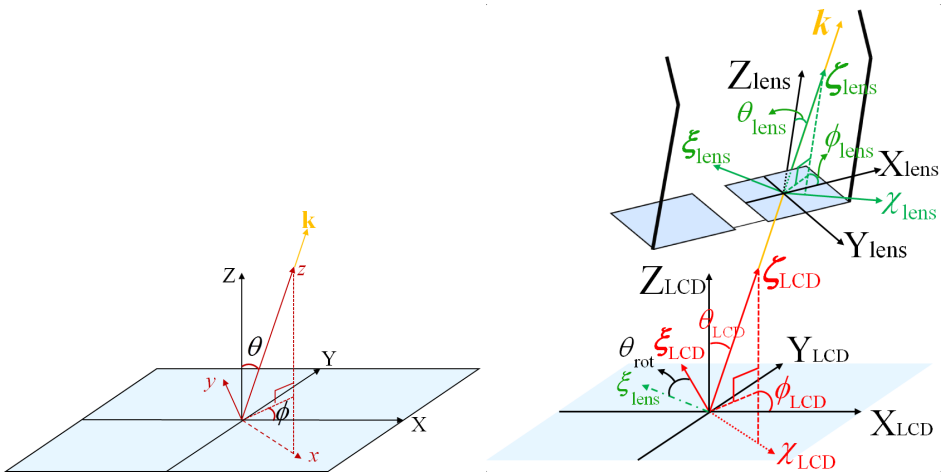

(a) θ, ϕ and $\mathbf{k}$ (b) Axes of coordinates

Figure A.2: Angles used in LCD and glasses coordinates used in Eq. (A.1-A.6)

$$\psi_{wp} = -\frac{1}{2}\arctan\left(\frac{\Delta n_{\parallel}\sin(2\phi - \phi_{wp})\cos\theta}{\frac{1}{2}\Delta n_{\parallel}\cos(2\phi - \phi_{wp})(1+\cos^2\theta) + \Delta n_{\perp}\sin^2\theta}\right) \tag{A.4}$$

$$n_{\xi} - n_{\eta} = -\Delta n_{\parallel}\cos\theta/\sin(2\psi_{wp}) \tag{A.5}$$

$$\Gamma = \frac{\pi(n_{\xi} - n_{\eta})d}{\lambda\cos\theta} \tag{A.6}$$

The Stokes vector is left multiplied by MMs which are 4x4 matrices that model LP and the wave plate (WP). WP includes the LC, FPR and QWP. Eq. (A.1) [YW06] is the MM for LP parameterized by the angle of transmittance axis: ψ_p in Eq. (A.2) [YW06]. The MM for the WP is given in Eq. (A.3) [YW06] which has two parameters ψ_{wp} in Eq. (A.4) [LL09] and Γ in Eq. (A.6) [LL09].

X, Y, Z in Fig. A.2 (a, b) are the axes of either the LP frame or the WP frame, among which Z denotes the surface normal of the LP or WP. $X-Y$ plane of LP, LC, FPR/ QWP is always parallel to the LCD/ glasses surface. For the LP, X in Fig. A.2 (a) denotes the transmittance axis (also the white arrows in LP in Fig. A.1). ϕ_p in Eq. (A.2) is the angle of the transmittance axis of the LP in the LCD coord. ϕ_{wp} in Eq. (A.4) is the angle of X axis of the LC, FPR/ QWP in the LCD/ glasses coord.

x, y, z in Fig. A.2 (a, b) are axes of the light coord. among which z is aligned with the wave vector $\mathbf{k}$ (unit vector of the propagation of the light), x lies in the incidence plane: $Z-\mathbf{k}$, y lies in plane $X-Y$, and $x-y$ denotes the wave plane. ϕ (in Eq. (A.2, A.4)) and θ (in Eq. (A.2, A.4, A.5, A.6)) in Fig. A.2 (a) are respectively the azimuthal angle and the polar angle of $\mathbf{k}$ in the XYZ frame. ψ_p is the angle from x to the projection of the LP transmittance axis onto the wave plane. In Fig. A.3, the

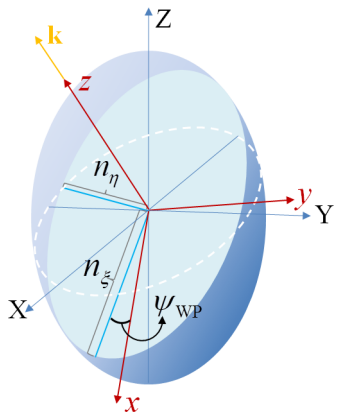

Figure A.3: Refractive index ellipsoid in coordinate.

refractive index ellipsoid (RIE) of the WP is parameterized by n_X, n_Y, n_Z as lengths of the semi-principal axes. And the intercession between the RIE and wave plane is an ellipse whose semi-major/ minor axis has the length of n_ξ/ n_η (in Eq. (A.5)) as the refraction index along axis ξ/ η. As Fig. A.2 (b) shows, ψ_{wp} is the angle from x to ξ. Γ denotes the phase difference between lights that polarize along ξ and η.

Since ψ_p and ψ_{wp} are defined in the wave plane in the light coordinate, and the orientation of the light coord. can be different in the LCD and in the glasses, it's necessary to illustrate these coord. systems: LCD coordinate, glasses coordinate, light coord. in the LCD, and light coord. in the lens. As Fig. A.2 (b) shows, we denote the LCD coord. as $[X_{LCD}, Y_{LCD}, Z_{LCD}]^T$, the light coord. in the LCD as $[x_{LCD}, y_{LCD}, z_{LCD}]^T$, the glasses coord. as $[X_{lens}, Y_{lens}, Z_{lens}]^T$, and the light coord. in the glasses as $[x_{lens}, y_{lens}, z_{lens}]^T$. And note in Fig. A.2 (b) how the orientation of the wave plane $x_{LCD} - y_{LCD}$ changes to $x_{lens} - y_{lens}$ as the LCD and the glasses orient differently.

Table A.1: Parameters used for LC, FPR and QWP [YW06] [LL12]

Parameters	Description	Values
d_{LC}	LC Cell gap	$4\mu m$
$n_{X,LC}$	n_X of LC	1.565
$n_{Y,LC}$	n_Y of LC	1.479
$n_{Z,LC}$	n_Z of LC	1.479
d_{FPR}	thickness of RMS-001	$0.86\mu m$
$n_{X,FPR}$	n_X of RMS-001	1.680
$n_{Y,FPR}$	n_Y of RMS-001	1.521
$n_{Z,FPR}$	n_Z of RMS-001	1.521
d_{PC}	thickness of PC film	$13.75\mu m$
$n_{X,PC}$	n_X of PC film	1.590
$n_{Y,PC}$	n_Y of PC film	1.580
$n_{Z,PC}$	n_Z of PC film	1.585

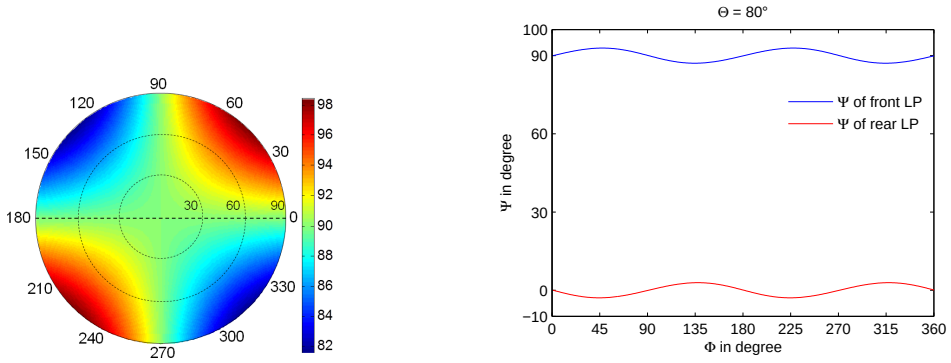

(a) $\psi_{front} - \psi_{rear}$ (b) ψ_{front} & ψ_{rear}

Figure A.4: Result of ψ_p in the LP

A.2 Results of ψ and Γ in CP LCD

In the modeling, we apply parameters of in-plane switching (IPS) for LC, RMS-001 Merck reactive LC for FPR and PC film for QWP in the glasses, among which IPS and reactive LC are uniaxial and PC film is biaxial. As Fig. A.1 shows, ϕ_p of the rear/ front LP is 0°/ 90°. ϕ_{wp} of the left-eye-field/ right-eye-field FPR and the left-eye/ right-eye QWP are both 45°/ 135°. For the bright/ dark state of the LC, ϕ_{wp} of the IPS is 45°/ 0°. All the parameters used for the IPS, FPR and QWP are listed in Table A.1. We assume the wavelength to be 550 nm (green).

Fig. A.4 (a) shows how the difference between ψ_p of the front and the rear LP

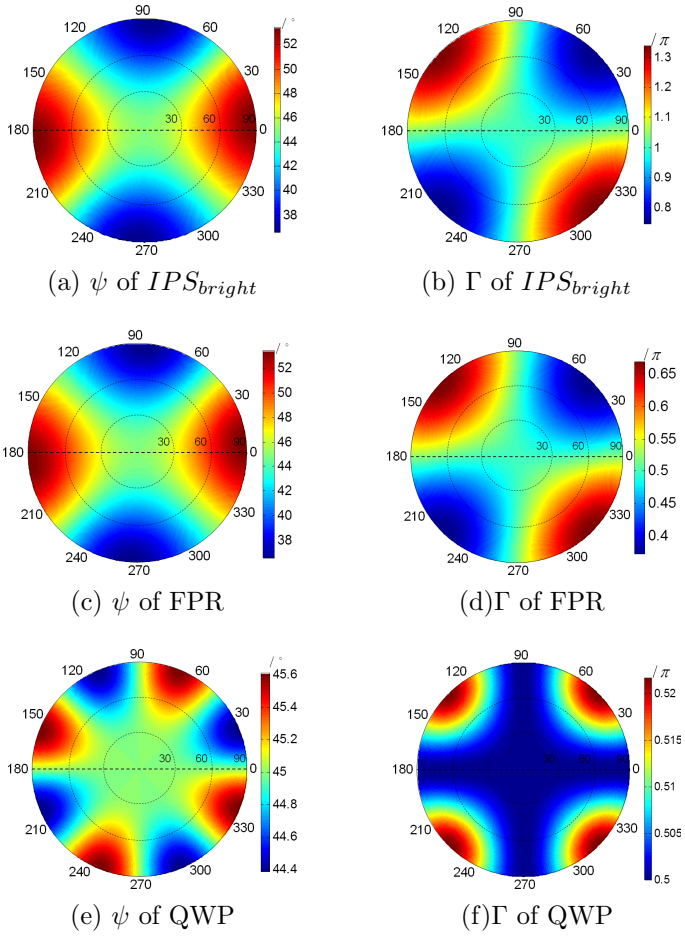

(a) ψ of IPS_{bright} (b) Γ of IPS_{bright}

(c) ψ of FPR (d)Γ of FPR

(e) ψ of QWP (f)Γ of QWP

Figure A.5: ψ and Γ in (a, b): bright-state IPS (LC), (c, d): left-eye FPR, (e, f): left-eye QWP.

changes with θ (as radial coord. in Fig. A.4 (a) and all the polar plots in this paper) and ϕ (as the angular coord. in Fig. A.4 (a) and all the polar plots in this paper) in the LCD coord. We can see in Fig. A.4 (a) that $\psi_{front} - \psi_{rear}$ deviates from 90° in oblique incidence especially at off-axis azimuthal angles: $45°, 135°, 225°, 315°$. This indicates ψ_{rear} and ψ_{front} are non orthogonal. Fig. A.4 (b) shows how individually ψ_p of the front and the rear LP changes when $\theta = 80°$. From Eq. (A.4), we can calculate ψ_{wp} of the LC, FPR and QWP respectively. Note from Fig. A.2 (b) as the incident angle rotates around Z, x also rotates while ξ stays around the longest principal axis of the RIE. To better observe ψ_{wp}, we subtract from it the rotation of x. And the resulted ψ_{wp}s of the bright-state LC, left-eye-field FPR and left-eye QWP are shown in Fig. A.5 (a, c, e) respectively, and they all shift from the corresponding

ϕ_{wp} as the incident angle becomes oblique. Comparing Fig. A.5 (a, c) with Fig. A.5 (e), we can see that ψ_{wp} in the QWP has smaller shifting compared with those in the IPS and FPR. It is because PC film for the QWP is biaxial whose value of n_Z is between n_X and n_Y (Table. A.1), while IPS for the LC and Merk LC for the FPR are uniaxial whose n_Zs are the same as n_Xs. And the shape of the RIE of the PC film better counter balances the deviation of ψ_{wp} from ϕ_{wp} at oblique incidence.

In Fig. A.5 (b, d, f), Γs of the bright-state LC, left-eye-field FPR and the left-eye QWP are shown respectively. We observe at oblique incidence Γ shifts away from π in the LC and from $\pi/2$ in the FPR and the QWP. This shifting in Γ is cause by the deviation of ψ_{wp} in the LC, FPR and QWP.

The deviation from orthogonality of ψ_ps in the crossed LP and the shifting from π of Γ in the bright-state IPS only cause light to leak from the backlight to after the front LP. This leakage lowers the contrast in the 2D images only but results in no binocular crosstalk. However, the shifting of Γ from $\pm\pi/2$ in the FPR causes light to be elliptically rather than circularly polarized (or S_3 to deviate from -1/ +1 in the left-eye/ right-eye field), and thus yield crosstalk after the glasses. Similarly, the shifting of Γ from $\pm\pi/2$ in the QWP of the glasses also results in crosstalk.

To see the combined influence that LP, FPR and the passive glasses have on the luminance of the display, lets first simplify the entire display into a "single-pixel display", and FPR into an uniform QWP for either the left-eye or the right-eye field as Fig. A.6 (a, b) shows. We then assume the input back light is lambertion, $[1, 0, 0, 0]^T$ at normal incidence, of wavelength 550nm (green light). We also assume the surface of the lens is always normal to the incident light (as shown in Fig. A.6 (a, b)) for all viewing angles. Luminance of the single-pixel display under full viewing angle from the set up in Fig. A.6 (a, b) is shown in Fig. A.7. The results in Fig. A.7 are luminance after the left-eye lens with combinations in the display of bright/ dark pixel with left-eye/ right-eye pixel. We can see that for the simple set up in Fig. A.6 (a, b), and for single-colored light, the leakages in Fig. A.7 (b, c, d) are insignificant.

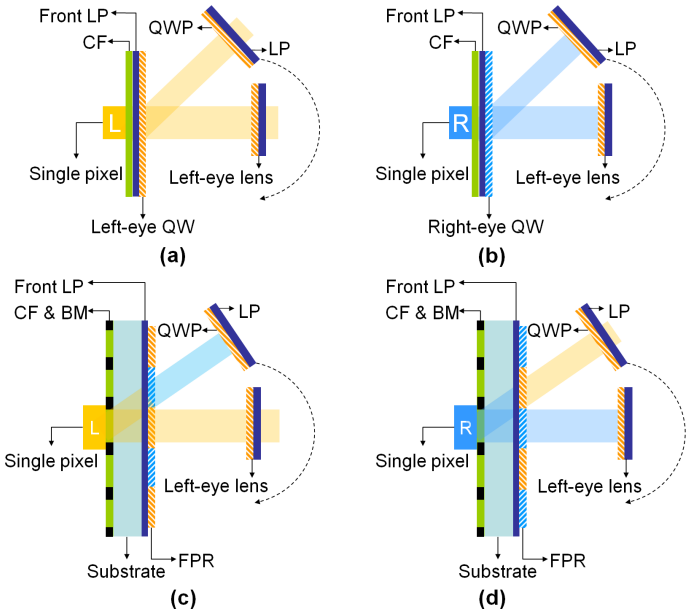

Figure A.6: Set up for the test of single-pixel luminance: (a, c) left-eye pixel after left-eye lens, (b, d)Right-eye pixel after left-eye lens

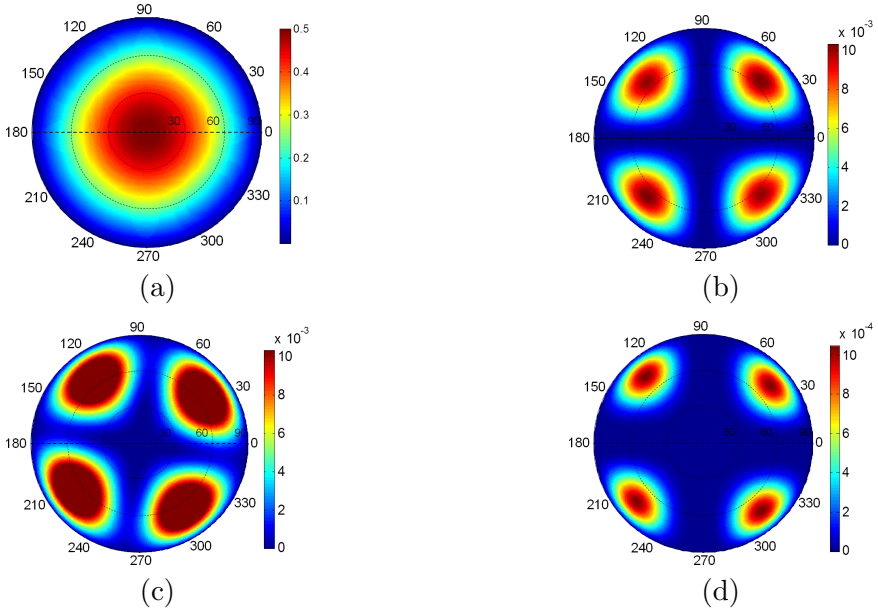

Figure A.7: Singl-pixel luminance after left-eye lens from set up in Fig. A.6: (a, b) left-eye pixel, (c, d) right-eye pixel, (a, c) bright pixel, (b, d) dark pixel

Appendix B

Comparison of Simulation with Real Display

In Fig. B.1, at view A, the camera is vertically aligned to a quarter of the screen height from screen top at the distance of $1m$. At view B, the camera is vertically aligned to a quarter of the screen height from screen bottom at the distance of $1m$. At view C, the camera is vertically aligned to a quarter of the screen height from screen top at the distance of $0.8m$. At view D, the camera is vertically aligned to a quarter of the screen height from screen bottom at the distance of $0.8m$.

In Fig. B.2, two viewing locations are tested: vertically aligned to the screen top at the distance of $1m$ (left two columns), and vertically aligned to the screen bottom at the distance of $1m$ (right two columns). From left to right, the 1^{st} and 3^{rd} columns are resulted from simulation, and the 2^{nd} and 4^{th} columns show the real CP LCD. Note that the tiltedness of the display in photos are corrected by Homography tranform. The real CP LCD is LG 47LH55 (1080p) [Cor09].

(a) Screen shot, view A.

(b) Simulation, view A.

(c) Screen shot, view B.

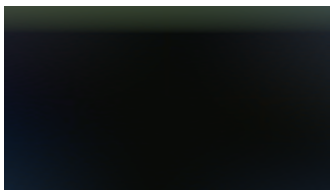

(d) Simulation, view B.

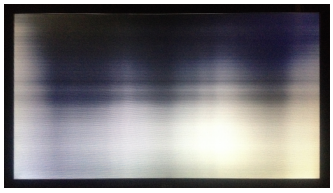

(e) Screen shot, view C.

(f) Simulation, view C.

(g) Screen shot, view D.

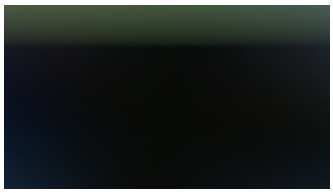

(d) Simulation, view D.

Figure B.1: Screen pictures (after homography transform) and the corresponding simulations.

Figure B.2: Results of "Books" [SP07] (top row) in left view, "Dwarves" [SP07] (center row) in right view, and "Dolls" [SP07] (bottom row) in left view.

Bibliography

[BBZ96] Benedicte Bascle, Andrew Blake, and Andrew Zisserman. Motion deblurring and super-resolution from an image sequence. *Computer VisionECCV'96*, pages 571–582, 1996.

[Ber72] D. W. Berreman. Optics in Stratified and Anisotropic Media: 4 X 4-Matrix Formulation. *Journal Of The Optical Society Of America*, 62(4):502–510, April 1972.

[BL11] P. Boher and T. Leroux. Optical Characterization of Different Types of Stereoscopic 3D Displays. In *Exhibitor Forum SID Conference*. The Society for Information Display, May 19 2011.

[BLBC10] P. Boher, T. Leroux, T. Bignon, and P. V. Collomb. Multispectral polarization viewing angle analysis of circular polarized stereoscopic 3d displays. In *Proceedings of SPIE Stereoscopic Displays and Applications XXI*, pages 0R1–0R12, 2010.

[BPJ+11] J.V. Baar, S. Poulakos, W. Jarosz, D. Nowrouzezahrai, R. Tamstorf, and M. Gross. Perceptually-based compensation of light pollution in display systems. In *Proceedings of the ACM SIGGRAPH Symposium on Applied Perception in Graphics and Visualization*, pages 45–52. ACM, 2011.

[BTB+11] Marcus Barkowsky, Sylvain Tourancheau, Kjell Brunnström, Kun Wang, and Börje Andrén. Crosstalk measurements of shutter glasses 3d displays. In *SID Symposium Digest of Technical Papers*, volume 42, pages 812–815. Wiley Online Library, 2011.

[BWS05] A. Blasiak, J. Wehrwein, and D. Scharstein. 2005 Stereo datasets with ground truth. http://vision.middlebury.edu/stereo/data/, 2005.

[CCCH09] C.Y. Chiang, T.S. Chen, Y.C. Chang, and Y.P. Huang. 54.2: The effect of crosstalk for stereoscopic 3d dynamic moving images. In *SID Symposium Digest of Technical Papers*, volume 40, pages 808–811. Wiley Online Library, 2009.

[CG66] F. W. Campbell and R. W. Gubisch. Optical Quality of The Human Eye. *The Journal of Physiology*, 186:558–578, 1966.

[Cor09] LG Corporation. LG 47LH55 LCD. http://www.lg.com/us/tvs/lg-47LH55-lcd-tv, 2009.

[DKS12] J.H. Lee D.H. Kang, E.J. Lee and J.K. Song. Perceptual Strength of 3-D Crosstalk in Both Achromatic and Color Images in Stereoscopic 3-D Displays. *IEEE Transactions on Image Processing*, 21(7):3253–3261, July 2012.

[DN11] C. Doutre and P. Nasiopoulos. Optimized contrast reduction for crosstalk cancellation in 3d displays. In *IEEE 3DTV Conference, Antalya, Turkey*, pages 1–4, May 2011.

[Ham97] Stephen T Hammett. Motion blur and motion sharpening in the human visual system. *Vision Research*, 37(18):2505–2510, 1997.

[HHS10] D.G. Lee M.J. Lim H.K. Hong, J.W. Jang and H.H. Shin. Analysis of angular dependence of 3-d technology using polarized eyeglasses. *Journal of the SID*, 18(1):8–12, 2010.

[HLW05] Thomas X Hong, Qiand Wu, Ruibo Lu, and Shin-Tson Wu. Wide-view circular polarizer consisting of a linear polarizer and two biaxial films. *Optics express*, 13(26):10777–10783, 2005.

[Hon12] HyungKi Hong. Reduction of spatially non-uniform 3d crosstalk for stereoscopic display using shutter glasses. *Displays*, 33(3):136–141, 2012.

[HR12] I.P. Howard and B.J. Rogers. *Perceiving in Depth, Volume 2: Stereoscopic Vision*. Oxford University Press, 2012.

[HTLH00] K.C. Huang, C.H. Tsai, K. Lee, and W.J. Hsueh. Measurement of contrast ratios for 3d display. *Proceedings of SPIE Input/Output and Imaging Technologies II*, 4080:78–86, 2000.

[HW05] Q. Hong and X. Wu. Designs of wide-view and broadband circular polarizers. *Optics Express*, 13(20):8318–8331, Oct 2005.

[HWZ+05] Qi Hong, Thomas Wu, Xinyu Zhu, Ruibo Lu, and Shin-Tson Wu. Designs of wide-view and broadband circular polarizers. *Optics express*, 13(20):8318–8331, 2005.

[JKD00] B. Lacotte J. Konrad and E. Dubois. Cancellation of image crosstalk in time-sequential displays of stereoscopic video. *IEEE Transactions on Image Processing*, 9(5):897–908, 2000.

[KRL+11] Taeho Kim, Joong Min Ra, Jun Hak Lee, Seong Hak Moon, and Kwang-Yeol Choi. 3d crosstalk compensation to enhance 3d image quality of plasma display panel. *Consumer Electronics, IEEE Transactions on*, 57(4):1471–1477, 2011.

[LHW58] R. L. Lamberts, G. C. Higgins, and R. N. Wolfe. Measurement and analysis of the distribution of energy in optical images. *Journal of The Optical Society of America*, 48(7):487–490, 1958.

[Lie97] A. Lien. A detailed derivation of extended jones matrix representation for twisted nematic liquid crystal displays. *Liquid Crystals*, 22:171–175, Aug 1997.

[Lip87] L. Lipton. Factors Affecting Ghosting in Time-multiplexed Plano-stereoscopic CRT Display Systems. In *SPIE True 3D Imaging Techniques and Display Technologies*, pages 75–78, 1987.

[LL09] C.T Lee and H.Y. Lin. Analytic expressions of optical retardation of biaxial compensation films for liquid crystal displays. *Journal of Optics A: Pure Appl.*, 11, August 2009.

[LL10] C.T Lee and H.Y. Lin. Designs of broadband and wide-view patterned polarizers for stereoscopic 3d displays. *Optics Express*, 18, No. 26:27079–27094, Jan 2010.

[LL12] C.T Lee and H.Y. Lin. Ultra-wide-view patterned polarizer type stereoscopic lcds using patterned alignment. *Optics Express*, 20, No.2:1700–5, Jan 2012.

[LLT+09] J. C. Liou, K. Lee, F. G. Tseng, J. F. Huang, W. T. Yen, and W. L. Hsu. Shutter Glasses Stereo LCD with a Dynamic Backlight. In *Proceedings of SPIE Stereoscopic Displays and Applications XX*, number 72370X, pages 1–8. SPIE, Feb 2009.

[LW94] J.S. Lipscomb and W.L. Wooten. Reducing Crosstalk between Stereoscopic Views. In *Proceedings of SPIE Stereoscopic Displays and Virtual Reality Systems*, volume 2177, pages 92–96. SPIE, 1994.

[LWH11] Y. Tu L. Chen P. Zhang T. Zhang L. Wang, K. Tuenissen and I. Heynderickx. Crosstalk evaluation in stereoscopic displays. *IEEE Journal of Display Technology*, 7(4):208–214, April 2011.

[LXP12] T. Ebrahimi L. Xing, J.You and A. Perkis. Assessment of stereoscopic crosstalk perception. *IEEE Transactions on Multimedia*, 14(2):326–337, April 2012.

[Ma04] Yi Ma. *An invitation to 3-d vision: from images to geometric models*, volume 26. springer, 2004.

[MZN15] A. E. Robinson M. Zeng and T. Q. Nguyen. Modeling, prediction, and reduction of 3d crosstalk in circular polarized stereoscopic lcds. *Image Processing, IEEE Transactions on*, 24(12):5516–5530, 2015.

[Pat07] Robert Patterson. Human factors of 3-d displays. *Journal of the Society for Information Display*, 15(11):861–871, 2007.

[PC83] Michael Potmesil and Indranil Chakravarty. Modeling motion blur in computer-generated images. *ACM SIGGRAPH Computer Graphics*, 17(3):389–399, 1983.

[PFD05] Hao Pan, Xiao-Fan Feng, and Scott Daly. Lcd motion blur modeling and analysis. In *Image Processing, 2005. ICIP 2005. IEEE International Conference on*, volume 2, pages II–21. IEEE, 2005.

[PSI05] L.M.J. Meesters P.J.H. Seuntins and W.A. IJsselsteijn. Perceptual attributes of crosstalk in 3d images. *Displays*, 26:177–183, Oct 2005.

[RMDM04] J. E Richman, K. G. McAndrew, D. Decker, and S. C. Mullaney. An evaluation of pupil size standards used by police officers for detecting drug impairment. *Journal of the American Optometric Association*, 75(3):175–182, March 2004.

[SJMR14] Hosik Sohn, Yong Ju Jung, and Yong Man Ro. Crosstalk reduction in stereoscopic 3d displays: Disparity adjustment using crosstalk visibility index for crosstalk cancellation. *Optics express*, 22(3):3375–3392, 2014.

[SLF07] F.A. Smith, R.V. Liere, and B. Frhlich. Three Extensions to Subtractive Crosstalk Reduction. In *13th Eurographics Virtual Environments symposium, Weimar, Germany*, pages 1–9. IPT-EGVE, July 2007.

[SMI05] Pieter JH Seuntiëns, Lydia MJ Meesters, and Wijnand A IJsselsteijn. Perceptual attributes of crosstalk in 3d images. *Displays*, 26(4):177–183, 2005.

[SP07] Daniel Scharstein and Chris Pal. Learning conditional random fields for stereo. In *Computer Vision and Pattern Recognition, 2007. CVPR'07. IEEE Conference on*, pages 1–8. IEEE, 2007.

[TWA11] Inna Tsirlin, Laurie M Wilcox, and Robert S Allison. The effect of crosstalk on depth magnitude in thin structures. In *IS&T/SPIE Electronic Imaging*, pages 786313–786313. International Society for Optics and Photonics, 2011.

[Vie] Best 3D TV Screen Size and Viewing Distance. http://www.best-3dtvs.com/guides/best-screen-size-viewing-distance/.

[WH10] A. J. Woods and C. R. Harris. Comparing levels of crosstalk with red/cyan, blue/yellow, and green/magenta anaglyph 3D glasses. pages 0Q1–0Q12. in Proceedings of SPIE Stereoscopic Displays and Applications XXI, Jan. 2010.

[WKL12] G.D. Lee J.H. Lee B.K. Kim H.C. Choi Y.J. Lim W.S. Kang, B.J. Mun and S.H. Lee. Optimal design of quarter-wave plate with wideband and wide viewing angle for three-dimensional liquid crystal display. *Journal of Applied Physics*, 111:103119:1–6, May 2012.

[Woo12] A.J Woods. Crosstalk in stereoscopic displays: a review. *Journal of Electronic Imaging*, 21(4):040902(1)–040902(21), 2012.

[WSM01] Stefan Winkler, Animesh Sharma, and David McNally. Perceptual video quality and blockiness metrics for multimedia streaming applications. In *Proceedings of the international symposium on wireless personal multimedia communications*, pages 547–552, 2001.

[WWZW04] Haiying Wang, Thomas X Wu, Xinyu Zhu, and Shin-Tson Wu. Correlations between liquid crystal director reorientation and optical response time of a homeotropic cell. *Journal of Applied Physics*, 95(10):5502–5508, 2004.

[XYEP10] L. Xing, J. You, T. Ebrahimi, and A. Perkis. A perceptual quality metric for stereoscopic crosstalk perception. In *Proceedings of 17th International Conference on Image Processing, Hongkong*, pages 4033–4036. IEEE, Sep. 2010.

[YS90] Yei-Yu Yeh and Louis D Silverstein. Limits of fusion and depth judgment in stereoscopic color displays. *Human Factors: The Journal of the Human Factors and Ergonomics Society*, 32(1):45–60, 1990.

[YUT08] Y Yoshihara, H Ujike, and T Tanabe. 3d crosstalk of stereoscopic (3d) display using patterned retarder and corresponding glasses. In *International Display Workshop, Niigata , Japan*, volume 15, pages 1135–1138, 2008.

[YW06] D.K. Yang and S.T. Wu. Fundamentals of Liquid Crystal Devices. pages ch.8.3, 208–216, 2006.

[YWS08] Y. Yang, J. Wanek, and M. Shahidi. Representing the retinal line spread shape with mathematical functions. *Journal Zhejiang University*, 9:996–1002, Dec. 2008.

[YY09] Young-Cheol Yang and Denge-Ke Yang. Analytic expressions of optical retardation of biaxial compensation films for liquid crystal displays. *Journal of Optics A: Pure and Applied Optics*, 11(10):105502, 2009.

[Zen] M. Zeng. Modeling of the circularly polarized 3D LCD. http://tinyurl.com/kl9ohf2.

[ZGW06] Xinyu Zhu, Zhibing Ge, and Shin-Tson Wu. Analytical solutions for uniaxial-film-compensated wide-view liquid crystal displays. *Journal of Display Technology*, 2(1):2, 2006.

[ZN13] M. Zeng and T. Nguyen. Crosstalk modeling, analysis, simulation and cancellation in passive-type stereoscopis lcd displays. In *The 38th International Conference on Acoustics, Speech, and Signal Processing , Vancouver*. IEEE, April 2013.

[ZN14] M. Zeng and T. Nguyen. Crosstalk Modeling in Cricularly Polarized Stereoscopic LCDs. In *IEEE International Conference on Image Processing, Paris*. IEEE, Oct. 2014.